R94-970150-3

INTERFACIAL STUDIES OF COATED FIBER REINFORCED GLASS-CERAMIC MATRIX COMPOSITES

Prepared by

John Brennan, UTRC
Steven Nutt, Brown Univ.
Ellen Sun, Brown Univ.

FINAL REPORT

Contract F49620-92-C-0001

for

Air Force Office of Scientific Research
Bolling Air Force Base
Washington, DC 20332

December 31, 1994

UNITED TECHNOLOGIES RESEARCH CENTER

East Hartford, Connecticut 06108

REPORT DOCUMENTATION PAGE

Form Approved
OMB No. 0704-0188

1. AGENCY USE ONLY (Leave blank)	2. REPORT DATE	3. REPORT TYPE AND DATES COVERED
	31 December 1994	Final Report 11/1/92-10/31/94

4. TITLE AND SUBTITLE

INTERFACIAL STUDIES OF COATED FIBER REINFORCED GLASS-CERAMIC MATRIX COMPOSITES

5. FUNDING NUMBERS

F49620-92-C-0001

2306/BS

6. AUTHOR(S)

John Brennan, Steven Nutt, Ellen Sun

7. PERFORMING ORGANIZATION NAME(S) AND ADDRESS(ES)

United Technologies Research Center
400 Main Street
East Hartford, CT 06108

8. PERFORMING ORGANIZATION REPORT NUMBER

R94-970150-3

AFOSR-TR- 95 0074

9. SPONSORING / MONITORING AGENCY NAME(S) AND ADDRESS(ES)

Dr. Alexander Pechenik
Air Force Office of Scientific Research
Directorate of Chemistry and Materials Science
110 Duncan Ave, Suite B115
Bolling AFB DC 20332-0001

NA

10. SPONSORING / MONITORING AGENCY REPORT NUMBER

F49620-92-C-0001

11. SUPPLEMENTARY NOTES

12a. DISTRIBUTION / AVAILABILITY STATEMENT

APPROVED FOR PUBLIC RELEASE; DISTRIBUTION IS UNLIMITED.

12b. DISTRIBUTION CODE

13. ABSTRACT *(Maximum 200 words)*

The objective of this program is to develop an understanding of the relationships between the fiber, fiber coating or coatings, and the glass-ceramic matrix, that will lead to a composite system exhibiting high strength, high toughness, and good thermal and environmental stability to temperatures of 1200°C. To meet this objective, the chemistry and microstructure of the fiber/coating(s)/matrix interfacial region and how these influence the interfacial bonding, strength, and toughness of the particular composite system was investigated.

During the course of this program, emphasis was placed on the determination of the high temperature mechanical properties of the BMAS matrix/SiC over BN coated Nicalon fiber composite system, and how these properties relate to changes that may occur in the matrix, fiber coatings, or Nicalon fiber chemistry and microstructure. Specifically, short time flexural, short time tensile, tensile creep, and tensile fatigue testing was conducted in air to temperatures of 1200°C, all on the same composite sample. Flexural creep was also performed on similar composite samples and compared to the tensile creep results. In addition, Si_3N_4 over BN and BN by itself were evaluated as fiber coatings in the BMAS matrix/Nicalon fiber composite system. The effect of long-time heat-treatments in oxidizing and non-oxidizing environments were conducted on composites with different interface chemistries. With the collaboration of Brown University, SEM and TEM analyses of the composites after being subjected to the various stress and temperature conditions were conducted. From these studies, damage modes and microstructural and chemical changes that occurred as a result of these tests were determined. Results of these studies are presented.

14. SUBJECT TERMS	15. NUMBER OF PAGES
Ceramic composite interfaces, coated fiber/glass-ceramic composites, BMAS glass-ceramic matrix/coated Nicalon fiber composites	104
	16. PRICE CODE

17. SECURITY CLASSIFICATION OF REPORT	18. SECURITY CLASSIFICATION OF THIS PAGE	19. SECURITY CLASSIFICATION OF ABSTRACT	20. LIMITATION OF ABSTRACT
Unclassified	Unclassified	Unclassified	SAR

UNITED
TECHNOLOGIES
RESEARCH
CENTER

East Hartford, Connecticut 06108

R94-970150-3

Interfacial Studies of Coated Fiber Reinforced Glass-Ceramic Matrix Composites

FINAL REPORT

Contract F49620-92-C-0001

APPROVED BY: K. M. Prewo

K. M. Prewo, Manager of
Materials Sciences

DATE: 12/31/94

TABLE OF CONTENTS

INTERFACIAL STUDIES OF COATED FIBER REINFORCED GLASS-CERAMIC MATRIX COMPOSITES

I. INTRODUCTION AND BACKGROUND

During the past few years, the interest in fiber coatings as a means of controlling the fiber/matrix interfacial properties in ceramic matrix composites has increased[1-50]. Most of these studies have dealt with composite systems that bonded too strongly to achieve tough composite behavior, but some have attempted to find a replacement coating for carbon that would debond like carbon but have improved oxidative stability. Studies conducted at UTRC in this area in the past few years have concentrated on BN based coatings on both Nicalon polycarbosilane derived Si-C-O fibers (Nippon Carbon Co.) and HPZ hydridopolysilylazane derived Si-N-C-O fibers (Dow Corning Corp.) in glass-ceramic matrix composites[1,34,40-50].

From the work conducted at UTRC under the recently concluded AFOSR program in 1991[1], it was found that fiber coatings, such as chemically vapor deposited (CVD) BN and CVD SiC over BN, deposited on advanced refractory small diameter fibers such as Nicalon and HPZ fibers, can result in strong, tough, and oxidatively stable high temperature structural composites when these coated fibers are incorporated into glass-ceramic matrices such as lithium aluminosilicate (LAS) and barium-magnesium aluminosilicate (BMAS).

Interfacial analysis of the BN coated Nicalon fiber composites, utilizing both scanning Auger microprobe (SAM) depth profiling of fracture surfaces and transmission electron microscopy (TEM) of thin foils, indicated that during composite fabrication the BN coating next to the LAS matrix crystallized with concurrent Si and Al matrix element diffusion into it, and a significant amount of boron diffusion occurred from the BN coating into the LAS matrix. The boron diffusion into the LAS matrix prevented complete crystallization of the matrix to the high temperature β-spodumene structure, with the residual boron containing glassy regions contributing to the low elevated temperature strength of the composites. Interfacial debonding appeared to be enhanced in those regions of the BN coating where no matrix element diffusion occurred.

In order to prevent boron diffusion into the matrix during composite fabrication, a thin (200-300nm) diffusion barrier SiC overcoat was applied to the BN coated Nicalon

fibers. From SAM and TEM analyses, it was found that this SiC layer prevented boron diffusion into the matrix and matrix element diffusion into the BN, thus resulting in composites with superior elevated temperature properties compared to BN coated Nicalon fiber composites. Both LAS and BMAS matrix composites were fabricated with the SiC/BN coated Nicalon fibers, with the LAS and BMAS matrix composites resulting in high strengths and thermal and oxidative stability to ~1100°C and 1200°C, respectively.

A brief study was conducted into the interfacial properties, microstructure, and strength vs temperature for BN and SiC/BN coated HPZ fiber/BMAS matrix composites. As in the coated Nicalon fiber composites, it was found that the best elevated temperature properties were obtained with the dual SiC/BN coated HPZ fibers. Respectable flexural strength to 1200°C in air was obtained for this composite system. Similar to coated Nicalon fiber composites, interfacial debonding occurred in the BN layer that did not contain diffused matrix elements such as Si, Al, and Ba.

It thus appears that the BMAS matrix composite systems with both Nicalon and HPZ fibers coated with SiC over BN, provided that the matrix can be properly crystallized to barium osumilite, offer significant potential as tough, thermally stable, structural ceramic composites for applications to ~1200°C. The previous AFOSR contract (F49620-88-C-0062), which concluded in 1993, continued with the emphasis focused entirely on BN based coatings for HPZ fibers in glass-ceramic matrix composites[40]. The AFOSR contract (F49620-92-C-0001) discussed in this report has concentrated on BMAS glass-ceramic matrices reinforced with BN based coatings on Nicalon fibers.

From the work conducted under this program during 1992[41] and 1993[42], certain conclusions and recommendations were drawn:

1. The particular composite system studied in 1992, BMAS matrix/SiC over BN coated Nicalon fibers, was found to exhibit very good mechanical properties (flexural strength and tensile strength and stress-rupture) to temperatures of ~1200°C. Additional mechanical property tests conducted in 1993 focused on elevated temperature stress tests in oxidizing environments, including both flexural and tensile creep, and tensile fatigue. Under long-term creep conditions at 1100°C, steady-state creep was established after a period of transient creep, with very low creep rates in the range of 10^{-9} s^{-1}. Under cyclic tensile stress conditions with the maximum applied stress slightly above the proportional limit (matrix microcrack) stress, the composite survived 10^5 cycles at temperatures up to 1200°C.

2. Fiber indent testing conducted on both LAS and BMAS matrix composites by Dr. Paul Jero at WPAFB confirmed that the BN coated Nicalon fiber composites exhibited higher interfacial debond energies and frictional sliding stresses than the *in-situ* formed carbon interfaces in uncoated Nicalon fiber/glass-ceramic matrix composites, as expected from fiber debond length observations on composite fracture surfaces. However, the scatter in data for the SiC/BN coated Nicalon fiber composites was very high. This may be related to the differences in interfacial microstructure and chemistry observed from scanning Auger and TEM analyses, due predominantly to the disbonding of the SiC overcoating from the BN layer during composite fabrication allowing matrix element diffusion into the BN layer with subsequent BN crystallization and carbon/silica microlayer formation at the BN/Nicalon fiber interface.

3. From both scanning Auger depth profiling of longitudinal composite fracture surfaces and HRTEM analysis of interfacial microstructure and chemistry, it was found that some of the BMAS matrix/SiC over BN coated Nicalon fiber composites exhibited distinct changes in interfacial chemistry and microstructure after certain heat-treatments or high temperature stress tests. These changes related to the crystallization of the turbostratic BN layer (due to matrix element diffusion) and the formation of a dual microlayer structure of carbon/silica at the BN/Nicalon fiber interface. However, it is not clear whether these changes were due to the thermal and/or stress history of the composite or to the detachment of the SiC layer from the BN layer during composite fabrication. This detachment was observed in several different composites and allowed the BMAS matrix to contact the BN layer, with subsequent rapid diffusion of matrix elements into it accompanied by BN recrystallization.

4. It was found that at elevated temperatures (>1100°C) under stress, the BMAS matrix tended to become unstable, in that phase separation by spinodal decomposition at the barium osumilite grain boundaries occurred, resulting in crystalline hexacelsian plus a siliceous glass. The two phase region was found to be magnesium deficient compared to the barium osumilite grains.

The overall objective of this program was to develop an understanding of the relationships between the fiber, fiber coating or coatings, and the glass-ceramic matrix, that will lead to a composite system exhibiting high strength, high toughness, and high thermal and environmental stability to temperatures of 1200°C. These relationships include the reactivity between the fiber and coating(s) during coating deposition, the reactivity between fiber/coating(s)/matrix constituents during composite processing, as well as the long time thermal and environmental stability of the composite system under conditions of use. Of prime importance is the understanding of the chemistry and

microstructure of the fiber/coating/matrix interfacial region, and how these influence the interfacial bonding, which, in turn, determines the strength and toughness (i.e., mode of fracture) of the particular composite system.

During the past year of this program, emphasis was placed on the determination of microstructural changes that may have occurred within the Nicalon fibers, fiber coatings, and BMAS matrix, as a function of elevated temperature tensile creep and fatigue testing, as well as long-time thermal aging. In addition, the effect on the BMAS matrix composite properties and microstructure when the SiC/BN fiber coating is changed to either a Si_3N_4/BN coating or a BN coating alone was evaluated. In addition, a slight change was made in the composition of the BMAS matrix in order to optimize the thermal stability of the crystalline barium osumilite matrix under elevated temperature, long time, aging conditions. With the collaboration of Brown University, SEM and TEM analyses of the composites after being subjected to the various stress and temperature conditions were conducted. From these studies, damage modes and microstructural and chemical changes that occurred as a result of these tests were determined.

II. TECHNICAL DISCUSSION

The research under this program during the past year was divided into four main tasks: I. Coated Fiber Characterization; II. Glass-Ceramic Matrix/Coated Fiber Composite Fabrication; III. Composite Mechanical and Thermal Testing; and IV. Microstructural and Microchemical Analysis of Composites. These tasks are set up to run concurrently and are iterative with one another.

During the past year, studies under this program have dealt with the composite system consisting of a barium-magnesium aluminosilicate (BMAS) matrix that contained SiC over BN, Si_3N_4 over BN, and BN coated Nicalon fibers. The fiber coatings were applied by a chemical vapor deposition process at 3M Co., St. Paul, MN.

A. Coated Nicalon Fiber Characterization

During the past year, two different lots of coated Nicalon fibers from 3M were utilized for BMAS matrix composite fabrication under this program, one with a Si_3N_4 over BN coating (#97037:38), and one with a BN coating only (#95223:73). In addition, previously fabricated composites with a SiC/BN coating (#97037:15) continued to be studied, especially in elevated temperature creep and fatigue. The coated fibers were subjected to tensile testing and scanning Auger microprobe (SAM) depth profiling in order to determine coating thickness and chemistry.

Figure 1 shows the SAM depth profile of the Si_3N_4 over BN coated Nicalon fiber (#92037:38), which was found to have a rather thin (~50-75nm) coating of silicon nitride over an ~300nm thick BN layer. There appeared to be a small amount (<3%) of boron and oxygen in the silicon nitride layer. The average tensile strength measured for this lot of coated fibers of 306 ksi (2110 MPa) corresponds to a Nicalon fiber strength of over 330 ksi (2280 MPa), assuming the coating does not contribute to the strength.

The SAM depth profile obtained for the BN coated Nicalon fiber lot #95223:73, indicated that the BN layer was quite stoichiometric, with ~15% C and very low oxygen (~3%), and was ~200-300nm thick, which is thinner than requested from 3M. The carbon is deliberately added to the BN precursor by 3M, who have found that the carbon addition minimizes reactivity during deposition between the BN and the Nicalon fibers. The measured tensile strength (15 fibers, 2.5 cm gage length) of 296±55 ksi (2039±378

MPa) indicates a modest decrease in UTS of the fiber, given the BN coating thickness of ~200-300nm.

Figure 2 shows the SAM depth profile obtained previously for the SiC/BN coated Nicalon fiber lot #97037:15, which was CVD coated at 3M under conditions that were designed to deposit ~400nm of BN, followed by only 100nm of SiC. While the surface of the SiC layer is somewhat carbon rich, most of the ~75-100nm thick layer appears to be relatively stoichiometric with no detected oxygen. The BN layer is quite stoichiometric, with ~15% C and very low oxygen, and is ~400nm thick. The measured tensile strength (15 fibers, 2.5 cm gage length) of this lot of coated fibers was 322±82 ksi (2220±565 MPa).

B. BMAS Glass-Ceramic Matrix/Coated Fiber Composite Fabrication

Three sixteen layer, 0/90° ply layup BMAS glass-ceramic matrix composites of dimensions 4"x4" (10 x 10 cm) were fabricated, one each from lots #97037:38 (BMAS/Si_3N_4/BN/Nicalon fiber composite #363-92), #95223:73 (BMAS/BN/Nicalon fiber composite #253-93), and #97037 (modified BMAS/SiC/BN/Nicalon fiber composite #129-94) coated Nicalon fibers. In addition, the twelve layer, 0/90° ply layup BMAS matrix composite (#95-93) of dimensions 6"x9" (15.2 x 22.8 cm) that was fabricated from the lot #97037:15 SiC/BN coated Nicalon fibers during the previous year, continued to be utilized for elevated temperature tensile creep and fatigue testing. The composite panels were hot-pressed under the usual conditions of a maximum temperature of 1420°-1440°C, 6.9 MPa pressure, for times of 5 to 10 min, in an Argon atmosphere.

After hot-pressing, the three 10 x 10 cm composite panels were then machined into both flexural test samples of dimensions ~0.2 x 0.1 x 4.0" (0.51 x 0.25 x 10 cm), and tensile samples of dimensions ~0.5 x 0.1 x 4.0" (1.25 x 0.25 x 10 cm) with a dogbone gage section of 0.2 " (0.51 cm) in width and 1.0" (2.54 cm) in length. The larger 15.2 x 22.8 cm composite panel was machined into both flexural and tensile samples as well, with the tensile samples being 6" (15.2 cm) in length compared to the previously utilized 4" (10 cm) long samples. The tensile samples had a gauge section that was 2" (5.1 cm) long by 5/16" (8 mm) wide for the short time tensile and tensile creep tests, and 3" (7.6 cm) long by 3/16" (5 mm) wide for the tensile fatigue tests. Those composites to be tested in the "ceramed" or matrix crystallized condition were heat-treated in argon to 1200°C for 24 hrs in order to crystallize the BMAS matrix to the barium osumilite phase.

C. Composite Thermomechanical Testing and Microstructural Characterization

During the past year, this task consisted of completing the flexural creep testing and analysis, as well as finishing the high temperature tensile creep and fatigue testing on BMAS matrix/SiC over BN coated Nicalon fiber composites that was initiated in 1993[42]. In addition, new studies were initiated on the effect of long-time thermal aging on BMAS/SiC/BN coated Nicalon fiber composites, and the mechanical and thermal testing of BN and Si_3N_4 over BN coated Nicalon fiber/BMAS matrix composites, as well as a brief study into the effect of BMAS matrix compositional changes on the high temperature stability of the barium osumilite crystalline matrix phase.

1. Flexural Creep Behavior of SiC/BN Dual Coated Nicalon Fiber Reinforced Glass-Ceramic Matrix Composites

This work was compiled into a manuscript and submitted for publication to the Journal of the American Ceramic Society in June, 1994[49], and is included in this report as Appendix I. This study reports the flexural creep behavior of the SiC/BN coated Nicalon fiber/BMAS matrix composite system, and the associated changes in microstructure as a function of creep testing. Flexural creep, creep-rupture, and creep-strain recovery experiments were conducted on the composite and the BMAS matrix material itself from 1000°-1200°C. The steady state creep rates were extremely low ($\sim 10^{-9} s^{-1}$) and were relatively insensitive to stress and temperature below ~1130°C. The creep-rupture strength of the composite at 1100°C was about 75-80% of the fast fracture strength,although creep-rupture occurred rapidly above 1160°C. Creep strain recovery experiments showed recovery of up to 90% under prolonged unloading. Experimental creep results from the composite and the matrix were compared, and microstructural observations by TEM were employed to assess the effectiveness of the fiber coatings and to determine the mechanism(s) of creep deformation and damage. Additional details on this study are found in Appendix I.

2. High Temperature Tensile Properties of Coated SiC Fiber Reinforced Glass-Ceramic Matrix Composites in Aerobic Environments

This work was also compiled into a manuscript and submitted for publication to the Journal of the American Ceramic Society in October, 1994[50], and is included in this report as Appendix II. The tensile properties of the BMAS matrix/SiC over BN coated Nicalon fiber composite system were investigated by conducting fracture, creep, and

fatigue experiments at temperatures from RT to 1200°C in air. The composite material exhibited excellent short time tensile properties to 1200°C. From the monotonic tensile fracture testing, no degradation in ultimate tensile strength was observed up to a test temperature of 1200°C in air. Under long-term creep conditions at 1100°C, steady state creep was established after a period of transient creep, with very low creep rates in the range of $10^{-9}s^{-1}$, which was similar to that found from flexural creep testing. Tensile fatigue experiments were conducted during which the maximum applied stress was above the proportional limit stress of the composite. From the results of these tests, it was determined that the composite could withstand 10^5 cycles at temperatures up to 1200°C.

Microscopic failure mechanisms of these composites were investigated by TEM and microstructural observations were correlated to the mechanical behavior. It was found that the SiC/BN dual fiber coatings were stable at the high test temperatures and effectively inhibited diffusion and reaction at the fiber/matrix interface, with the BN layer providing the weak interfacial bonding necessary to achieve damage tolerant fracture behavior. Limited oxidation of the SiC fibers occurred during prolonged exposure at high temperatures when oxygen diffused into the composite along microcracks in the matrix and/or in the BN interfacial layer. Under certain thermomechanical conditions, it was found that spinodal decomposition occurred in the intergranular glassy phase of the matrix, resulting in formation of crystalline hexacelsian and a silica glass. Additional details of this study are found in Appendix II.

3. Thermomechanical Stability of SiC/BN, Si_3N_4/BN, and BN Nicalon Fiber Coatings in BMAS Matrix Composites

a) SiC/BN Fiber Coatings

1) Thermal and Mechanical Testing

As was discussed in the previous Annual Report[42], short time flexural testing was conducted on BMAS matrix/SiC/BN Nicalon fiber composite #95-93 at RT, 1100°, 1200°, and 1300°C, as well as tensile testing at RT, 1100°, and 1200°C. All testing was performed in an ambient air environment. The results of these tests (Table I) indicated that the flexural and tensile strength of the SiC/BN coated Nicalon fiber composite #95-93 was very good from RT to 1200°C in air, only falling at 1300°C where the residual glass phase in the matrix becomes soft. The tensile properties of this composite are discussed in Appendix II.

During the past year, RT flexural testing was conducted on samples of this composite after heat-treatment at 1100°C for 266 hrs in air, argon, and a very high purity (HP) argon environment. The time of 266 hrs at 1100°C was chosen to match the tensile creep testing done last year on this composite. The results of the RT flexural tests conducted on these heat-treated composite samples are also shown in Table I. The samples heat-treated in air and argon were placed in an alumina tube furnace, with either gently flowing air or argon being passed through the tube. The sample heat-treated in HP argon was placed in a moly mesh furnace with extremely low oxygen partial pressure ($<10^{-12}$).

From the results shown in Table I, it can be seen that after heat-treatment in air for 266 hrs at 1100°C, the flexural strength and strain-to-failure decreased ~30% and 32% respectively. Similar heat-treatment in argon in the alumina tube furnace, also decreased the flexural strength and strain-to-failure significantly. In contrast, heat-treatment in pure argon resulted in a slight increase in both strength and strain-to-failure. The fracture surfaces of all of the RT flexural tested samples were examined in the SEM, and were found to be quite fibrous in nature. However, the near-surface regions of the samples heat-treated in air and in argon in the alumina tube furnace were found to be quite different than either an as-ceramed sample or the sample heat-treated in pure Ar. As seen in Fig. 3, the air heat-treated sample exhibits a considerable amount of debris adhering to the fiber surfaces, and evidence of porosity in the matrix regions near the composite surface. This was also true, but to a somewhat lesser extent, for the sample heat-treated in argon in the alumina tube furnace. In contrast, the sample heat-treated in pure argon appeared very similar to that of an as-ceramed sample, with no evidence of matrix porosity and the usual amount of fiber coating debris.

2) Microstructural Analysis

Samples of the flexural test pieces of composite #95-93 that were heat-treated in air and pure argon at 1100°C were cross-sectioned and polished for microstructural examination. As shown for polished edge sections that were exposed to the heat-treat environment in Figs. 4 and 5, no change in the microstructure was apparent for the sample heat-treated in pure argon (Fig. 4), while the sample heat-treated in air (Fig. 5) showed evidence of fiber and matrix reactions within ~5 fiber diameters of the sample surface. Figure 6 shows a TEM replica of a region of the air heat-treated composite near the composite surface. From this figure it can be seen that the BN layer appears to have been separated from the fibers by a reaction product, with the surface of the fibers being partially dissolved into the BMAS matrix. The microstructure of the matrix has also changed from the usual barium osumilite elongated grain structure into a two phase structure that appears to be a mixture of a crystalline phase and a glassy phase.

X-ray diffraction analyses were conducted on powdered composite samples before and after the 1100° C heat-treatments, as well as on the surface of the composites. Figure 7 shows the diffraction patterns for powdered samples of composite #95-93 as-ceramed and after the 1100°C, 266 hr heat-treatment in air. Essentially no change in crystalline structure was detected. This was also true for the other heat-treated samples, except that the amount of hexacelsian phase increased slightly for the sample heat-treated in argon in the alumina tube furnace, as was also noted previously[42] for the sample tensile stress-rupture tested for 266 hrs. No significant changes were noted in the interior of the composites after heat-treatment from TEM thin foil analyses, including the SiC/BN fiber coatings, except for the aforementioned increase in hexacelsian and a slight tendency to form nano-scale sublayers at the BN/fiber interface for the air heat-treated sample, as shown in Fig. 8. The hexacelsian formation is due to a spinodal decomposition of glassy grain boundary phase, and is discussed in more detail in Appendix II. The sublayers were carbon rich (fiber side) and silica rich (BN side) respectively, and were formed by the carbon-condensed solid state oxidation of the Nicalon fiber, as first described by Cooper and Chyung[51]. Other than the aforementioned changes, TEM analysis of the interiors of the heat-treated composites indicated that neither the microstructure nor the composition of the Nicalon fibers, or the SiC and BN coatings had changed significantly during the high temperature heat-treatments.

While no significant changes in the microstructure after 1100°C heat-treatment was found in the *interior* of the composites, X-ray diffraction analyses done on the composite surfaces showed significant differences as a function of heat-treat environment. Figure 9 shows the X-ray analyses of the surface of composite #95-93 after (A) ceraming in argon at 1200°C for 24 hrs, and (B) the 1100°C, 266 hr, HP argon heat-treatment. The as-ceramed composite exhibits highly oriented surface crystals of barium osumilite, with the 002 peak at 7.20Å being very strong compared to the other peaks. The major peaks are all barium osumilite, with only very minor peaks for hexacelsian and mullite. The broad peak at 3.37Å is from the residual graphite mold release on the composite surface, indicating that the ceraming atmosphere contains essentially no oxygen. After the 1100°C, 266 hr heat-treatment in the moly mesh furnace in argon, very little change is seen in the X-ray pattern, except that the amount of surface hexacelsian has increased. The broad graphite peak is still in evidence, indicating that the oxygen partial pressure was very low.

In contrast to the above composite samples, the X-ray diffraction analyses for the composite surfaces that were subjected to the 1100°C, 266 hr, heat-treatment in either air or argon in the alumina tube furnace were very different. As shown in Fig. 10A, the

heat-treatment in argon in the alumina tube furnace removed the residual graphite on the composite surface, with the amount of hexacelsian increasing dramatically. A relatively minor amount of celsian and silica (cristobalite) was also detected. It is obvious from the surface graphite removal that the argon heat-treatment in the alumina tube was contaminated by small amounts of oxygen, which evidently catalyzed hexacelsian formation. In air (Fig. 10B), the surface of the composite was transformed totally into celsian, with minor amounts of cristobalite. No barium osumilite or hexacelsian was evident.

In addition to the matrix changes in the surface region of the composite, reactions were also noted in the fiber/matrix interfacial region and the fiber itself near the composite surface after the 1100°C, 266 hr, air heat-treatment. This was visually seen in the light micrograph and TEM replica shown in Figs. 5 and 6. TEM thin foil analysis was also performed on a region of 0° plies, approximately 2-3 fiber diameters from the composite surface. As shown in Fig. 11, a reaction occurred on the fiber side of the interface, resulting in a two phase region that appears light and dark in the TEM image. Compositional analysis by EDS indicated that the light phase contained only silicon and oxygen. PEELS spectra collected from the light colored reacted phase and the BN coating layer are presented in Fig. 12. As was also found from EDS, the reacted phase contained only silicon and oxygen, while the BN layer contained boron, nitrogen, and a small amount of carbon. The carbon was present in the original as-deposited BN layer.

From the results of the composite sample heat-treated in air at 1100°C, it appears that the Nicalon fibers in the top ply of the composite undergo oxidation from oxygen diffusing from the environment through the BMAS matrix and SiC/BN layer. The reaction appears to create a silica glass plus a gaseous specie by:

$$2SiC_{(s)} + 3O_{2(g)} \Rightarrow 2SiO_{2(s)} + 2CO_{(g)} \qquad (1)$$

During this oxidation, the matrix phase transforms from barium osumilite to a crystalline celsian phase plus a glassy phase. The cause of this transformation and the apparent loss of magnesium from both the crystalline and glassy phases is not known.

It also appears that the Nicalon fibers (and the SiC overcoat) tend to oxidize more readily than the BN layer. This was also found for the #95-93 composite sample subjected to tensile fatigue testing at 1100°C, as discussed in last years Annual Report[42] (see Fig. 32) and in the tensile properties manuscript in Appendix II of this report (page 13 & Fig. 10). While this initially seems rather surprising, from the work of Pechentkovshaya, et al[52], the oxidation of hexagonal BN according to the reaction:

$$4BN_{(s)} + 5O_{2(g)} \Rightarrow 2B_2O_{3(s)} + 2NO_{2(g)} + N_{2(g)} \qquad (2)$$

at 1100°C, has a free energy of -222 KJ, compared to -557 KJ for the oxidation of SiC as given by reaction (1). Thus, SiC is more likely to react with oxygen than BN under similar conditions. While some BN may have oxidized as well, plugging of the interface with silica glass may have decreased oxygen ingress. For those fibers located very close to the composite surface that are obviously reacted quite severely, the SiC and BN interface coatings are also totally oxidized.

The degradation in composite flexural strength after 1100°C heat-treatment in both air and impure argon undoubtedly is caused by a variety of factors, including the oxidation of near-surface fibers, the formation of hexacelsian in the matrix, and the formation of porosity in the near-surface matrix due to gaseous reaction species such as CO. In the samples heat-treated in air, where degradation of near-surface fibers and the formation of matrix porosity was obvious, a reduction in flexural strength, which is particularly sensitive to surface effects, could be expected. This could also have been the case for the sample heat-treated in argon in the alumina tube furnace, where some surface oxidation did occur due either to a slight leak in the furnace closures or oxygen in the atmosphere from the alumina tube itself. While the surface region of this composite sample was not microstructurally analyzed in the TEM, degradation of surface fibers due to oxidation may have occurred. The formation of hexacelsian on the surface of this composite may have also been a contributing factor as well, since the high thermal expansion coefficient (8 x 10^{-6}/°C) of this phase, coupled with a rapid displacive transformation at ~300°C to an orthorhombic form with an accompanying 3% volume contraction, may have introduced significant residual stresses into the composite surface that could have contributed to the degradation of RT flexural strength.

In highly oxidizing environments, it appears that the BMAS matrix composite surface region transforms to a celsian BAS phase. This transformation may be induced by the formation of excess silica through the oxidation of the SiC fibers, and by the volatilization of MgO from the composite surface, although the mechanisms responsible for this are not clear. Celsian is a highly refractory crystalline phase (MP over 1700°C), with a thermal expansion coefficient (~2.29 x 10^{-6}/°C) that is very similar to that of barium osumilite (~3 x 10^{-6}/°C). The formation of this celsian phase may actually be beneficial to the long-time composite environmental stability by limiting diffusion of oxygen to the Nicalon SiC fibers. Under a related UTRC program, a 0/±45/90° BMAS matrix composite with SiC/BN coated Nicalon fibers was subjected to tensile stress-rupture testing at 1200°C in air at a stress level of 10 ksi (69 MPa), which is slightly higher than the proportional limit stress for this fiber layup. The composite remained at

this stress level for 11,725 hrs, which is ~1.35 yrs, when it finally fractured. The fracture surface, which is shown in Fig. 13, was quite fibrous except for a region around the periphery of the 0.2" x 0.1" (0.51 x 0.25 cm) composite cross-section in the gauge. Figure 14 shows a cross-section of this composite with reacted fibers and matrix porosity quite evident within 150-200μm of the composite surface. At higher magnification, as shown in Fig. 15, it appears that the oxidation of the Nicalon fibers occurred more rapidly in the 90° plys than in the 0° plys, in that the SiC/BN coatings on the fibers in the 0° ply next to the composite surface were intact within ~150μm of the composite surface, while those in the 90° plys were visibly reacted to a depth of at least 250μm. Thus, "pipeline" diffusion that initiates at cut ends of the fibers exposed at the composite surface, with oxygen transport occurring along the fiber/coating(s)/matrix interface, is evidently faster than "transverse" diffusion of oxygen through the matrix. TEM replica analysis of the composite (0° ply) near the surface and away from the surface, as shown in Fig. 16, reaffirms that, while the fibers and matrix near the surface are severely reacted, the microstructure of the bulk of the composite, including the SiC/BN fiber coatings, is unaffected by this severe environmental and mechanical exposure.

By comparing Fig. 14 to that shown in Fig. 5, it is apparent that the degradation of the BMAS matrix/SiC/BN coated Nicalon fiber composite due to oxidation of the near-surface regions is more severe (~150-250μm deep) after 11,750 hrs at 1200°C than after 266 hrs at 1100°C (~50μm deep), as should be expected. However, the kinetics of this diffusional oxidation reaction appear to be parabolic, which indicates that this type of composite should be able to withstand long-time environmental exposure in oxidizing atmospheres at elevated temperatures without major loss in load bearing capability. As an example of this, a BMAS matrix SiC/BN coated Nicalon fiber composite with 0/90° ply orientation is undergoing tensile stress-rupture testing at 1100°C in air under a stress of 20 ksi (138 MPa), which is well above the proportional limit stress. This sample currently has withstood these test conditions for over 14,000 hrs (1.6 yrs) without failure.

b) Si_3N_4/BN Fiber Coatings

The substitution of Si_3N_4 for the SiC layer in the BMAS matrix composites was attempted for two reasons. One relates to the lower thermal expansion coefficient of the silicon nitride compared to SiC, which may influence the bonding of the silicon nitride to the BN coated Nicalon fiber. It has been found[53,54] that turbostratic BN exhibits a significantly lower thermal expansion coefficient (~2 x 10^{-6}/°C) than SiC (~5 x 10^{-6}/°C). Debonding of the SiC layer from the BN during composite fabrication has been a problem in this composite system[42]. Another reason for utilizing silicon nitride as the diffusion barrier overcoat rather than SiC relates to the dielectric constant of silicon

nitride being much lower than that of SiC, which may be important for certain composite applications.

1) Thermal and Mechanical Testing

As discussed previously, the silicon nitride over BN coated Nicalon fiber from 3M (lot #97037:38, Fig. 1) was utilized to fabricate a 0/90° BMAS matrix composite (#363-92). This composite was flexural tested in 3-pt bending at RT, 1100°, and 1200°C. It was also scheduled for tensile testing at RT and elevated temperatures, but due to the observed microstructural changes that occurred in the composite during fabrication, as will be discussed in the next section, these tensile tests were put on hold.

The flexural properties of composite #363-92 are presented in Table II. Comparing these properties to that shown in Table I for the SiC/BN coated Nicalon fiber composite #95-93, it can be seen that the two composites exhibited mechanical behavior as a function of temperature that could be considered identical, within the scatter band usually encountered for these types of CMC's.

2) Microstructural Analysis

Microstructural analysis on composite #363-92 consisted of a scanning Auger depth profile of a fiber surface and matrix trough on a fracture surface that was created by splitting the composite in the plane of the fiber plys, and TEM thin foil analysis of the fiber/coating(s)/matrix interfacial region.

Figure 17 shows the scanning Auger (SAM) depth profile of the fiber surface and matrix trough of composite #363-92, combined into a single profile of the chemistry across the composite interface. It is apparent from this figure that the silicon nitride layer on the BN has reacted with and dissolved into the BMAS matrix during composite fabrication. There is also an indication that a subtle carbon (plus silica) layer sublayer may have formed at the Nicalon/BN interface. TEM thin foil analysis of the interfacial region of this composite, as shown in Fig. 18, substantiates the SAM observation that no silicon nitride overlayer is now present between the BN layer and the BMAS matrix. The BN layer has been coarsened in the region next to the matrix, as was found previously[42] for SiC/BN coated Nicalon fiber composites where the SiC layer had become detached during composite fabrication. While not definitive, the higher magnification micrograph (Fig. 17B) appears to show an indication of a very thin carbon/silica dual sublayer formation, which is caused by the carbon condensed oxidation of the Nicalon fibers[41,42,51].

It thus appears that silicon nitride coatings over BN are not suitable as diffusion barriers in glass-ceramic matrix composites, due to dissolution into the matrix during composite fabrication. Reaction of silicon nitride whiskers with LAS glass-ceramic matrices has been found from previous work on an AFOSR program in 1989[55], although total dissolution into the matrix was not observed. It is possible that a thicker and/or a more crystalline silicon nitride coating might be more stable, but this aspect was not pursued under this program.

c) BN Fiber Coatings

It was decided to investigate the effect of eliminating totally the diffusion barrier overcoat concept and fabricate composites with only a BN fiber coating. Originally, SiC diffusion barrier overcoating was found to be required in LAS matrix composites[1] due to boron diffusion from the BN into the matrix during composite fabrication leading to incomplete crystallization of the LAS matrix to β-spodumene during subsequent ceraming. With the BMAS crystalline barium osumilite system, this may not be as great a problem, since it has been observed that when debonding of the SiC layer from the BN during composite fabrication has occurred, the BMAS matrix next to the debonded region appears to be quite crystalline after the ceraming heat-treatment. In addition, it was noticed that in the Si_3N_4 over BN coated Nicalon fiber composite system just discussed, the BMAS matrix next to the BN layer (where the Si_3N_4 layer had dissolved in the matrix) was quite crystalline after ceraming. Eliminating the SiC CVD overcoating step would also lead to a reduction in cost and complexity of the final composite.

1) Thermal and Mechanical Testing

As discussed previously, the BN coated Nicalon fiber from 3M (lot #95223:73) was utilized to fabricate a 0/90° BMAS matrix composite (#253-93). This composite was flexural tested in 3-pt bending at RT, 1100°, and 1200°C, as well as RT flexural tested after long time (500 hrs) aging at 550°, 1000°, and 1100°C in either air or flowing oxygen. In addition, the elevated temperature (1100° and 1200°C) tensile properties of the composite were determined.

The flexural and tensile properties of composite #253-93 are presented in Table III. Comparing these properties to that shown in Table I for the SiC/BN coated Nicalon fiber composite #95-93, it can be seen that the flexural and tensile strengths measured from RT to 1100°C for the BN coated Nicalon fiber composite are as good or better than those measured for the SiC/BN coated Nicalon fiber composite. At 1200°C, the flexural and tensile strength and the tensile modulus drops somewhat for the BN coated Nicalon

fiber composite, but are still quite respectable. Essentially no decrease in RT flexural properties after 1000°C heat-treatment in oxygen are noted for composite #253-93, and only an 18% drop in flexural strength after 1100°C air exposure occurred. A rather significant drop in flexural strength was noted after the 550°C oxygen exposure, however. Previous SiC/BN coated Nicalon fiber BMAS matrix composites (#119-91) oxidized at 550°C did not suffer any degradation in flexural strength[41]. This environmental exposure condition is significant, since it has been found from previous work[41] on uncoated Nicalon fiber/BMAS matrix composites that formed an *in situ* carbon interfacial layer during composite fabrication, that significant strength degradation and loss of composite toughness can occur after exposure to oxygen at temperatures in the range of 550°C due to oxidation of the carbon interfacial layer.

2) Microstructural Analysis

Microstructural analysis on composite #253-93 consisted of TEM replica analysis of polished composite cross-sections, both as-pressed and after ceraming, as well as after thermal aging at 1100°C in air, TEM thin foil analysis in the ceramed, 550°, and 1100°C oxidized conditions, X-ray diffraction analysis of both powdered samples and surface regions for as-ceramed and 1100°C heat-treated composites, and scanning Auger depth profile analysis of the ceramed composite interfacial region.

TEM replica analysis of composite #253-93 in the as-pressed condition is presented in Figs. 19 and 20. From these figures, it can be seen that the BN coating is quite uniform in thickness (~200nm) and very well adhered to the Nicalon fibers. As stated previously, the BN coating as applied by 3M was somewhat thinner than desired. The BMAS matrix is primarily glassy in the as-pressed condition, as expected, with the usual amount of small mullite crystals. After ceraming at 1200°C for 24 hrs, as shown in Fig. 21, the BMAS matrix exhibits the usual lathe-like barium osumilite crystal structure. It is somewhat difficult from the TEM replica to determine the amount of glassy phase left in the matrix and if it has increased due to boron diffusion from the BN fiber coating, as compared to the SiC/BN coated fiber composites, but it doesn't appear that there is a significant amount of residual glassy phase. Subsequent X-ray diffraction analysis and TEM thin foil observations also indicate very little residual glassy phase in the matrix, as will be discussed later.

The scanning Auger depth profile analysis across the fiber/BN/matrix interfacial region for a ceramed sample of composite #253-93 is presented in Fig. 22. From this figure, it can be seen that a thin carbon rich layer has developed at the BN/Nicalon fiber interface, at which location the fiber/matrix interface separated, a significant amount of silicon and oxygen diffusion has occurred into the BN layer from the matrix, and diffusion

of matrix and fiber coating elements such as B, Al, Ba, and Mg, has taken place into the Nicalon fibers to a depth of ~500nm.

TEM thin foil analysis of composite #253-93, as shown in Fig. 23, indicated that rather thick (~25-40nm) sublayers (one dark and one light colored) have formed at the BN/Nicalon fiber interface. These sublayers, while seen previously in SiC/BN coated Nicalon fiber composites, especially when the SiC layer has detached from the BN *and* the BN is relatively thin[42], or after long-time, high temperature heat-treatment (see Fig. 8), are much thicker than usual. The usual coarsening of the BN next to the BMAS matrix has also occurred to a depth ~half way through the 250nm thick BN layer. The chemistry of the dual sublayers was determined by PEELS analysis, focusing the probe on the individual layers. As shown in Fig. 24, the PEELS spectra was obtained from the Nicalon fiber (point 1), the light colored sublayer (point 2), the dark colored sublayer (point 3), and the uncoarsened BN layer (point 4), and indicated that, as expected, the light sublayer was carbon rich while the dark sublayer was primarily silica.

Carbon plus silica sublayer formation between Nicalon fibers and BN coatings have been found previously for CVI SiC matrix composites[27,28]. From these studies, it was determined that the sublayers, which were on the order of 40-80nm in thickness, were formed as a result of decomposition of the Nicalon fibers during the hundreds of hours utilized for the CVI SiC infiltration step at ~1000°C. From experiments done on uncoated Nicalon fibers in vacuum at 1000°C for hundreds of hours, thus simulating the CVI infiltration process, the same authors found identical carbon plus silica layer formation on the surface of the fibers. Thus, oxidation of the fibers from an outside source, as suggested by Cooper, et al[51], to form the sublayers may not be necessary in all cases. Interestingly, in the CVI SiC composites, the interfacial crack deflection occurred between the BN and silica layers, not in the carbon sublayer as found for the BMAS matrix composite #253-93. Recent work[56] in CVI SiC matrix/Nicalon fiber composites, where the BN fiber coating was varied in thickness from 0.15 to 2.7μm, found that a BN layer thickness of ~0.5μm was optimal for obtaining maximum composite mechanical properties, with thin BN coatings exhibiting discontinuities in the C/SiO_2 double layer that reportedly contributed to low tensile rupture and impact properties, and thick BN coatings resulting in low elastic modulus due to excessive amounts of BN (27%) in the matrix of the composite.

As mentioned previously, long-time (500 hrs) heat-treatments at temperatures from 550°C to 1100°C in oxidizing environments were conducted on composite #253-93. Heat-treatment for 500 hrs at 1000°C in flowing oxygen did not decrease the flexural strength of the composite, while heat-treatments at 1100°C in air and 550°C in

oxygen did lead to 18% and 37% strength reductions, respectively. Optical and TEM replica analysis of a composite cross-section near the surface, as shown in Figs. 25 and 26, indicated that after the 1100°C air heat-treatment, oxidation of the Nicalon fibers near the composite surface, coupled with matrix compositional changes and void formation, undoubtedly caused the reduction in flexural strength, as was also seen for the SiC/BN coated Nicalon fiber composite #95-93 (Fig. 5). Interestingly, although the time at 1100°C was 500 hrs, compared to 266 hrs for composite #95-93, the extent of visible reaction with the Nicalon fibers and BN coatings was slightly *less* for the BN coated Nicalon fiber composite (Figs. 25 and 26), than for the SiC/BN coated Nicalon fiber composite (Fig. 5), as was the corresponding loss in flexural strength. For composite #253-93, as shown in Fig. 26, the visibly reacted fibers extended to a depth from the surface of only ~3 fiber diameters, compared to ~5 fiber diameters for the SiC/BN coated Nicalon fiber composite #95-93.

X-ray diffraction analysis of composite #253-93 in the ceramed condition, showed that the crystalline content of the BMAS matrix was essentially identical to that presented previously for composite #95-93, i.e., primarily barium osumilite plus very minor mullite and hexacelsian, with highly oriented barium osumilite on the composite surface (see Figs. 7A and 9A). After the 1100°C, 500 hr, air heat-treatment, no change in the X-ray diffraction pattern was noted for the powdered composite compared to the as-ceramed, however the surface of the composite changed to almost totally celsian, with minor barium osumilite and silica (cristobalite) peaks, as shown in Figs. 27A and 27B, respectively. This change in the crystalline structure of the surface of BMAS matrix composites on heat-treatment in oxidizing environments at elevated temperatures from barium osumilite to celsian has been discussed previously.

TEM thin foil analysis was conducted on composite #253-93 after the 1100°C and 550°C oxidizing heat-treatments. As shown in Fig. 28, after the 1100°C air heat-treatment for fibers that were oriented in the 90° direction, i.e., where pipeline diffusion down the fiber/matrix interface from an exposed composite edge is likely, significant changes were seen in the interfacial structure, when compared to the as-ceramed composite shown in Fig. 23. For the 1100°C heat-treated composite, in most cases the silica sublayer was noticeably absent, while the carbon rich sublayer remained. In contrast, after the 550°C exposure, as shown in Fig. 29, the carbon layer was absent and a glassy layer was now present between the BN layer and the Nicalon fiber. In both heat-treated samples, the BN layer was coarsened throughout its thickness, in contrast to that shown in Fig. 23 where the coarsening of the BN layer progressed less than halfway though it from the matrix side.

From the TEM analyses, it appears that for the 1100°C heat-treatment, the carbon sublayer was stable and protected from oxidation by the glazing that occurs on the composite surface, leading to "plugging" of the interface by glassy phase. However, the silica sublayer apparently diffused into the BN layer during the 1100°C, 500 hr exposure, leading to the coarsening of the BN layer. It has been found previously that diffusion of elements such as Si and O into the initially turbostratic BN layer causes coarsening of the BN into a structure consisting of disarrayed hexagonal BN "platelets" within an amorphous, or glassy phase. While the coarsened BN is not as susceptible to crack blunting and diversion as turbostratic BN, the presence of the carbon sublayer at the Nicalon/BN interface still contributes to the tough behavior and relatively high strength seen for the 1100°C heat-treated composite.

In contrast to 1100°C heat-treatment, the 550°C heat-treatment leads to degradation of the carbon sublayer, apparently by "pipeline" oxidation down the fiber/matrix interface from cut ends of fibers exposed on the composite surface. Coarsening of the BN layers in the 550°C heat-treated composite throughout their thickness is somewhat surprising, although the example shown in Fig. 29 has a rather thin BN layer (~175nm) that may have been coarsened as a result of matrix element diffusion during composite fabrication, and not as a result of the 550°C heat-treatment. In any case, the low fracture strength of this composite is undoubtedly due to the combination of a coarsened BN layer coupled with the absence of a carbon sublayer, with the result being no easy path for crack deflection at the fiber/matrix interface.

d) Fiber Indent Testing

Samples of composites #95-93, #363-92, and #253-93, with SiC/BN, Si_3N_4/BN, and BN coated Nicalon fibers, respectively, were sent to Dr. Paul Jero at Wright-Patterson AFB (AFML) for fiber indent testing in order to determine the debond energies and frictional sliding stresses for the three different interfaces. Dr. Jero utilized a push-in type of test on polished composite sections ~3 mm thick, with the fibers being pushed oriented in the 0° direction for the 0/90° composites. The loading probe was a truncated diamond cone with a 10 micron flat and 55° included angle. Tests were run at 12.7 microns/minute crosshead speed, with fiber displacement being calculated from the time and the known crosshead speed. Between 15 and 18 fibers were pushed from each sample.

The data was analyzed utilizing both the Kerans and Parthasarathy[57] and the Marshall and Oliver[58] approaches. The Marshall and Oliver (M&O) analysis yields a τ value that corresponds to a frictional sliding stress (in MPa), and a bonding component

(G) that can be referred to as the debond fracture energy, crack extension force, or strain energy release rate. It is related to the toughness, or stress intensity K of the interface. In this report it will be referred to as simply the debond energy (in J/m^2), and gives a measure of the bonding at the fiber/coating/matrix interface.

The calculated values for τ and G by the Marshal and Oliver approach for the three composites in the ceramed condition are listed in Table IV, along with data for the RT flexural strength, proportional limit stress, and strain-to-failure of the composites. A significant amount of scatter in the data was found, especially for composite #363-92. In addition, the preparation of polished sections of the composites was found to be very difficult for composite #95-93, with the possibility that damage to the interface may have occurred during indent sample preparation, accounting for the low values of τ and G for this composite. In general, the composite with the highest proportional limit stress and lowest strain-to-failure (#363-92) exhibited the highest values of τ and G, but other than that, no correlation can be made between the interfacial debond and frictional sliding data and the resultant composite properties, *or* to the interfacial chemistry and structure of each composite. Intuitively, one might think that the formation of a carbon sublayer in composite #253-93 would result in a lower debond energy and frictional sliding stress than the turbostratic BN interface in composite #95-93, but that was not the case. As mentioned previously, damage during sample preparation may have lead to the low values for τ and G in composite #95-93. Additional work is needed in the test procedures and sample preparation for these types of tests in order to obtain meaningful data.

4. Modified BMAS Matrix/SiC/BN Coated Nicalon Fiber Composites

Towards the end of the current program, a brief investigation was carried out into modifying the BMAS matrix composition such that composites could be fabricated with ceramed matrices that did not contain the undesirable hexacelsian phase. This phase has been found to form in minor amounts in previous BMAS matrix composites, as was shown in the X-ray diffraction data for composite #95-93 in Fig. 7. By adjusting the MgO content in the BMAS composition, a composite (#129-94) was fabricated that did not contain hexacelsian on subsequent crystallization of the matrix, only the barium osumilite phase and a somewhat increased minor amount of mullite, as shown in Fig. 30A. After an 1100°C, 266 hr heat-treatment in air, however, a very minor amount of hexacelsian was noted, as shown in Fig. 30B.

The mechanical properties of this composite are listed in Table V, and indicate that while the RT flexural properties are somewhat lower than that previously recorded for composite #95-93, the elevated temperature flexural and tensile properties are as

high, or higher than composite #95-93. Essentially no reduction in RT flexural strength was noted for the composite heat-treated in air at 1100°C for 266 hr, in contrast to the 30% drop in strength for composite #95-93, although as mentioned, the RT flexural properties were not as high initially as those for composite #95-93. No additional microstructural or chemical analyses were done on this composite due to time limitations; however, the preliminary results obtained indicate that the general area of matrix modifications to stabilize the barium osumilite phase in these types of composites warrant further investigation.

III. CONCLUSIONS AND RECOMMENDATIONS FOR FUTURE WORK

From the work conducted under this program during the past three years, it has been demonstrated that the ceramic composite system based on the reinforcement of a barium-magnesium aluminosilicate (BMAS) glass-ceramic matrix with CVD SiC over BN coated Nicalon SiC fibers exhibits the mechanical properties necessary for potential application as a high temperature, lightweight component for advanced gas turbine engine structures in Air Force aircraft. The mechanical properties of this system, including flexural strength, flexural creep, tensile strength, tensile creep and fatigue, and tensile stress-rupture at temperatures up to 1200°C in aerobic environments have been demonstrated. In particular, it has been shown that this composite system can withstand stress levels at elevated temperature for long periods of time and/or many cycles that are *higher* than the proportional limit, or matrix microcracking, stress of the composite. This indicates that the fiber/matrix interface consisting of CVD SiC over BN is performing as it should, i.e., a weakly bonded yet environmentally stable system that allows the deflection and diversion of matrix cracks such that the composite system behaves in a pseudo-ductile or "tough" manner, and when it fails does so in a graceful, non-catastrophic fracture mode.

It has also been shown that Si_3N_4 is not a good choice for a substitute for the SiC diffusion barrier overcoating, due to dissolution into the glass-ceramic matrix during composite fabrication. However, a thicker and more crystalline silicon nitride than that examined under this program could be viable and may warrant further consideration. The use of a BN layer by itself was demonstrated to result in excellent BMAS composite properties with very little effect on matrix crystallization, contrary to that found for LAS matrix composites, but without the SiC diffusion barrier overcoating, diffusion of matrix elements into the BN led to the formation of dual sublayers of carbon and silica at the BN Nicalon fiber interface, as well as coarsening of the BN. The formation of these sublayers at the BN/Nicalon interface were shown to be unstable at elevated temperatures in oxidizing environments, even as low as 550°C. However, the utilization of a thicker and possibly more crystalline BN could affect the formation of these sublayers and thus the composite environmental stability.

It is recommended that future work in glass-ceramic matrix composite systems concentrate on the development of more reliable and reproducible fiber coatings, based on the use of BN as the primary debond coating. It is imperative that consistent fiber coatings be produced from run to run, and that the chemistry and thickness of the

coatings remain consistent, not only from run to run, but within the fiber arrays in both continuously coated tows and batch coated cloth. The debonding of the SiC overcoat layer is still a concern, and should be addressed by exploring the use of functionally graded coatings such that there is no abrupt interface between the SiC and BN. This should minimize thermal expansion mismatch problems, and the associated stresses that apparently lead to the debonding of the SiC layer. In addition, the stability of the BMAS matrix system under long-time exposures in aerobic environments still requires study. While this system has shown excellent properties to temperatures approaching 1200°C for relatively short periods of time, the long-time stability of the barium osumilite crystalline phase is still a concern. Interfacial microstructural and microchemical analysis should still play a major role in future investigations, in that it is the nature of these interfaces that controls the mechanical properties and influences the thermal and environmental stability of these composites.

In addition, the utilization of new, more thermally stable fibers, such as the "High Nicalon" oxygen free fiber from Nippon Carbon Co., may enable higher temperature coatings to be applied to the fibers without fiber degradation. These coatings may be more crystalline and/or purer versions of the ones previously studied under this program, or new fiber coating concepts such as porous, layered, or fugitive interface coatings. More thermally stable fibers and fiber coatings will then allow different composite fabrication techniques to be explored, such as glass transfer molding in the case of glass-ceramic matrix composites, that require higher temperatures for composite consolidation than the usual hot-pressing routes. Glass transfer molding has the advantage of being able to form net shape composites with rather complex configuration, by injecting a molten glass into a preform containing a woven fiber array. As usual, the ability to coat the fiber arrays with reproducible, uniform coatings that will not be degraded during composite consolidation, will be the key to the success of this approach to CMC fabrication.

As was explored during the current program, the ability of the composite and especially its interfacial phases to withstand high temperature stress states, both static and cyclic, in aerobic environments and continue to function in a compliant, fracture tough manner, will determine the eventual usefulness of the system in advanced gas turbine structural components.

IV. ACKNOWLEDGEMENTS

The authors would like to thank Mr. Jim O'Kelly of 3M for coating the Nicalon fibers under study, Dr. Bruce Laube of UTRC for the SAM analyses, Mr. Gerald McCarthy of UTRC for the TEM replica analyses, Mr. Stan Kustra of UTRC and Mr. David Murphy of P&W for the composite mechanical testing, and Ms. Laura Austin of UTRC for the fabrication of the coated fiber composites, and to Dr. Alexander Pechenik of AFOSR for his sponsorship of this program.

Ms. Ellen Y. Sun, who conducted the HRTEM study at Brown University, was awarded a Ph.D in the Division of Engineering at Brown University, Providence, RI. on September 12, 1994. The title of her thesis was "Fiber-Reinforced Glass-Ceramic Matrix Composites for High-Temperature Applications: Control of Interfaces".

Papers published to date under AFOSR support include:

1. "SiC-Whisker-Reinforced Glass-Ceramic Composites: Interfaces and Properties", John J. Brennan and Steven R. Nutt, J. Am. Ceram. Soc. 75, [5] 1205-16 (1992)

2. "Interfacial Studies of Fiber Reinforced Glass-Ceramic Matrix Composites", John J. Brennan, Symposium on High Temperature Ceramic Matrix Composites, 6th European Conference on Composite Materials, Sept. 20-24, 1993, Bordeaux, France, pp 269-283, Woodhead Publishing Ltd, Abington Cambridge, England.

3. "Evolution of Interface Microstructure in a Dual-Coated Silicon Carbide Fiber-Reinforced BMAS Glass-Ceramic Composite", Ellen Y. Sun, Steven R. Nutt, and John J. Brennan, Proceedings of the American Ceramic Society '93 Annual Meeting Symposium on Advances in Ceramic Matrix Composites, pp 199-210, Oct. 1993

4. "Interfacial Microstructure and Chemistry of SiC/BN Dual Coated Nicalon Fiber Reinforced Glass-Ceramic Matrix Composites", Ellen Y. Sun, Steven R. Nutt, and John J. Brennan, J. Am. Ceram. Soc. 77, [5] 1329-39 (1994)

5. "Flexural Creep and Creep-Rupture Behavior of SiC/BN Dual Coated Nicalon Fiber Reinforced Glass-Ceramic Matrix Composites, Ellen Y. Sun, Steven R. Nutt, and John J. Brennan, Cer. Engr. & Sci. Proc., Vol. 15, No. 4, 57-64 (1994).

6. "Interfacial Diffusion and Reaction Mechanisms in Coated Fiber Reinforced Glass-Ceramic Composites", Ellen Y. Sun, Steven R. Nutt, and John J. Brennan, Cer. Engr. & Sci. Proc., Vol. 15, No. 5, 943-950 (1994).

7. "Interfaces in BN Coated Fiber Reinforced Glass-Ceramic Matrix Composites", John J. Brennan, Scripta Metallurgica et Materialia, Vol. 31, No. 8, pp. 959-964, 1994.

8. "Microscopic Failure Mechanisms in SiC Fiber-Reinforced Glass-Ceramic Composites", Ellen Y. Sun, Steven R. Nutt, and John J. Brennan, Proceedings of the 1994 TMS Spring Meeting (Symposium on Control of Interfaces in Metal and Ceramic Composites)

Papers submitted for publication to date include:

1. "Flexural Creep Behavior of SiC/BN Dual Coated Nicalon Fiber Reinforced Glass-Ceramic Matrix Composites", Ellen Y. Sun, Steven R. Nutt, and John J. Brennan, submitted to the Journal of the American Ceramic Society.

2. "High-Temperature Tensile Properties of Coated SiC Fiber Reinforced Glass-Ceramic Matrix Composites in Aerobic Environments", Ellen Y. Sun, Steven R. Nutt, and John J. Brennan, submitted to the Journal of the American Ceramic Society.

Papers Presented at Meetings to date and not submitted for publication include :

1. "Interfacial Reaction in BN Coated HPZ Fiber Reinforced Glass-Ceramic Matrix Composites", J. J. Brennan, presented at the 17th Annual Conf. on Composites, Materials, and Structures, Cocoa Beach, Fla. Jan. 10-15, 1993 (paper #140).

2. "Glass and Glass-Ceramic Matrix Composites", J. J. Brennan, presented at the 95th Annual Meeting of the Am. Cer. Soc, Cincinnati, OH, April 19-22, 1993 (Invited Paper #SII-81-93).

V. REFERENCES

1. Brennan, J. J.: Interfacial Studies of Coated Fiber Reinforced Glass-Ceramic Matrix Composites, Annual Report R91-918185-2 on AFOSR Contract F49620-88-C-0062, Sept. 30, 1991.

2. Rice, R. W.: BN Coating of Ceramic Fibers for Ceramic Fiber Composites, US Patent 4,642,271, Feb. 10, 1987.

3. Brennan, J.J.: The Evaluation of Dow Corning Fibers, UTRC Annual Report R86-917103-12 on Contract F33615-83-C-5006, Feb., 1986.

4. Singh, R.N.: Fiber-Matrix Interfacial Characteristics in a Fiber-Reinforced Ceramic-Matrix Composite, J. Am. Cer. Soc., 72 (9), 1989, 1764-1767.

5. Tredway, W.K., and Prewo, K.M.: Improved Performance in Monofilament Fiber Reinforced Glass Matrix Composites Through the Use of Fiber Coatings, Mat. Res. Soc. Symp. Proc. Vol. 170, 1990, 215-221.

6. Brennan, J.J.: Interfacial Studies of Chemical Vapor Infiltrated (CVI) Ceramic Matrix Composites, Final Report R90-917779-5 on ONR Contract N00014-87-C-0699, March 31, 1990.

7. Lowden, R.A., and Stinton, D.P.: Interface Modification in NICALON/SiC Composites, Ceram. Engr. Sci. Proc., 9 [7-8], 1988, 705-722.

8. Doughan, C.A., Lehman, R. L., and Greenhut, V.A.: Interfacial Properties of C-Coated Alumina Fiber/Glass Matrix Composites, Ceram. Engr. Sci. Proc. 10 [7-8], 1989, 912-924.

9. Jurewicz, A.J.G., Kerans, R.J., and Wright, J.: The Interfacial Strengths of Coated and Uncoated SiC Monofilaments Embedded in Borosilicate Glass, ibid, 925-937.

10. Hay, R.S., and Hermes, E.E.: Sol-Gel Coatings on Continuous Ceramic Fibers, ibid., 11 [9-10], 1990, 1526-1538.

11. Gulden, T.D., Hazlebeck, D.A., Norton, K.P., and Streckert, H.H.: Ceramic Fiber Coating by Gas-Phase and Liquid-Phase Processes, ibid., 1539-1553.

12. Bender, B.A., Jessen, T.L., and Lewis III, D.: Interfacial Microstructure and Mechanical Properties of SiC/$ZrTiO_4$ Composites Hot-Pressed in CO, ibid., [7-8], 964-973.

13. Lackey, W.J., Hanigofsky, J.A., Groves, M.T., and Heaney, J.A.: Continuous Fiber Coating System, ibid., 12 [7-8], 1991, 1048-1063.

14. Hay, R.S.: Sol-Gel Coating of Fiber Tows, ibid., 1064-1074,

15. Hazlebeck, D.A., Glatter, I.Y., and Streckert, H.H.: Novel Sol-Gel Coating Techniques for Ceramic Tows: In-Situ Curing vs Reaction Bonding, ibid., 1075-1085.

16. Mah, T., Keller, K., Parthasarathy, T.A., and Guth, J.: Fugitive Interface Coating in Oxide-Oxide Composites: A Viability Study, ibid., [9-10], 1802-1818.

17. Lee, K.N., and Jacobson, N.S.: Fiber Coating/Matrix Reactions in Silicon-Based Ceramic Matrix Composites, ibid., 13 [7-8], 1992, 29-36.

18. Carpenter, H.W., and Bohlen, J.W.: Fiber Coatings for Ceramic Matrix Composites, ibid, 238-256.

19. Bender, B.A., Jessen, T.L., Ingel, R.P., and Lewis III, D.: High-Temperature Exposure of BN-Coated Polymer-Derived SiC Fiber/$ZrTiO_4$ Composites, ibid., [9-10], 889-896.

20 Tortorelli, P.F., Nijhawan, S., Riester, L., and Lowden, R.A.: Influence of Fiber Coatings on the Oxidation of Fiber-Reinforced SiC Composites, ibid., 14 [7-8], 1993, 358-366.

21. Lowden, R.A., Schwarz, O.J., and More, K.L.: Improved Fiber Coatings for Nicalon/SiC Composites, ibid., 375-384.

22. Xiao, Y., Tan, B.J., Willis, W.S., Suib, S.L., and Galasso, F.S.: Syntehsis and Characterization of Al_2O_3-Coated SiC Yarns, ibid., 548-555.

23. Shen, L., Willis, W.S., Galasso, F.S., and Suib, S.L.: Coating of BN Interfaces on Ceramic Yarns from Boric Acid and Ammonia, ibid., 556-562.

24. Fareed, A.S., Schiroky, G.H., and Kennedy, C.R.: Development of BN/SiC Duplex Fiber Coatings for Fiber-Reinforced Alumina Matrix Composites Fabricated by Directed Metal Oxidation, ibid., [9-10], 794-801.

25. Keller, K.A., Mah, T., Parthasarathy, T.A., and Cooke, C.: Fugitive Interfacial Carbon Coatings for Oxide/Oxide Composites, ibid., 878-879.

26. Llorca, J., and Singh, R.N.: Influence of Fiber and Interfacial Properties on Fracture Behavior of Fiber-Reinforced Ceramic Composites, J. Am. Cer. Soc. 74 [11] 2882-90 (1991).

27. Naslain, R., Dugne, O., and Guette, A.: Boron Nitride Interphase in Ceramic-Matrix Composites, ibid., [10] 2482-88 (1991).

28. Dugne, O., Prouhet, S., Guette, A., Naslain, R., Fourmeaux, R., Khin, Y., Sevely, J., Rocher, J.P., and Cotteret, J.: Interface characterization by TEM, AES, and SIMS in tough SiC (ex-PCS) fibere-SiC (CVI) matrix composites with a BN interphase, J. Mat. Sci., 28 (1993) 3409-3422.

29. Vaidya, R.U., Fernando, J., Chawla, K.K., and Ferber, M.K.: Effect of fiber coating on the mechanical properties of a Nextel-480-fiber-reinforced glass matrix composite, Matls. Sci. & Engr., A150 (1992) 161-169.

30. Ha, J.S., Chawla, K.K., and Engdahl, R.E.: Effect of processing and fiber coatingon fiber-matrix interaction in mullite fiber-mullite matrix composites, ibid., A161 (1993) 303-308.

31. Morgan, P.E.D., and Marshall, D.B.: Functional interfaces for oxide/oxide composites, ibid., A162, 1-2, (1993) 15-26.

32. Chyung, K., and Dawes, S.B.: Fluormica coated Nicalon fiber reinforced glass-ceramic composites, ibid., 27-34.

33. Cain, M.G., Daniel, A.M., and Lewis, M.H.: Presynthesized interfaces for ceramic matrix composites via fibre coating, Materials Letters, 17 (1993) 246-252.

34. Brennan, J.: Interfacial Studies of Fiber Reinforced Glass-Ceramic Matrix Composites, Proceedings of High Temperature CMC's, 6th European Conf. on Composite Materials, Bordeaux, France, Sept. 20-24, 1993, Woodhead Publishing, Ltd, Abington Cambridge, England, 1993, 269-284.

35. Kerans, R.: Control of Fiber-Matrix Interface Properties in Ceramic Composites, ibid., 301-312.

36. Davis, J., and Evans, A.G.: Fiber Coatings for Sapphire-Reinforced Alumina Composites, ibid., 329-336.

37. Lowden, R.A., More, K.L., Schwarz, and Vaughn, N.L.: Improved Fiber-Matrix Interlayers for Nicalon/SiC Composites, ibid., 345-352.

38. Hay, R.: Fiber-Matrix Interfaces for Oxide Fiber-Oxide Matrix Composites, ibid., 385-392.

39. Ricca, N., Guette, A., Camus, G., and Jouin, J.M.: SiC (ex-PCS)/MAS Composites With a BN Interphase: Microstructure, Mechanical Properties and Oxidation Resistance, ibid., 455-464.

40. Brennan, J., Allen, W., McCluskey, P., and Jarmon, D.: Processing and Properties of Coated HPZ Fiber Reinforced Glass-Ceramic Matrix Composites, Final Report R93-970104-2 on AFOSR Contract F49620-88-C-0062, March 31, 1993.

41. Brennan, J., Allen, W., Nutt, S., and Sun, Y.: Interfacial Studies of Coated Fiber Reinforced Glass-Ceramic Matrix Composites, Annual Report R92-970150-1 on AFOSR Contract F49620-92-C-0001, Nov. 30, 1992.

42. Brennan, J., Nutt, S., and Sun, E.: Interfacial Studies of Coated Fiber Reinforced Glass-Ceramic Matrix Composites, Annual Report R93-970150-2 on AFOSR Contract F49620-92-C-0001, Nov. 30, 1993.

43. Sun, E., Nutt, S., and Brennan, J.: "Evolution of Interface Microstructure in a Dual-Coated Silicon Carbide Fiber-Reinforced BMAS Glass-Ceramic Composite", Ceramic Transactions 38, Advances in Ceramic Matrix Composites, ed. Bansal, N., pp 199-210 (1993).

44. Sun, E., Nutt, S., and Brennan, J.: "Interfacial Microstructure and Chemistry of SiC/BN Dual Coated Nicalon Fiber Reinforced Glass-Ceramic Matrix Composites", J. Am. Ceram. Soc. 77, [5] 1329-39 (1994)

45. Sun, E., Nutt, S., and Brennan, J.: "Flexural Creep and Creep-Rupture Behavior of SiC/BN Dual Coated Nicalon Fiber Reinforced Glass-Ceramic Matrix Composites, Cer. Engr. & Sci. Proc., Vol. 15, No. 4, 57-64 (1994).

46. Sun, E., Nutt, S., and Brennan, J.: "Interfacial Diffusion and Reaction Mechanisms in Coated Fiber Reinforced Glass-Ceramic Composites", ibid., Vol. 15, No. 5, 943-950 (1994).

47. Brennan, J.: "Interfaces in BN Coated Fiber Reinforced Glass-Ceramic Matrix Composites", Scripta Metallurgica et Materialia, Vol. 31, No. 8, pp. 959-964, 1994.

48. Sun, E., Nutt, S., and Brennan, J.: "Microscopic Failure Mechanisms in SiC Fiber-Reinforced Glass-Ceramic Composites", Proceedings of the 1994 TMS Spring Meeting (Symposium on Control of Interfaces in Metal and Ceramic Composites)

49. Sun, E., Nutt, S., and Brennan, J.: "Flexural Creep Behavior of SiC/BN Dual Coated Nicalon Fiber Reinforced Glass-Ceramic Matrix Composites", submitted to the Journal of the American Ceramic Society.

50. Sun, E., Nutt, S., and Brennan, J.: "High-Temperature Tensile Properties of Coated SiC Fiber Reinforced Glass-Ceramic Matrix Composites in Aerobic Environments", submitted to the Journal of the American Ceramic Society.

51. Cooper, R.F. and Chyung, K.: Structure and Chemistry of Fibre-Matrix Interfaces in SiC Fibre-Reinforced Glass-Ceramic Composites: An Electron Microscopy Study, J. Mat. Sci. 22 (1987) 3148-3160.

52. Pechentkovskaya, L.E., and Nazarchuk, T.N.: "Effect of the Different Crystal Structure of Boron Nitride on its High-Temperature Stability in Oxygen", Soviet Powder Metallurgy and Metal Ceramics, Dec. 1981.

53. Moore, A.W., and Strong, S.L.: "Variations in the Structure and Morphology of Pyrolytic Boron Nitride", Ceram. Eng. Sci. Proc. 10[7-8], pp 846-856, 1989.

54. US Patent #5,275,844, "Process for Forming a Crack Free BN Coating on a Carbon Substrate", Jan., 1994.

55. Brennan, J.J.: Interfacial Studies of Whisker and Coated Fiber Reinforced Ceramic Matrix Composites, Annual Report R90-918185-1 on AFOSR Contract F49620-88-C-0062, May 31, 1990.

56. Prouhet, S., Camus, G., Labrugere, C., and Guette, A.: Mechanical Characterization of Si-C(O) Fiber/SiC (CVI) Matrix Composites with a BN-Interphase, J. Am. Cer. Soc., 77 [3] 649-56 (1994).

57. Kerans, R.J., and Parthasarathy, T.A.: Theoretical Analysis of the Fiber Pullout and Pushout Tests, ibid, 74 [7] 1585-96 (1991)

58. Marshall, D.B., and Oliver, W.C.: Measurement of Interfacial Mechanical Properties in Fiber-Reinforced Ceramic Composites, ibid., 70 [8], 1987, 542-48.

Table I

Mechanical Properties in Air for BMAS Matrix/SiC/BN Coated Nicalon Fiber Composite #95-93 (0/90°)

Flexural Properties

Temperature	σ - ksi(MPa)	PL - ksi(MPa)	E - msi(GPa)	ε_f - %
RT	74 (510)	23 (159)	15.3 (105)	0.73
RT (1100°C, 266hrs, air)	52 (360)	-	17.0 (117)	0.50
RT (1100°C, 266hrs, Ar)	58 (400)	-	19.0 (131)	0.38
RT (1100°C, 266hrs, HP Ar)	83 (574)	-	15.5 (107)	0.81
1100°C	73 (501)	21 (145)	8.8 (61)	1.10
1200°C	65 (448)	15 (103)	7.0 (48)	1.19
1300°C	44 (303)	7 (48)	6.8 (47)	0.90

Tensile Properties

Temperature	UTS - ksi(MPa)	PL - ksi(MPa)	E - msi(GPa)	ε_f - %
RT	34.4 (237)	13.8 (95)	19.1 (132)	0.63
1100°C	39.5 (272)	12.8 (88)	10.6 (73)	0.70
1200°C	44.0 (304)	10.2 (70)	8.6 (59)	0.88

Table II

Mechanical Properties in Air for BMAS Matrix/Si_3N_4 Over BN Coated Nicalon Fiber Composite #363-92 (0/90°)

Flexural Properties

Temperature	σ - ksi(MPa)	PL - ksi(MPa)	E - msi(GPa)	ε_f - %
RT	78 (537)	28 (193)	17.5 (121)	0.67
1100°C	84 (578)	24 (158)	9.8 (68)	1.10
1200°C	56 (386)	11.0 (76)	9.2 (63)	0.96

Table III

Mechanical Properties in Air for BMAS Matrix/BN Coated Nicalon Fiber Composite #253-93 (0/90°)

Flexural Properties

Temperature	σ - ksi(MPa)	PL - ksi(MPa)	E - msi(GPa)	ε_f - %
RT	90 (620)	18 (124)	20.6 (142)	0.77
RT (550°C, 500 hrs, O_2)	57 (392)	19 (131)	14.1 (97)	0.59
RT (1000°C, 500 hrs, O_2)	86 (593)	20 (140)	17.7 (122)	0.66
RT (1100°C, 500 hrs, air)	74 (513)	20 (140)	17.1 (118)	0.56
1100°C	82 (568)	20 (140)	9.2 (63)	1.13
1200°C	48 (329)	8.3 (57)	7.0 (48)	1.03

Tensile Properties

Temperature	UTS - ksi(MPa)	PL - ksi(MPa)	E - msi(GPa)	ε_f - %
RT		Not Determined		
1100°C	48 (331)	8.8 (61)	8.6 (59)	1.14
1200°C	40 (276)	7.5 (52)	6.2 (43)	1.10

Table IV

Results of Fiber Indent Testing of Ceramed BMAS Matrix/Nicalon Fiber Composites With SiC/BN, Si_3N_4/BN, and BN Coated Fibers

Comp. #	Fiber Coating	RT σ-ksi(MPa)	PL - ksi(MPa)	ε_f - %	τ-MPa (M&O)	G-J/m^2(M&O)
95-93	SiC/BN	74 (510)	23 (159)	0.73	17.6±12.4	2.5±2.3
363-92	Si_3N_4/BN	78 (537)	28 (193)	0.67	92.6±57.8	17.6±18.9
253-93	BN	90 (620)	18 (124)	0.77	37.7±14.2	11.0±7.2

Table V

Mechanical Properties in Air for Modified BMAS Matrix/SiC/BN Coated Nicalon Fiber Composite #129-94 (0/90°)

Flexural Properties

Temperature	σ - ksi(MPa)	PL - ksi(MPa)	E - msi(GPa)	ε_f - %
RT	61 (420)	21.8 (150)	20.9 (144)	0.48
RT (1100°C, 266 hrs, air)	58 (400)	20 (140)	18.1 (125)	0.46
1100°C	61 (420)	16.6 (114)	11.7 (81)	0.69
1200°C	74 (509)	26 (179)	10.6 (73)	1.24

Tensile Properties

Temperature	UTS - ksi(MPa)	PL - ksi(MPa)	E - msi(GPa)	ε_f - %
RT		Not Determined		
1100°C	44 (304)	9.5 (66)	12.2 (84)	0.69
1200°C	41 (282)	8.7 (60)	8.7 (60)	0.89

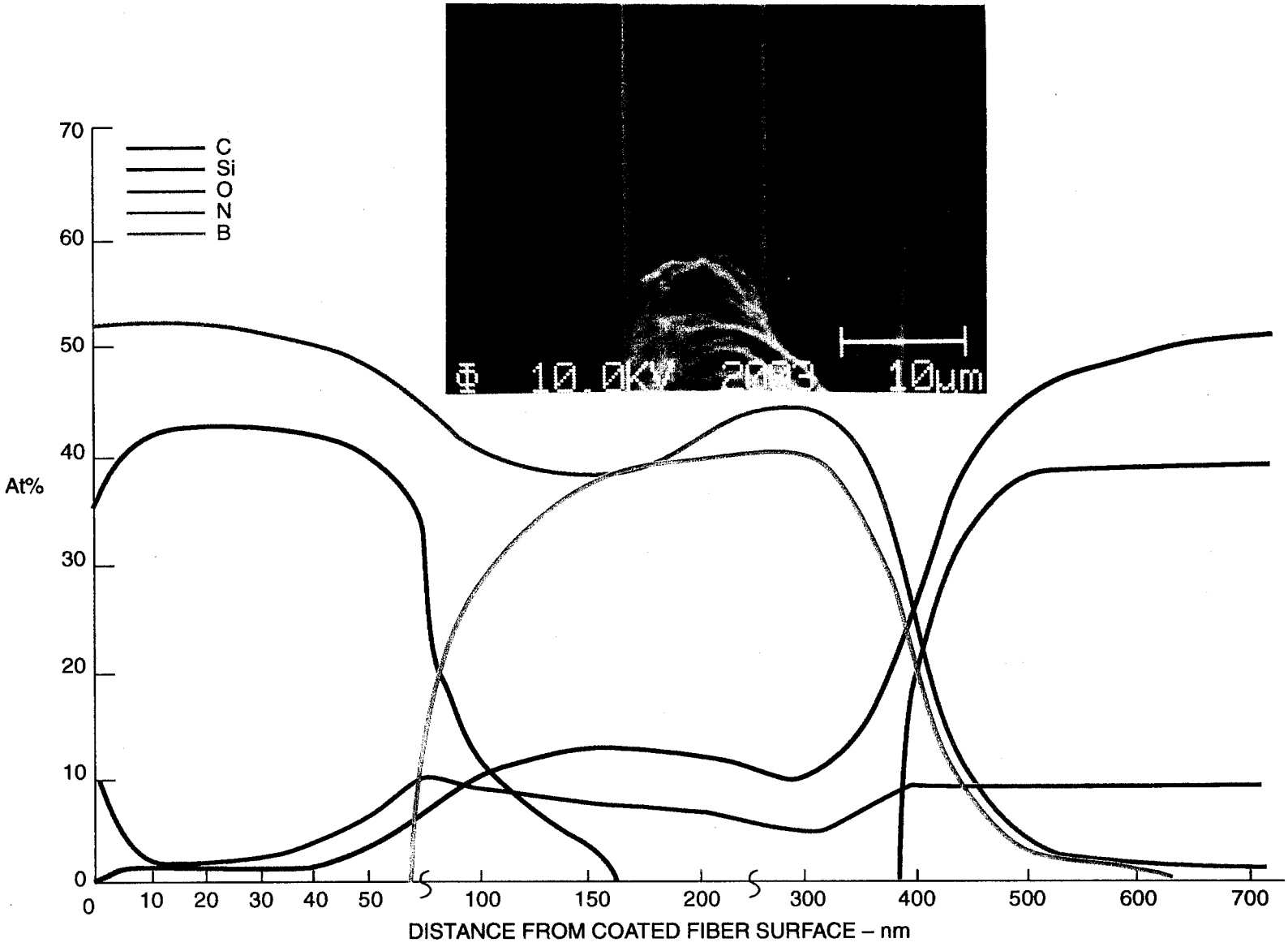

Figure 1 SAM Depth Profile 3M Si_3N_4 Over BN Coated Nicalon Fiber - #97037:38

PG315.12

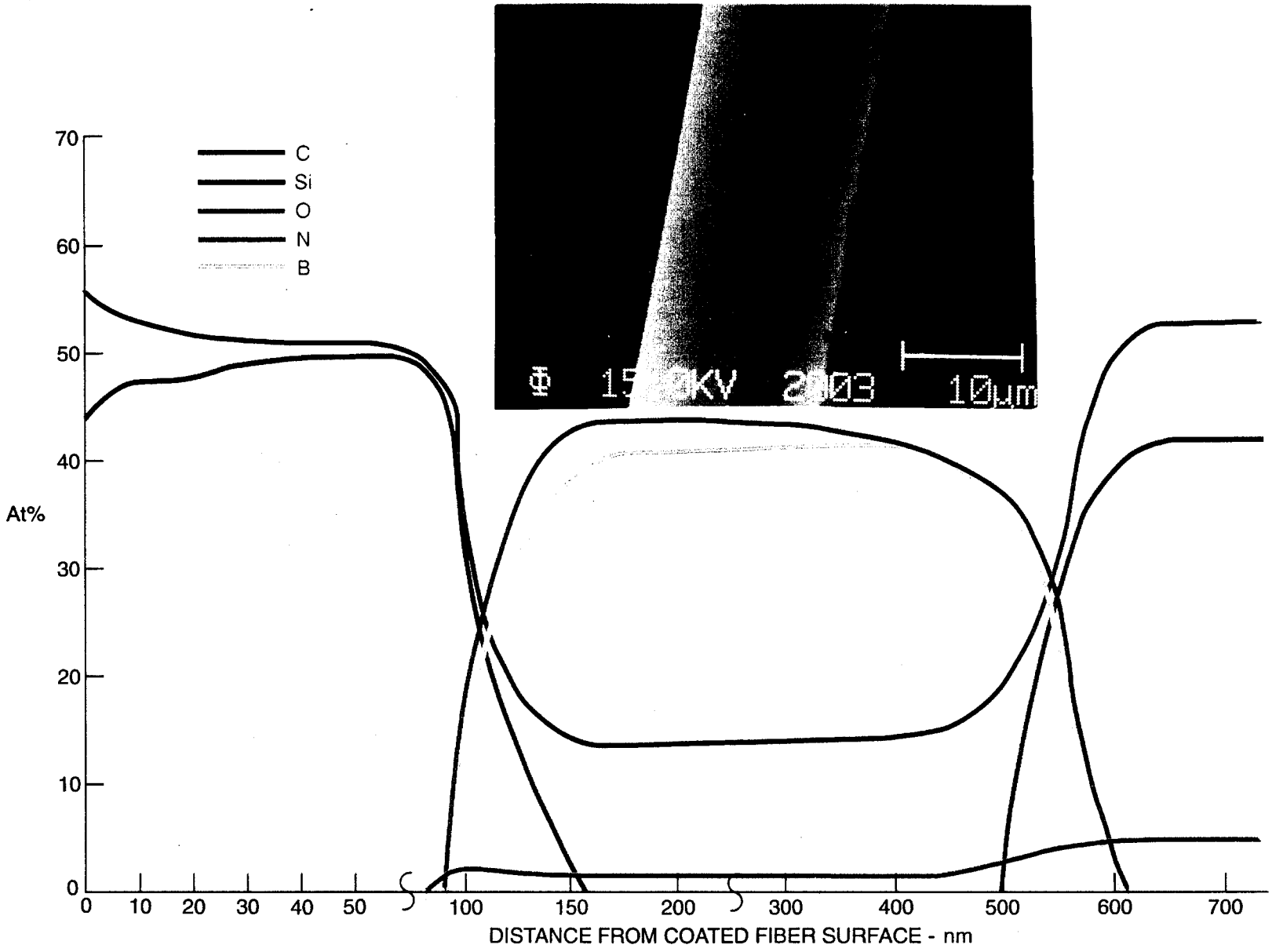

Figure 2 SAM Depth Profile 3M SiC/BN Coated Nicalon Fiber – Lot #97037:15

PG315.13

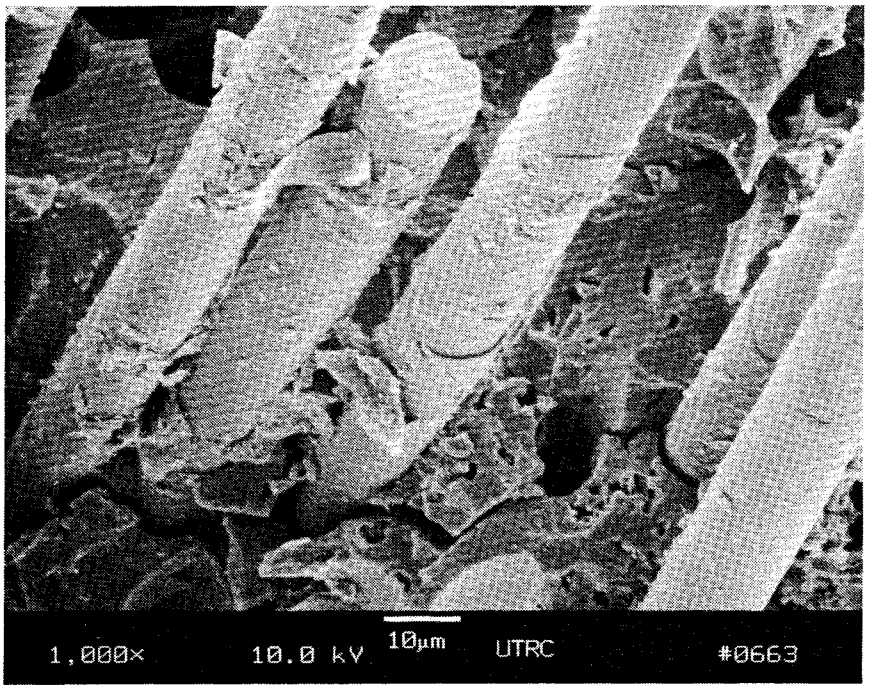

A.

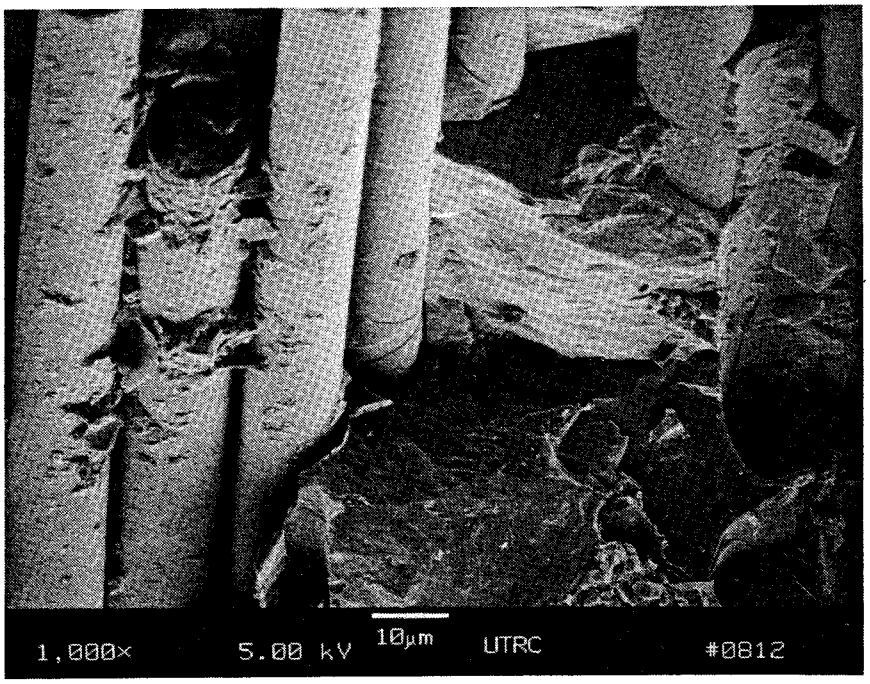

B.

Figure 3 Fracture Surfaces of BMAS/SiC/BN/Nicalon Fiber Composite #95-93 After 1100°C, 266 Hrs in Air (A) and Pure Argon (B)

NO FIBER DEGRADATION

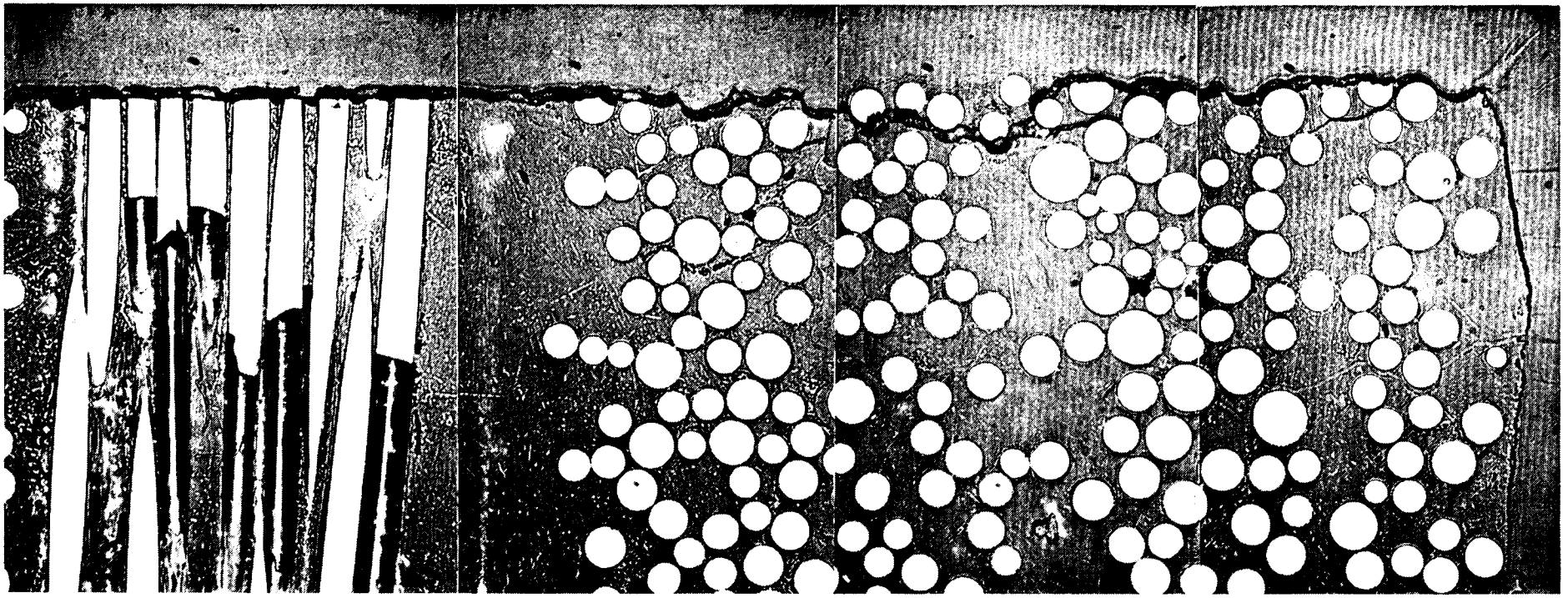

PG315.11

Figure 4 Optical Micrograph of SiC/BN Coated Nicalon Fiber/BMAS Matrix Composite #95-93-18-2 (266 Hrs, 1100°C, AR)

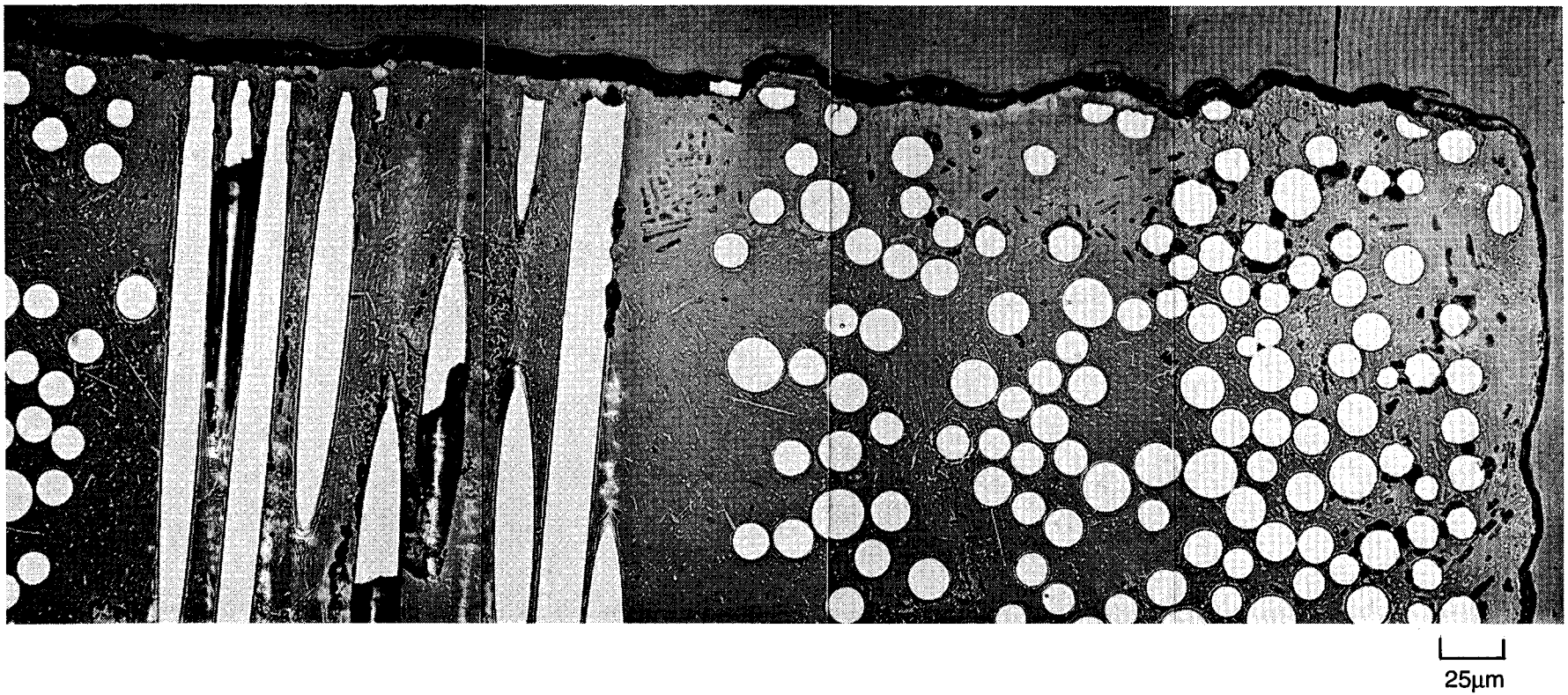

PG315.10

Figure 5 Optical Micrograph of SiC/BN Coated Nicalon Fiber/BMAS Matrix Composite #95-93-18-1 (266 Hrs, 1100°C, Air)

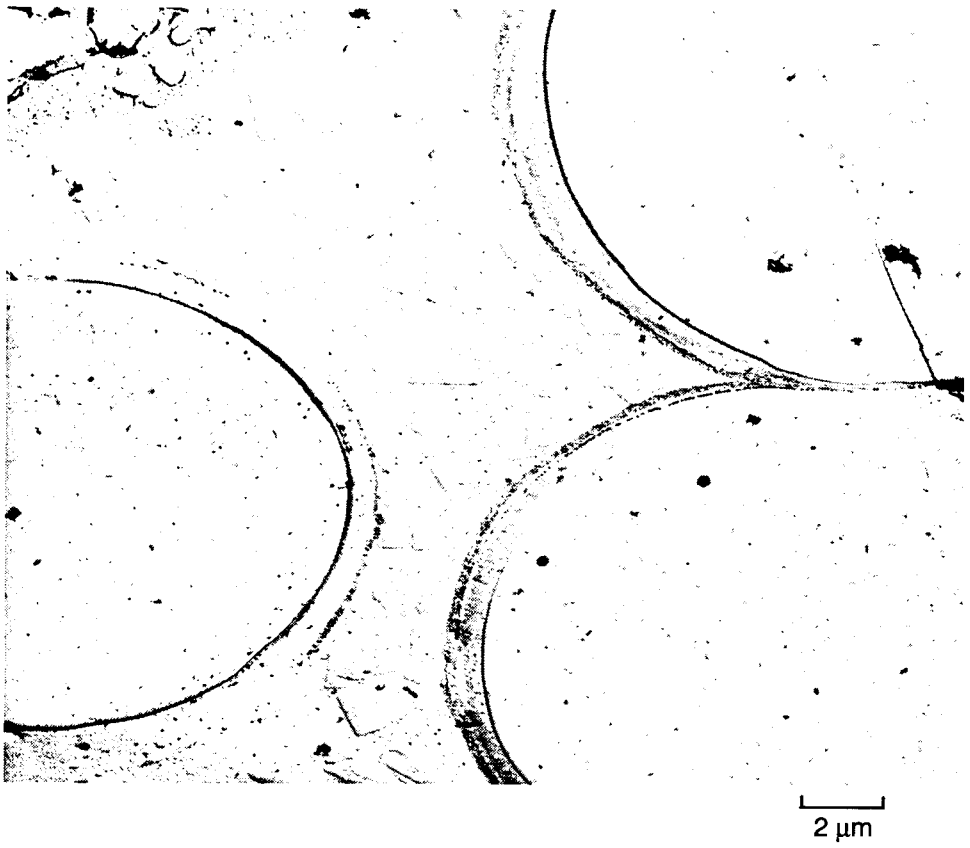

Figure 6 TEM Replica Characterization of the Surface Region of BMAS/SiC/BN Nicalon Fiber Composite #95-93 (1100°C, 266 Hrs, Air)

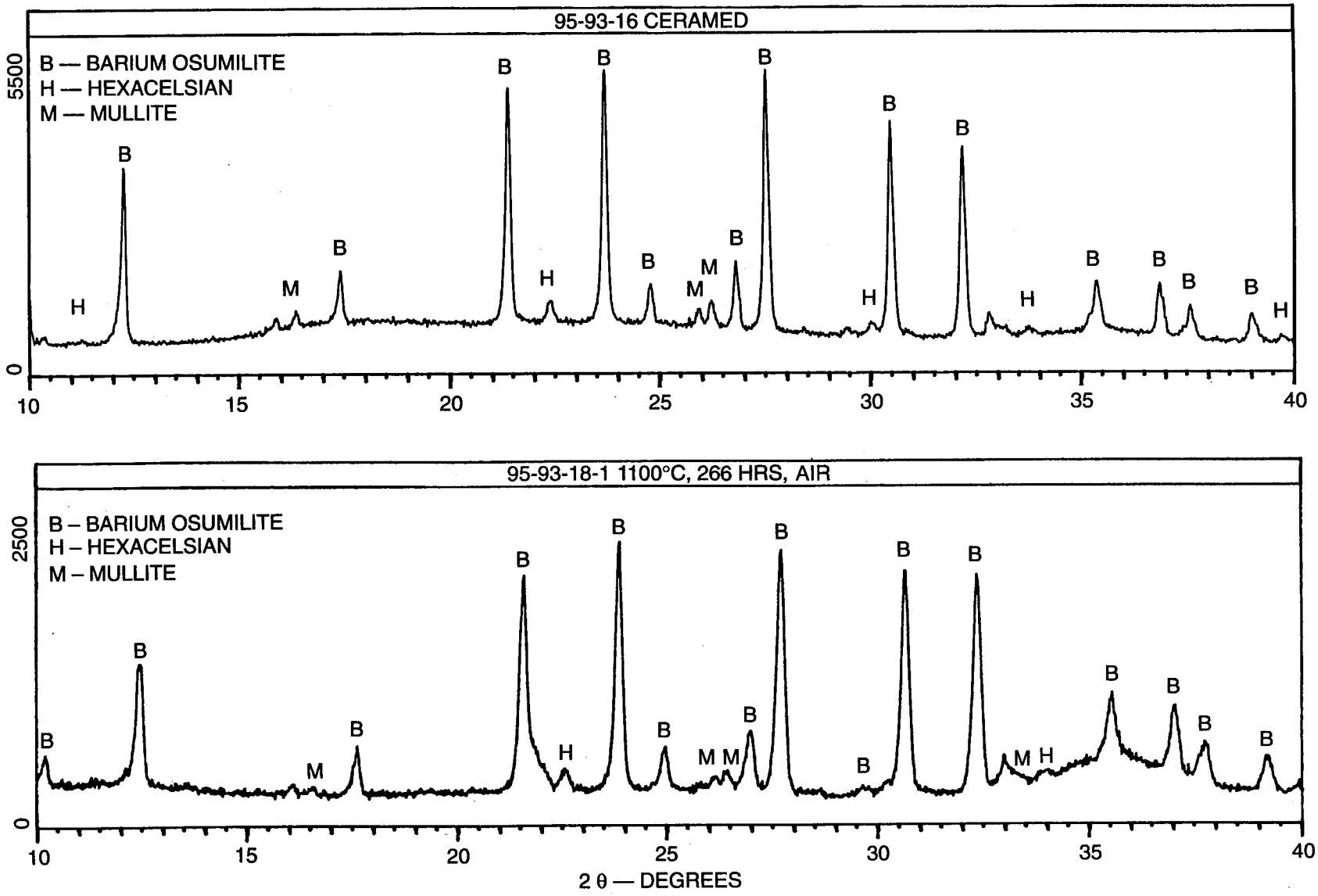

PG315.9

Figure 7 **X-ray Diffraction Analysis of BMAS Matrix/SiC/BN Coated Nicalon Fiber Composite #95-93, As-Ceramed (Top) and After 1100°C, 266 Hrs, Air (Bottom)**

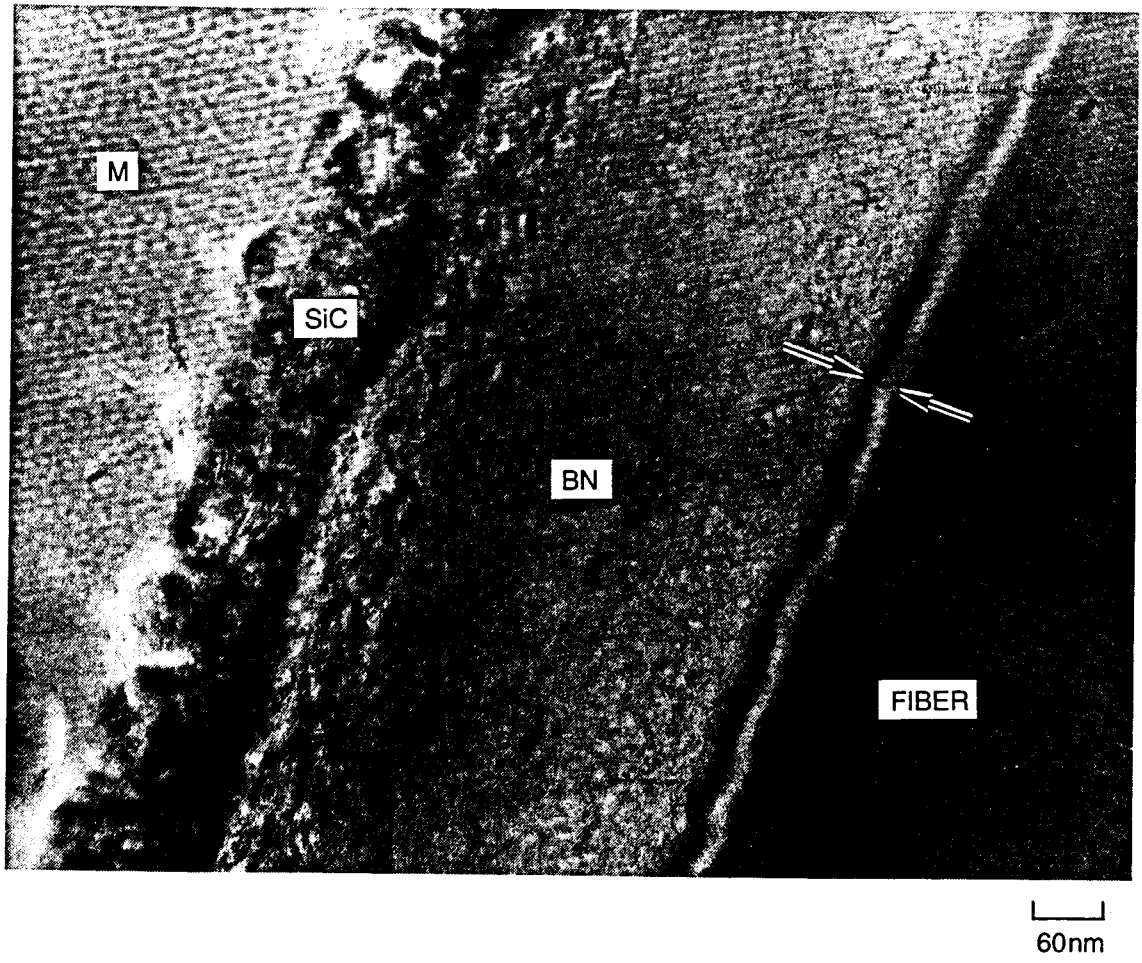

Figure 8 TEM Thin Foil Characterization of Interior Region of BMAS Matrix Composite #95-93 After Heat-Treatment at 1100°C, 266 Hrs, Air

PG315.16

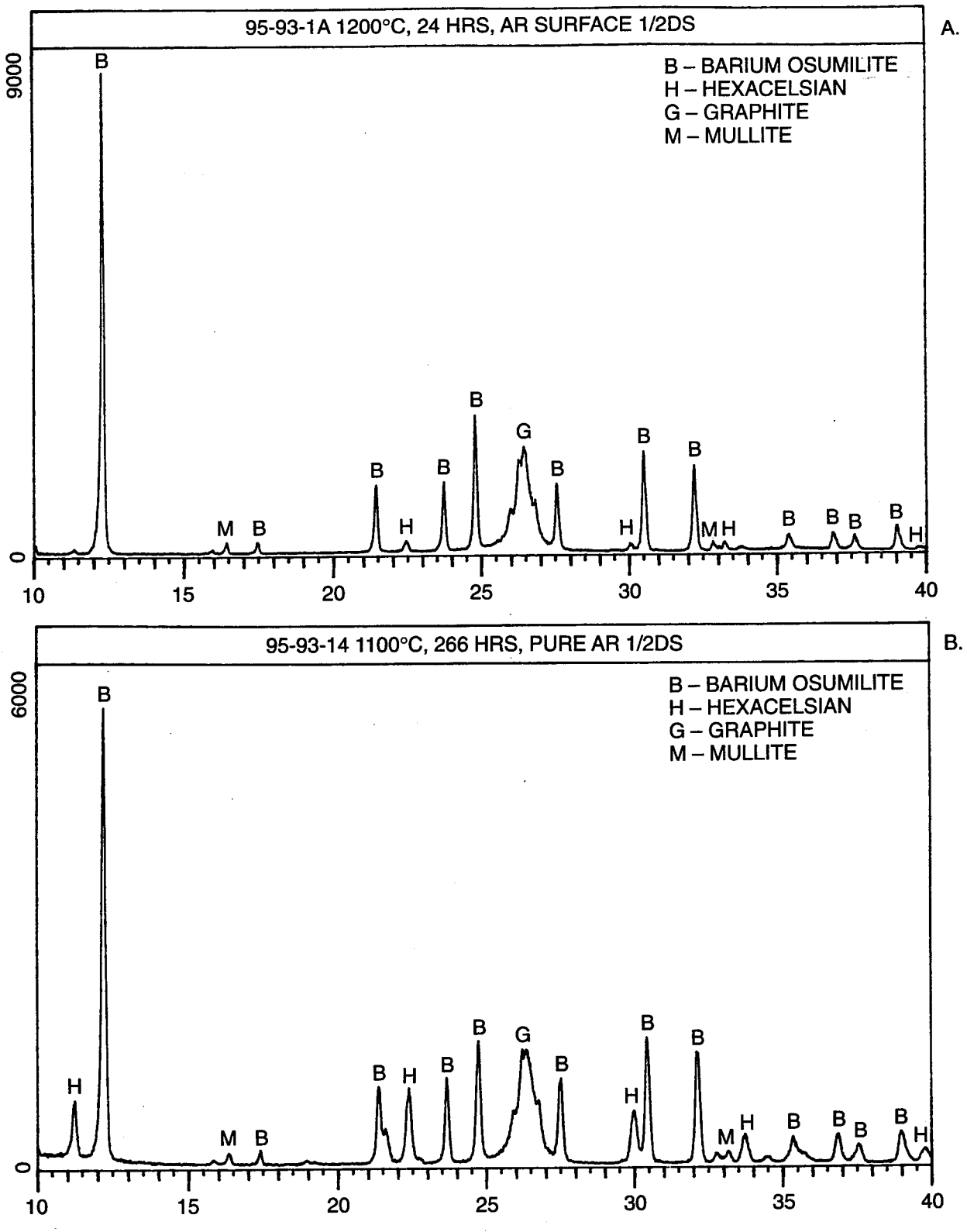

Figure 9 X-ray Diffraction Analysis of the Surface of BMAS/SiC/BN Nicalon Fiber Composite #95-93 After (A) Ceraming at 1200°C, 24 Hrs, AR, and (B) 1100°C, 266 Hrs, HP AR

PG315.7

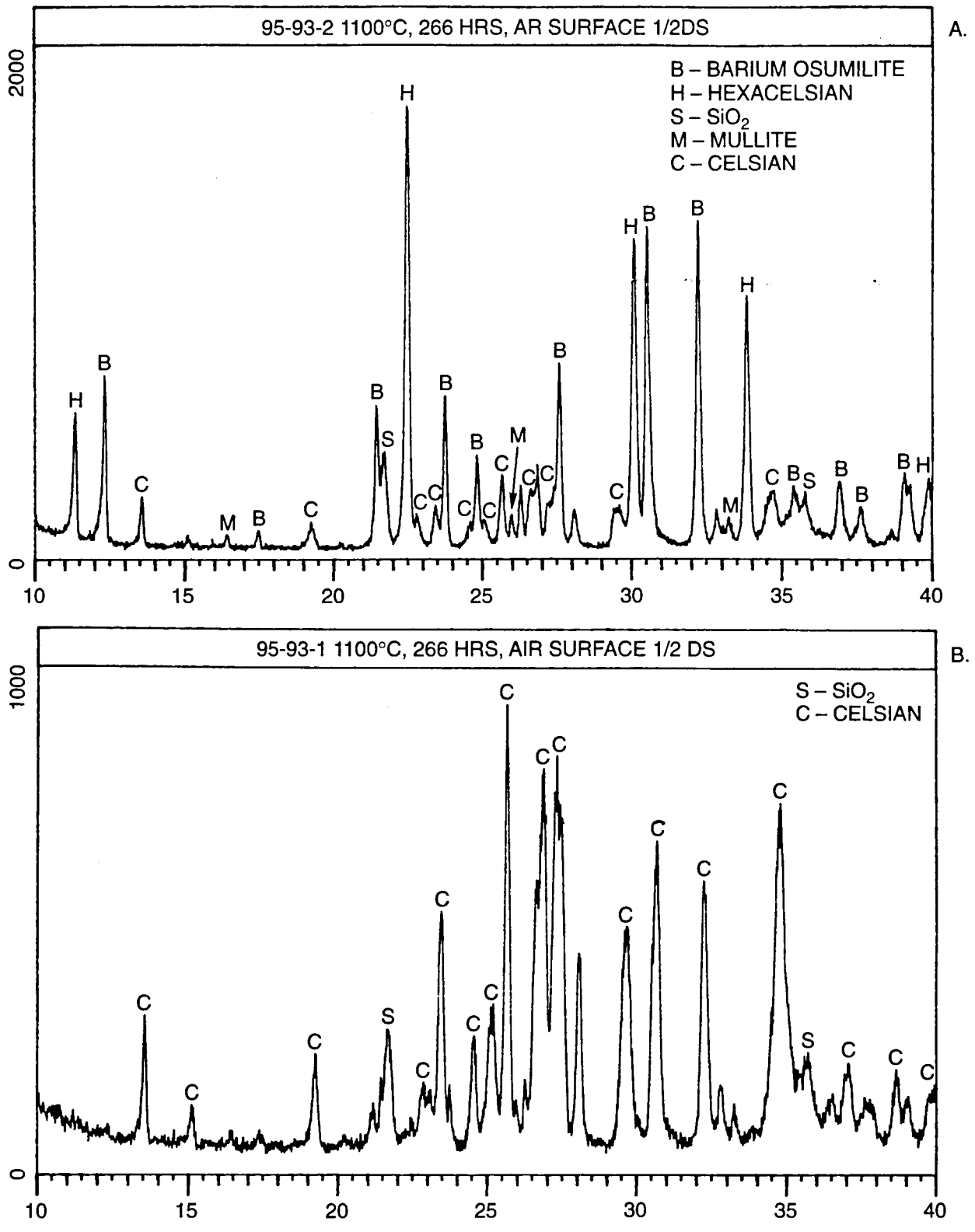

Figure 10 X-ray Diffraction Analysis of the Surface of BMAS/SiC/BN Nicalon Fiber Composite #95-93 After Heat-Treatment at 1100°C, 266 Hrs, in (A) Impure Argon, and (B) Air

PG315.8

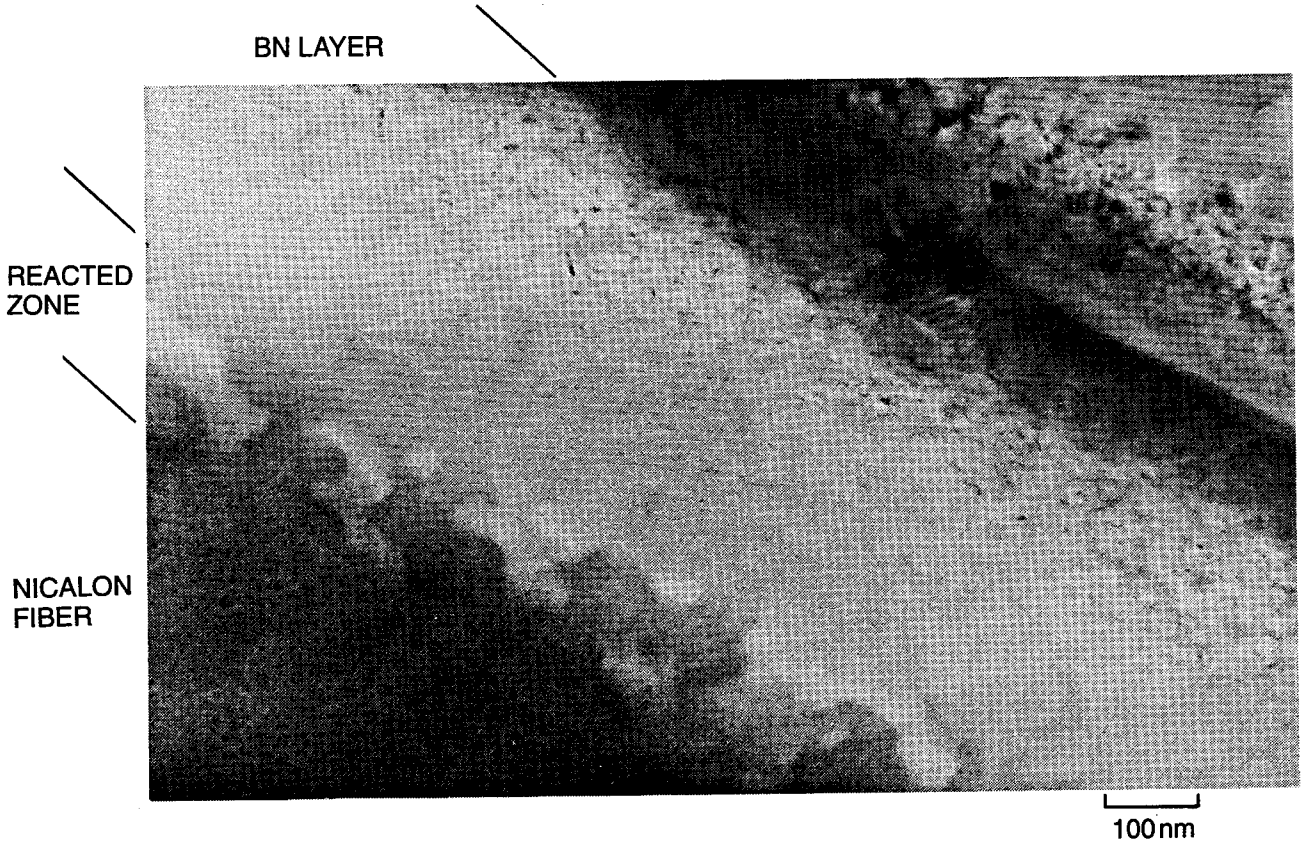

Figure 11 Interfacial Region Near the Surface of BMAS/SiC/BN Nicalon Fiber Composite #95-93 (1100°C, 266 Hrs, Air)

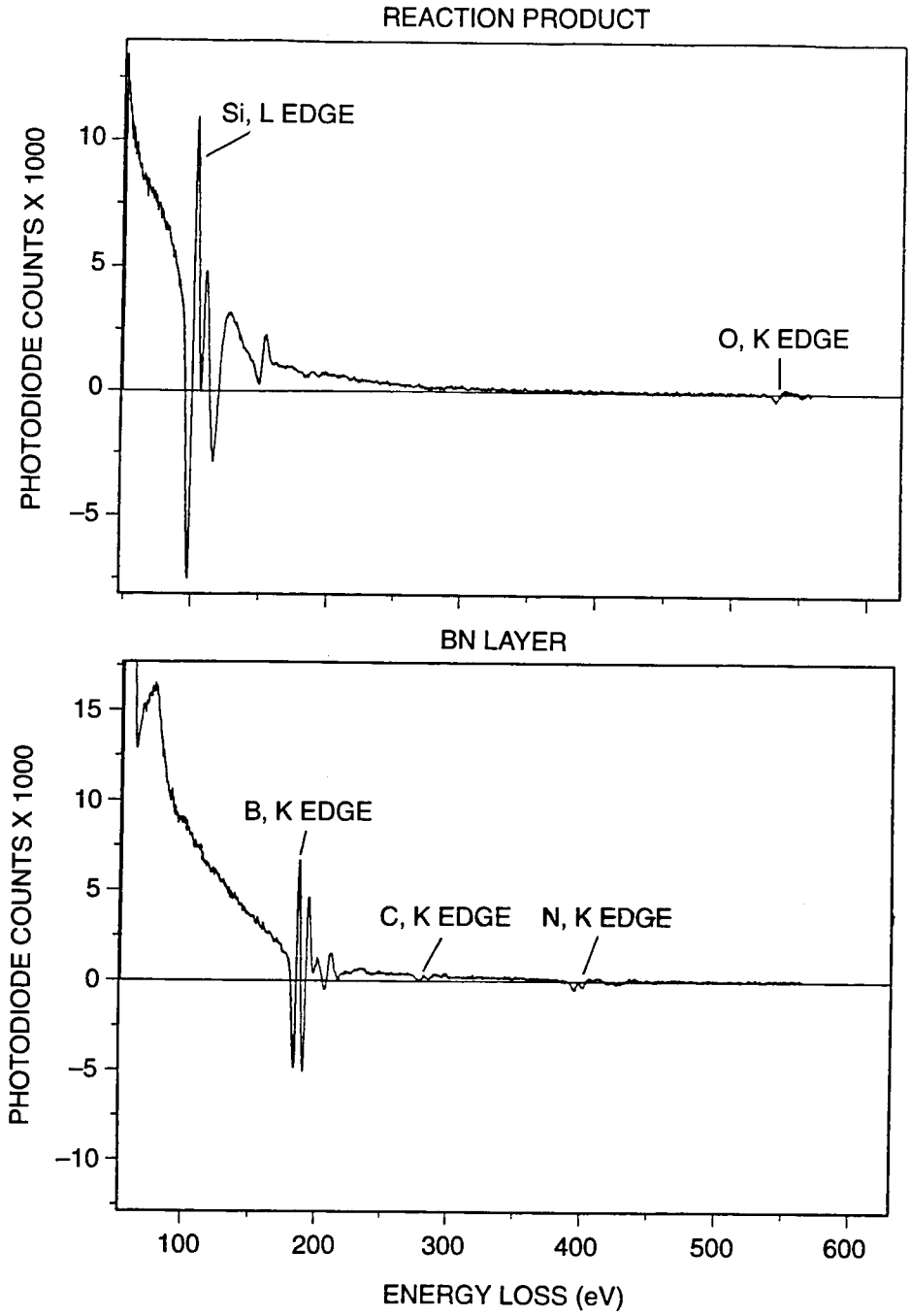

Figure 12 PEELS Data Collected from the Regions Shown in Figure 11

PG315.3

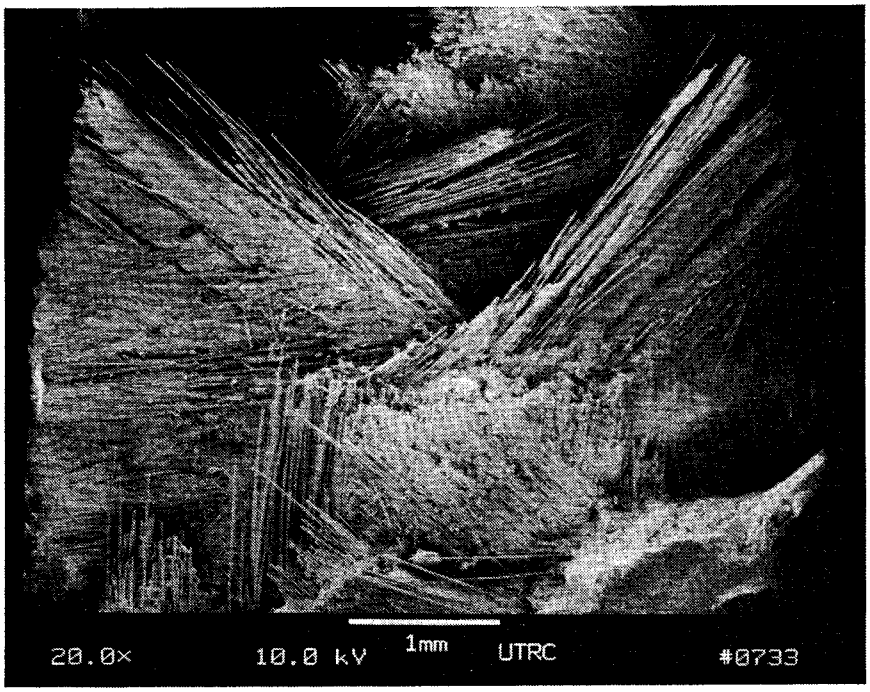

A. OVERALL FRACTURE SURFACE

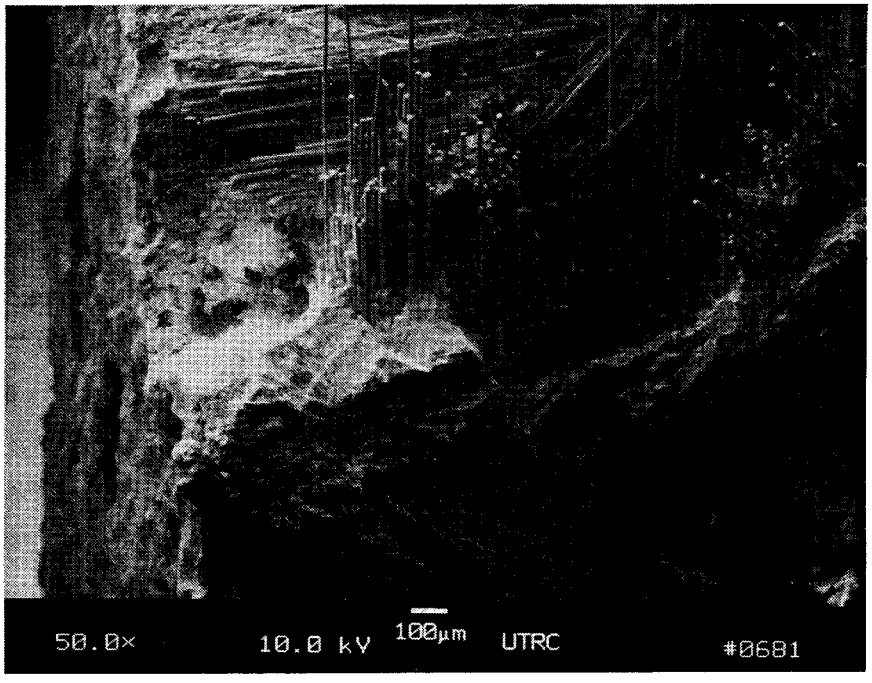

B. BRITTLE EDGE REGION

Figure 13 Fracture Surface of a 0/±45/90° BMAS/SiC/BN Nicalon Fiber Composite #23-92 (Tensile Stress-Rupture Tested at 1200°C in Air, 69 MPa, 11,725 Hrs)

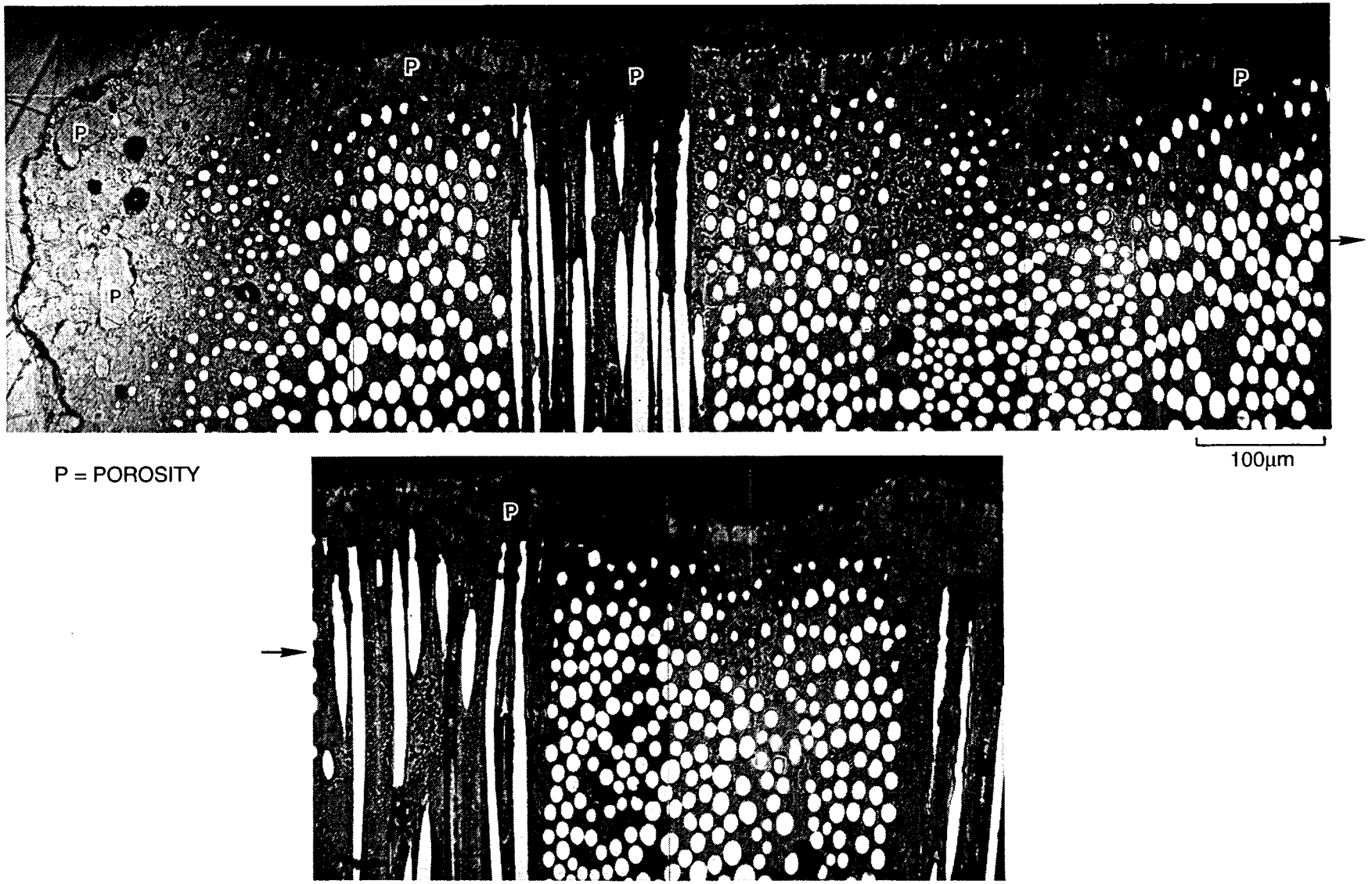

PG315.19

Figure 14 Optical Micrographs of BMAS/SiC/BN/Nicalon Composite #23-29-9 (Tensile Stress-Rupture/ 1200°C/69 MPa/11,725 Hrs)

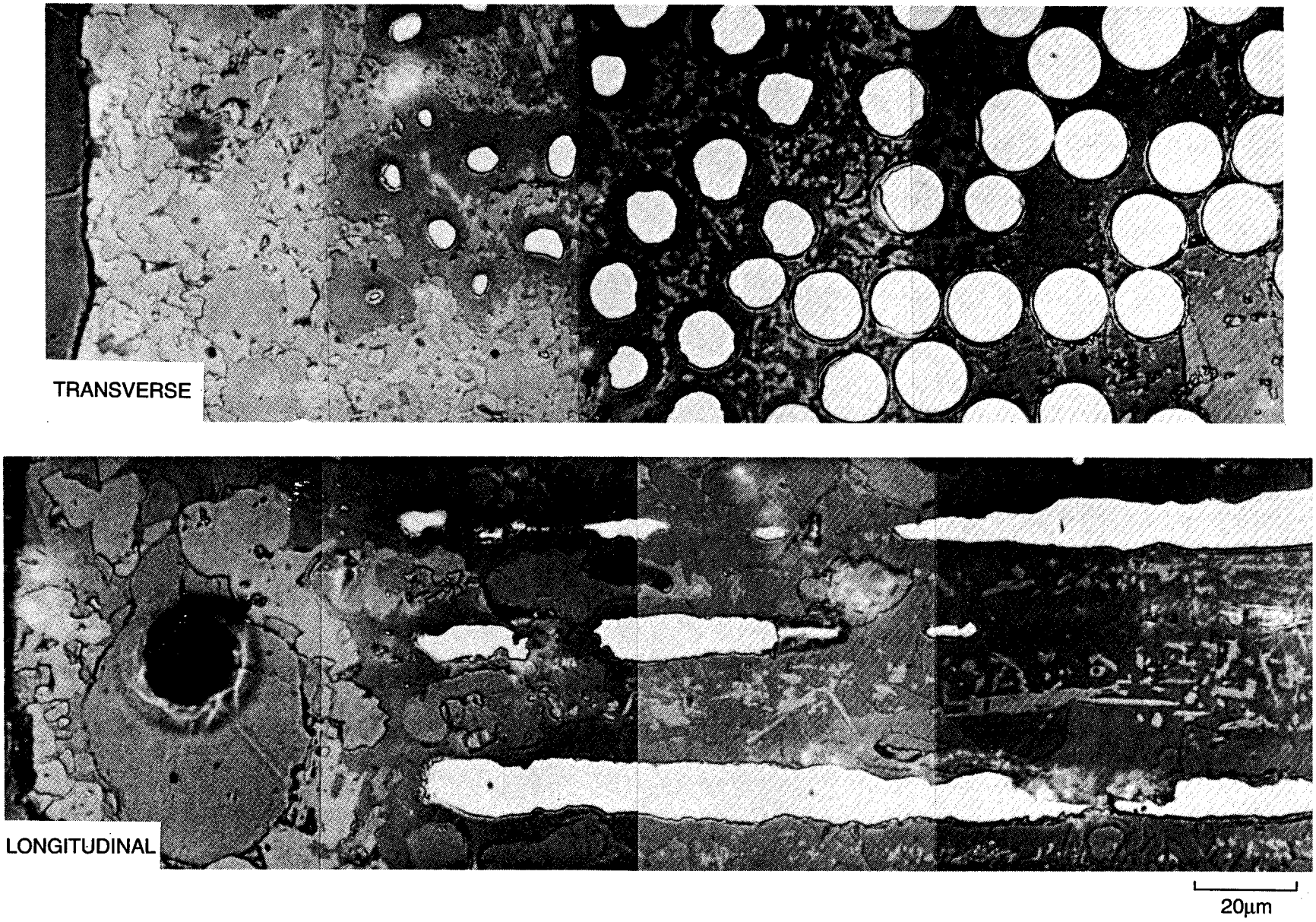

PG315.20

Figure 15 Optical Micrographs of BMAS/SiC/BN/Nicalon Composite #23-29-9 (Tensile Stress-Rupture/ 1200°C/69 MPa/11,725 Hrs)

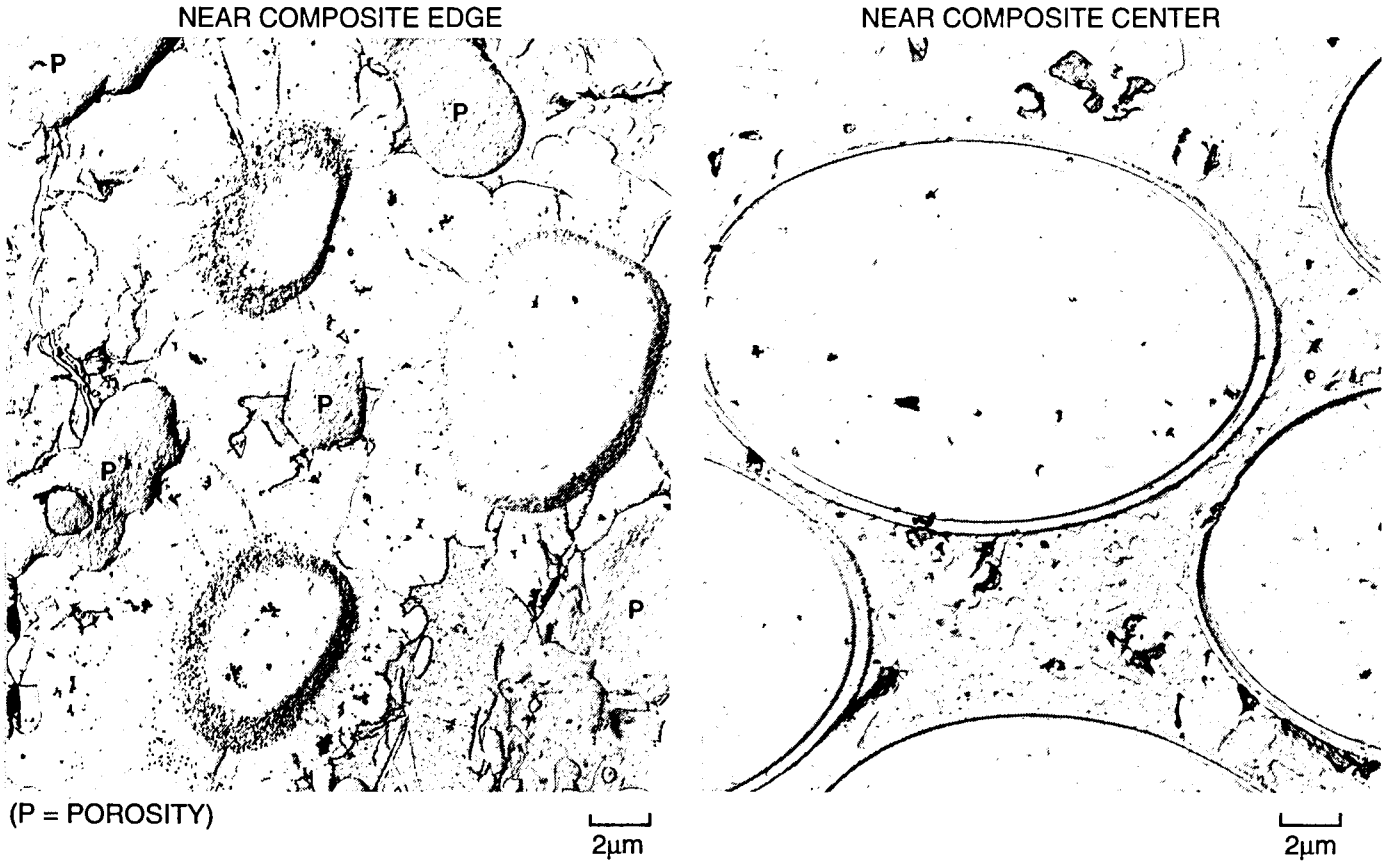

Figure 16 TEM Replica Characterization of BMAS/SiC/BN Coated Nicalon Fiber Composite #23-92-9 (Tensile Stress-Rupture Tested at 1200°C, 69 MPa, 11,725 Hrs)

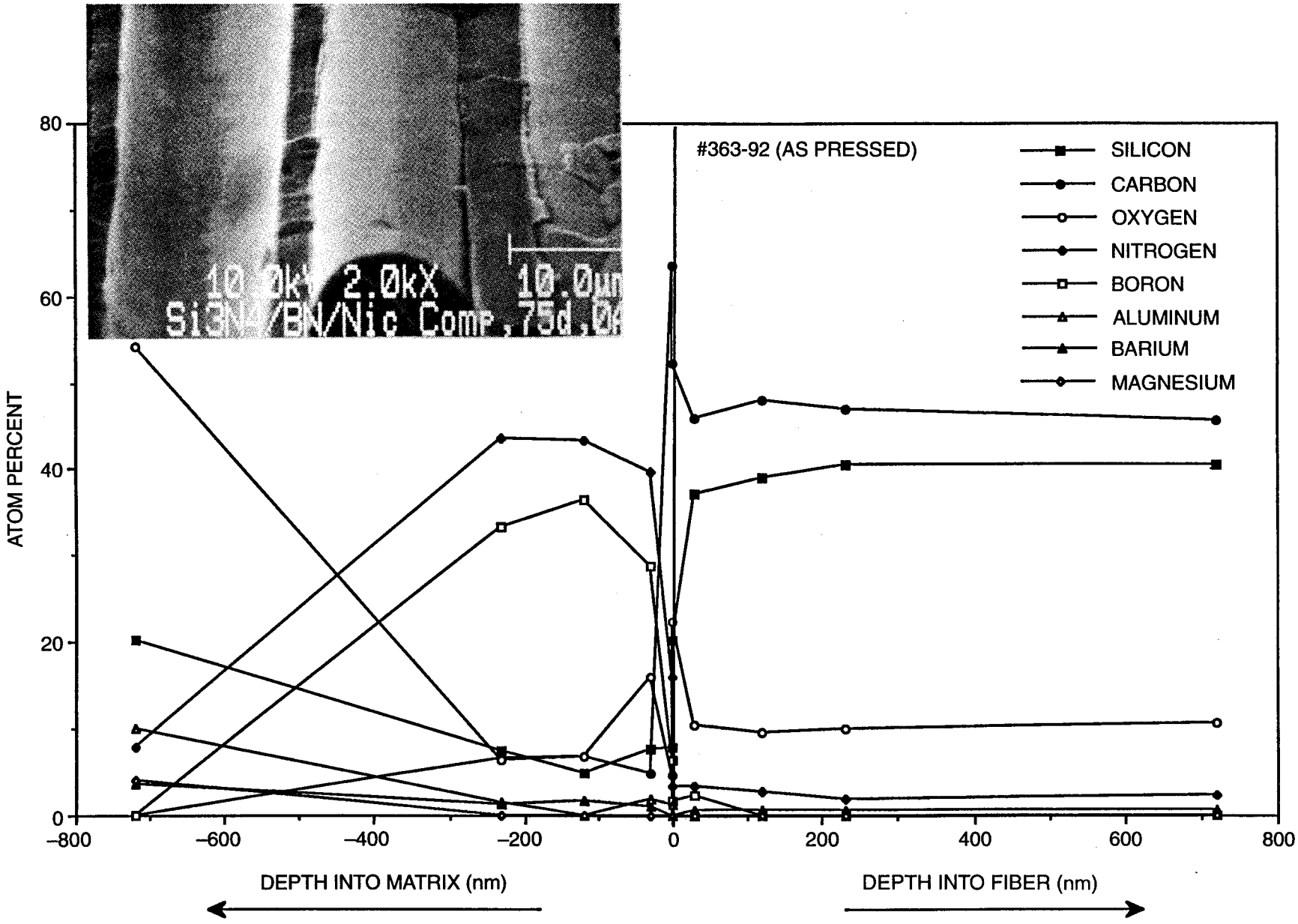

PG315.2

Figure 17 SAM Depth Profile – Interfacial Chemistry of BMAS Matrix/Si_3N_4/BN Coated Nicalon SiC Fiber Composite

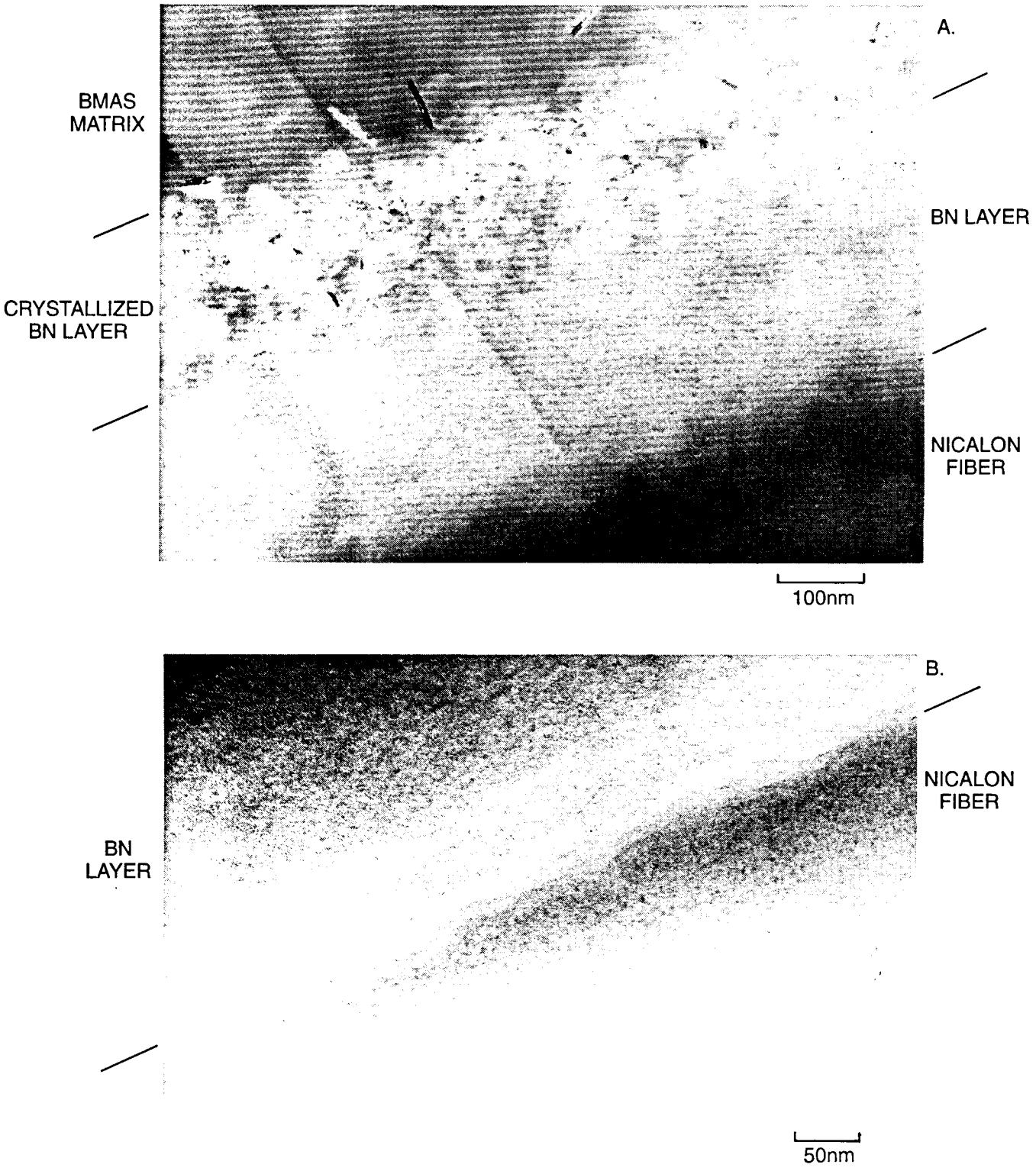

Figure 18 TEM Thin Foil Analysis of Interfacial Region in BMAS Matrix/Si_3N_4/BN Coated Nicalon Fiber Composite #363-92 (As-Pressed)

PG315.22

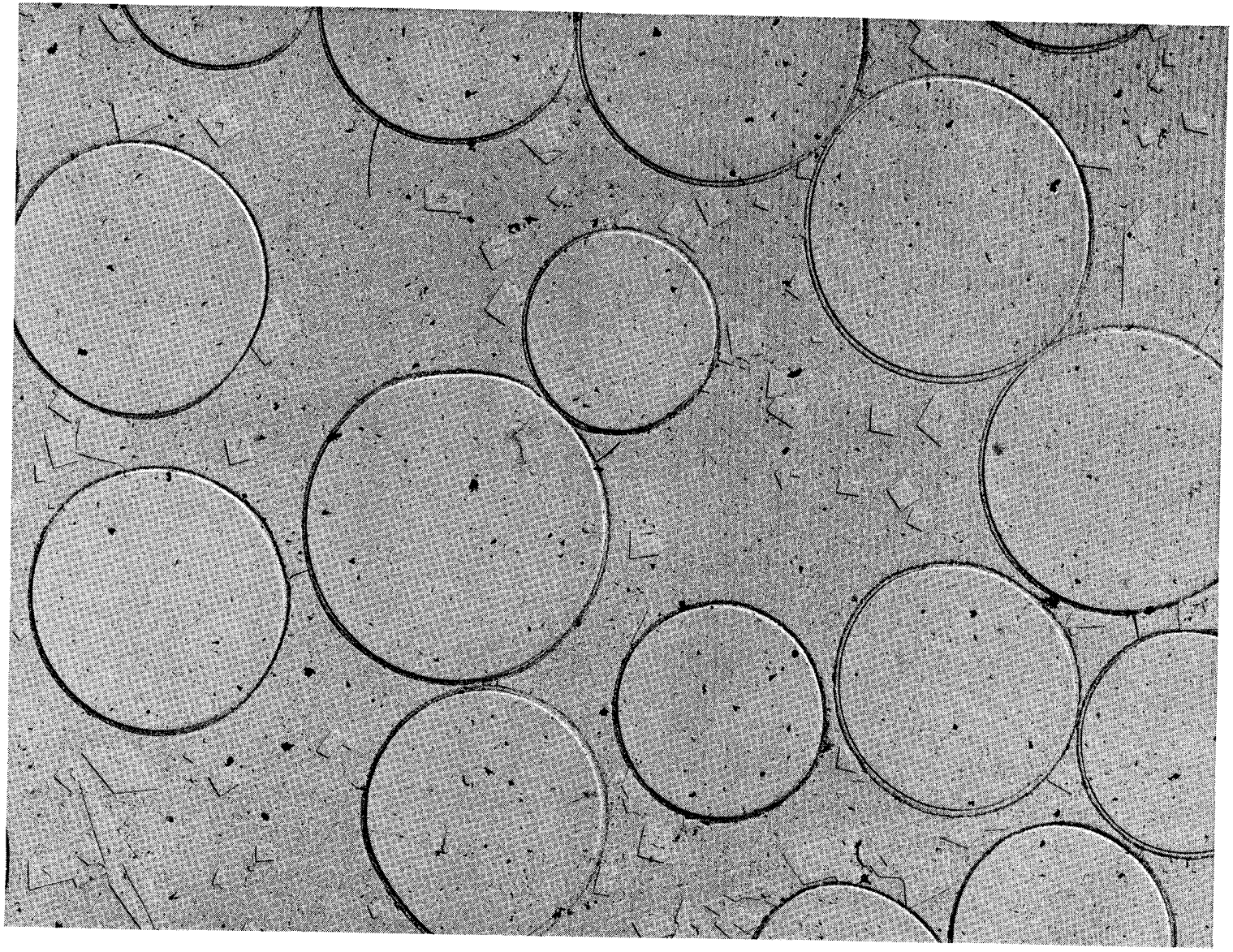

Figure 19 TEM Replica Characterization of BMAS/BN Coated Nicalon Fiber Composite #253-93 (As Pressed)

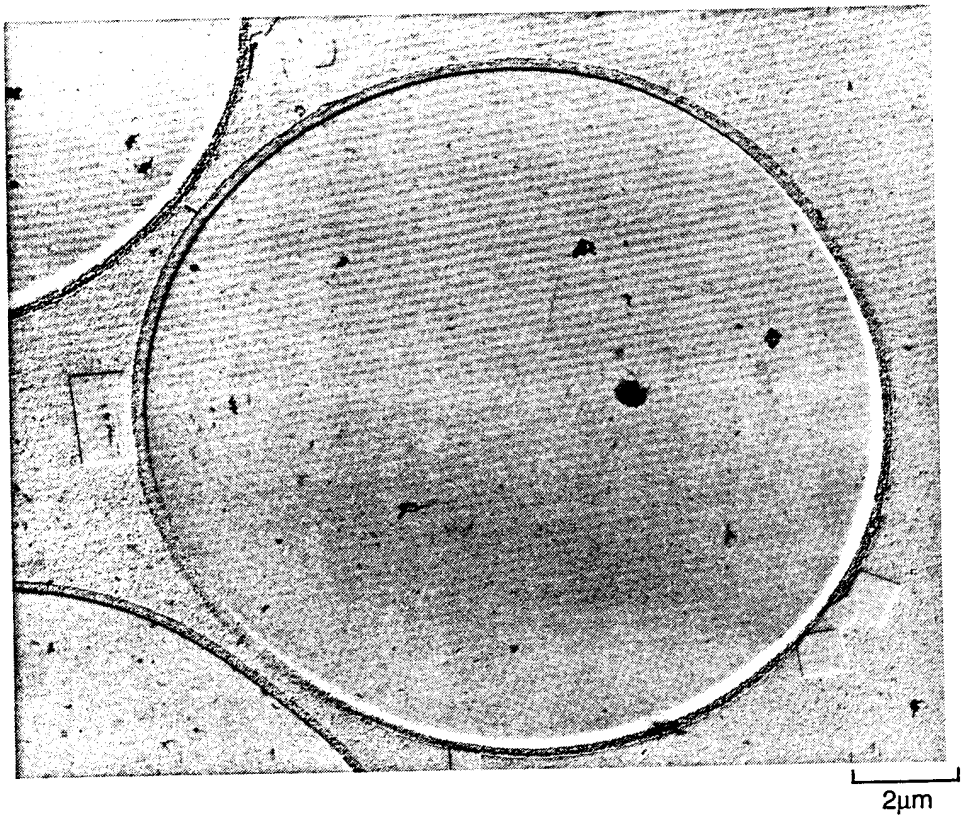

Figure 20 TEM Replica Characterization of BMAS/BN Coated Nicalon Fiber Composite #253-93 (As Pressed)

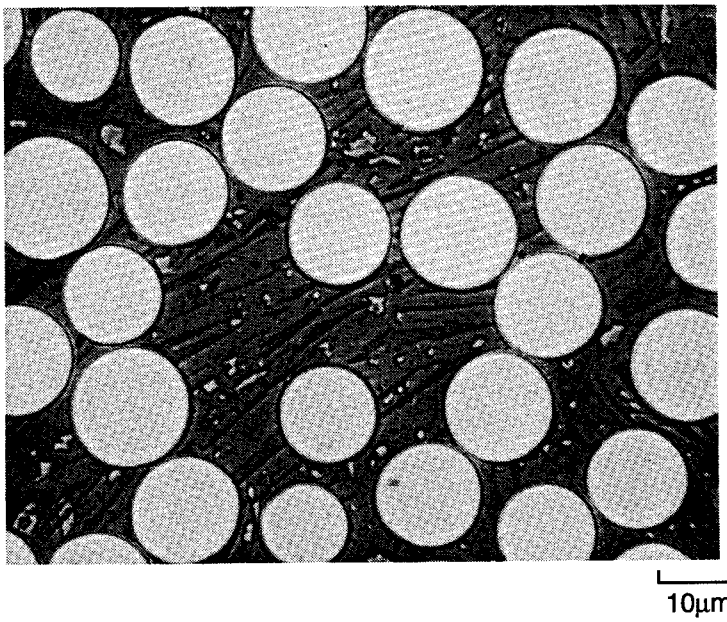

Figure 21 Optical and TEM Replica Characterization of BMAS/BN Coated Nicalon Fiber Composite #253-93 (Ceramed)

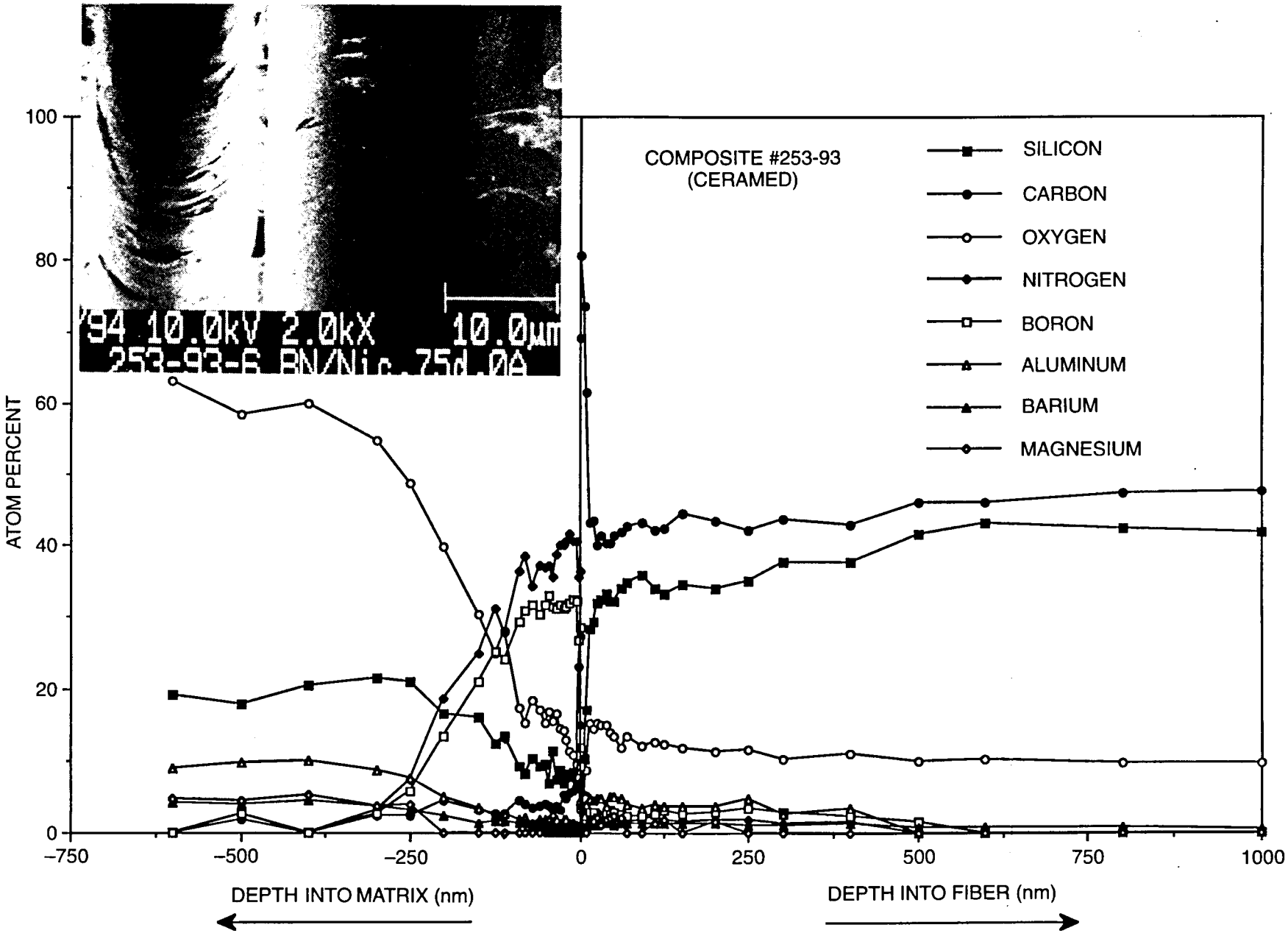

PG315.1

Figure 22 SAM Depth Profile – Interfacial Chemistry of BMAS Matrix/BN Coated Nicalon SiC Fiber

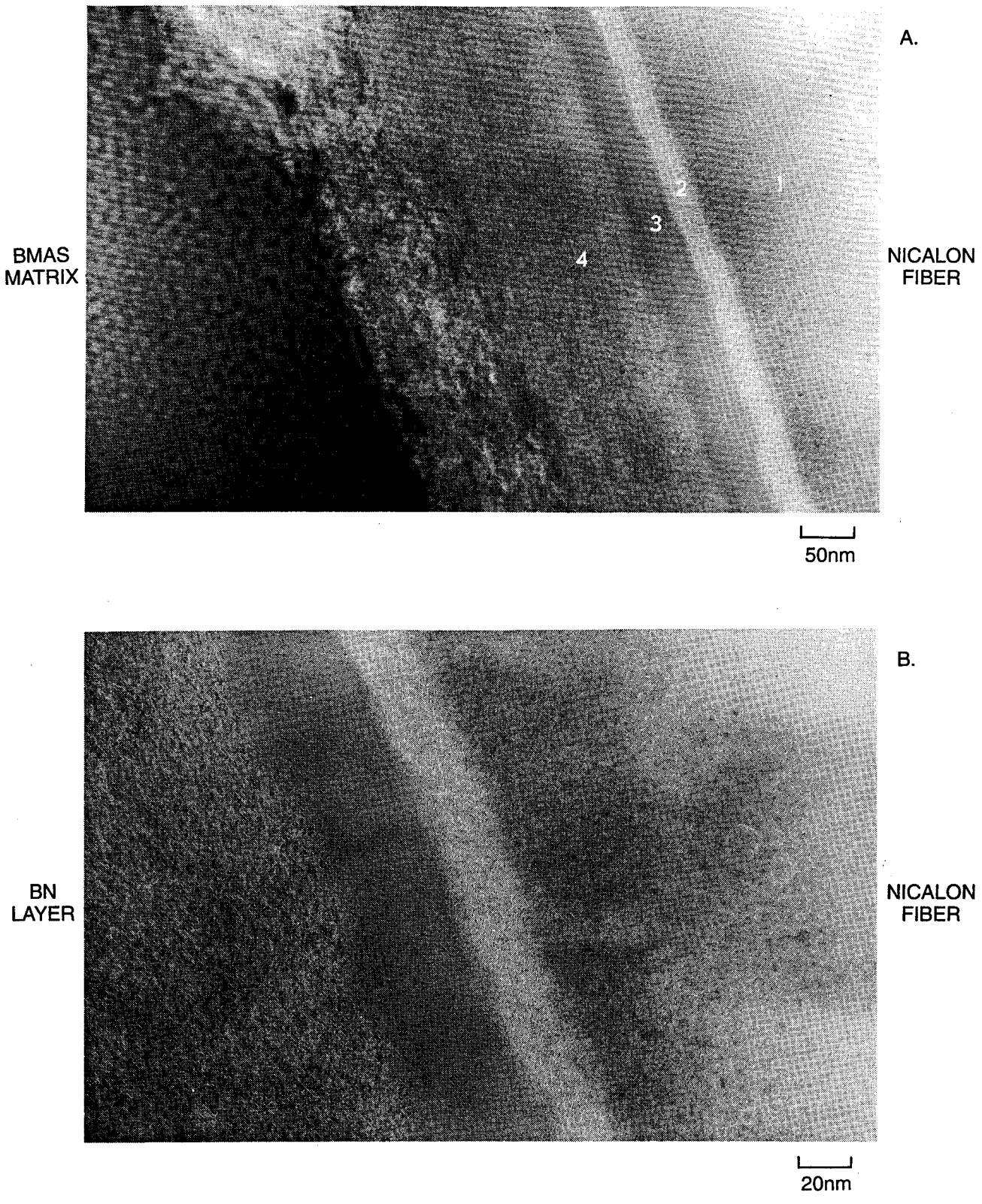

Figure 23 TEM Thin Foil Analysis of Interfacial Region in BMAS Matrix/BN Coated Nicalon Fiber Composite #253-93 (Ceramed)

PG315.26

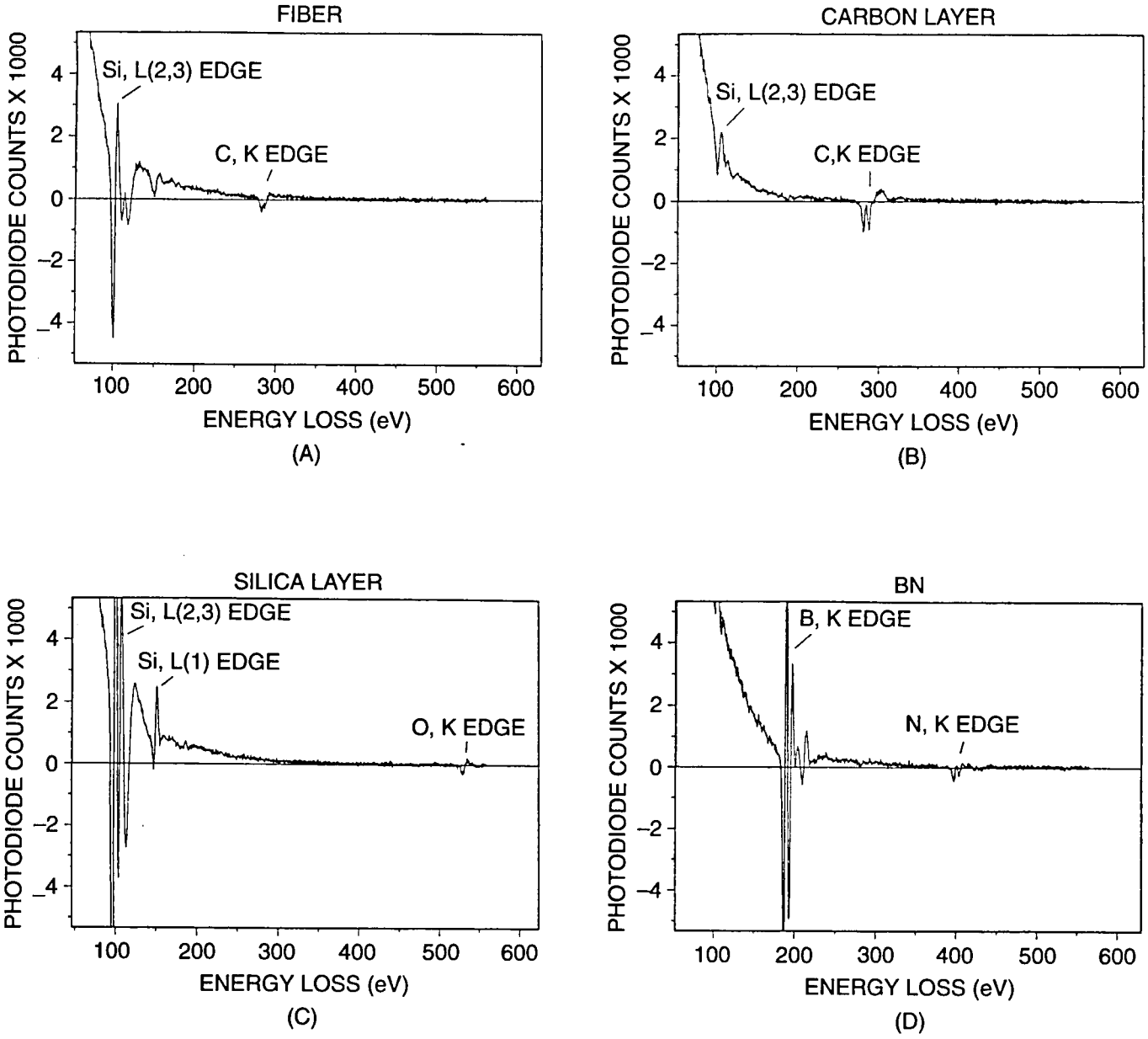

Figure 24 PEELS Spectra Collected from Points 1–4 in Figure 23: (a) Point 1, the Nicalon Fiber; (b) Point 2, the Light Sublayer; (c) Point 3, the Dark Sublayer; and (d) Point 4, the BN Layer

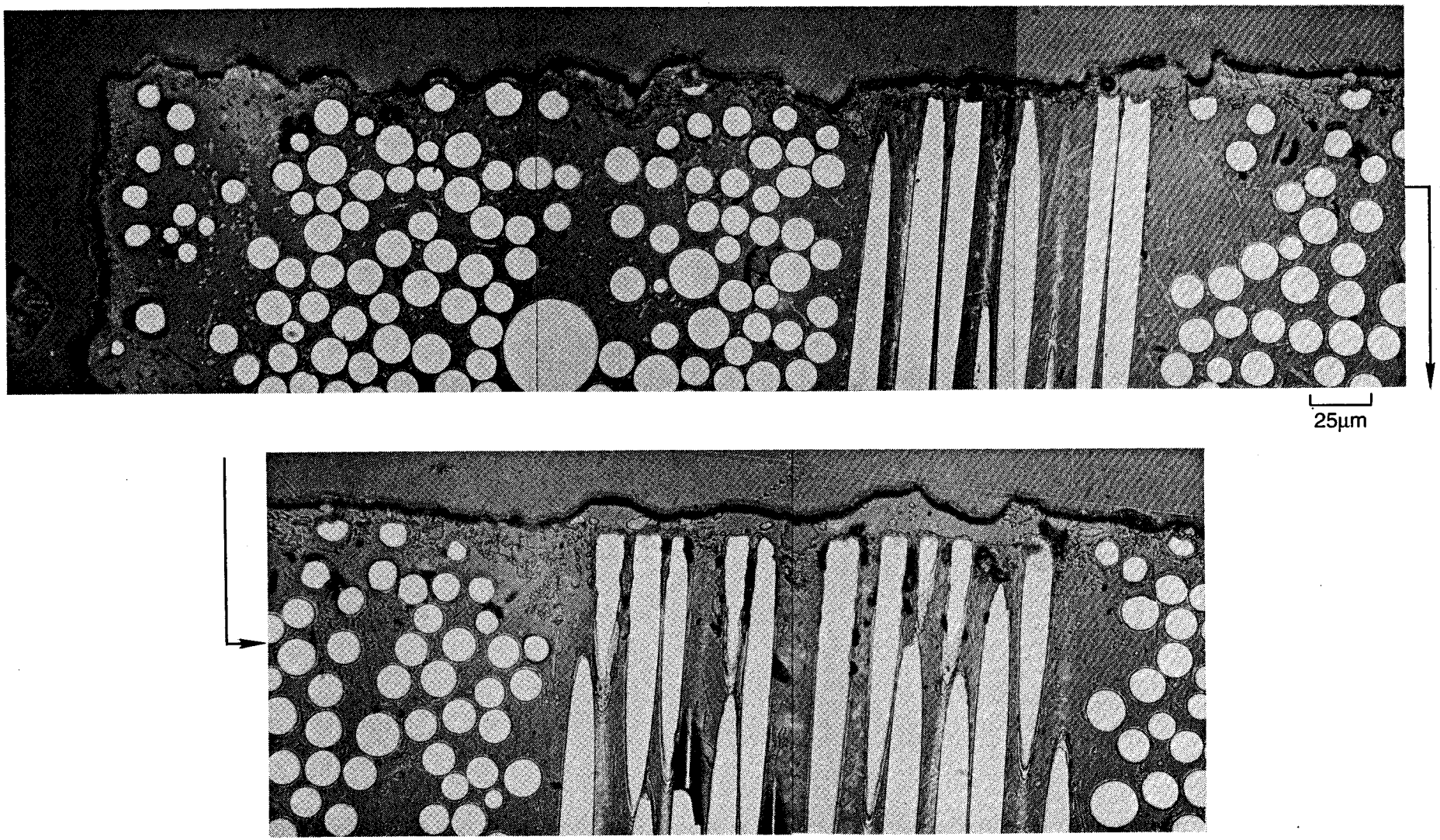

Figure 25 Optical Micrograph of BMAS Matrix/BN-Coated Nicalon Fiber Composite #253-93 (1100°C/500 Hrs./Air)

PG315.27

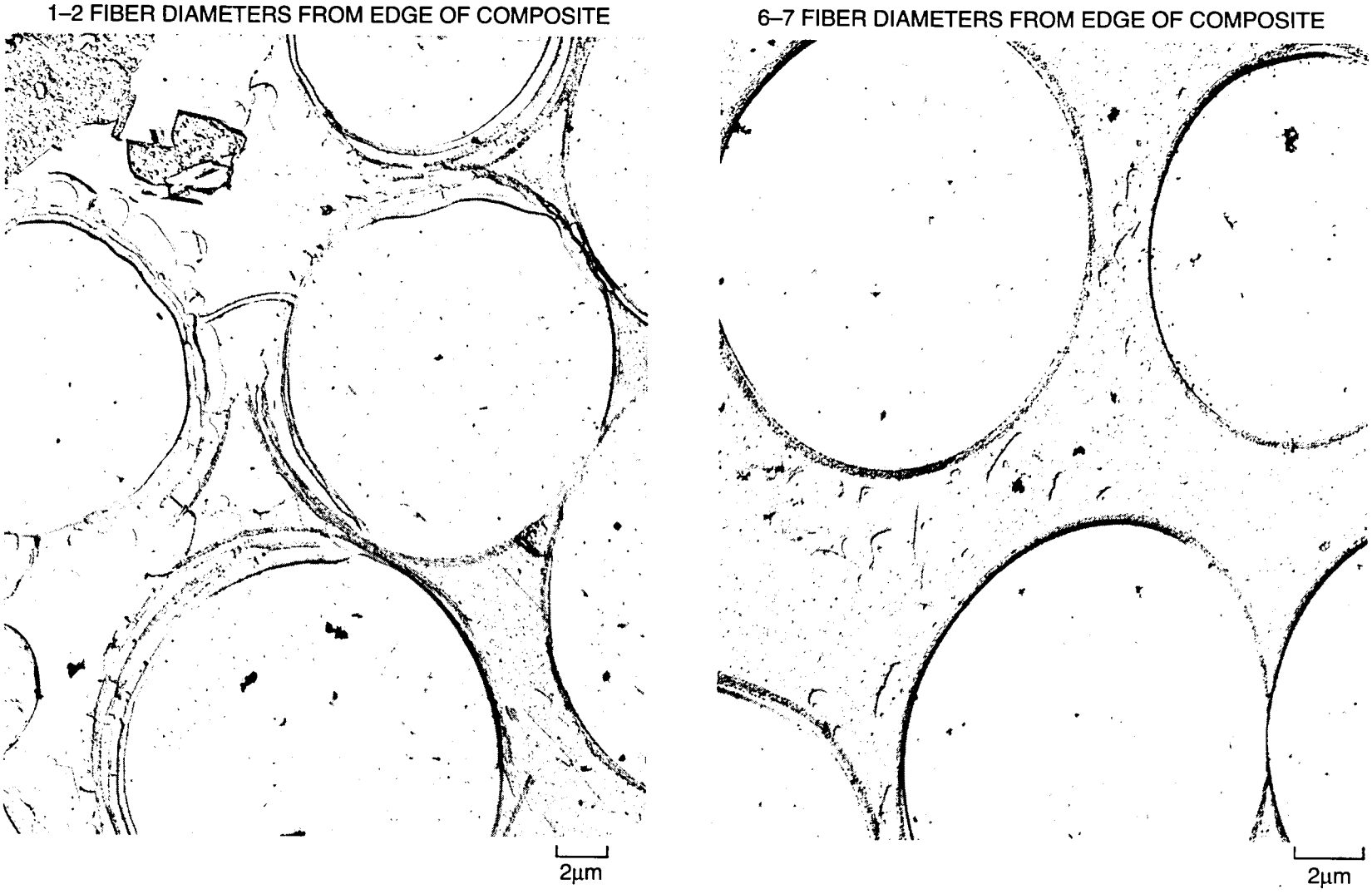

Figure 26 TEM Micrographs of BMAS Matrix/BN-Coated Nicalon Fiber Composite #253-93 (1100°C/500 Hrs/Air)

PG315.28

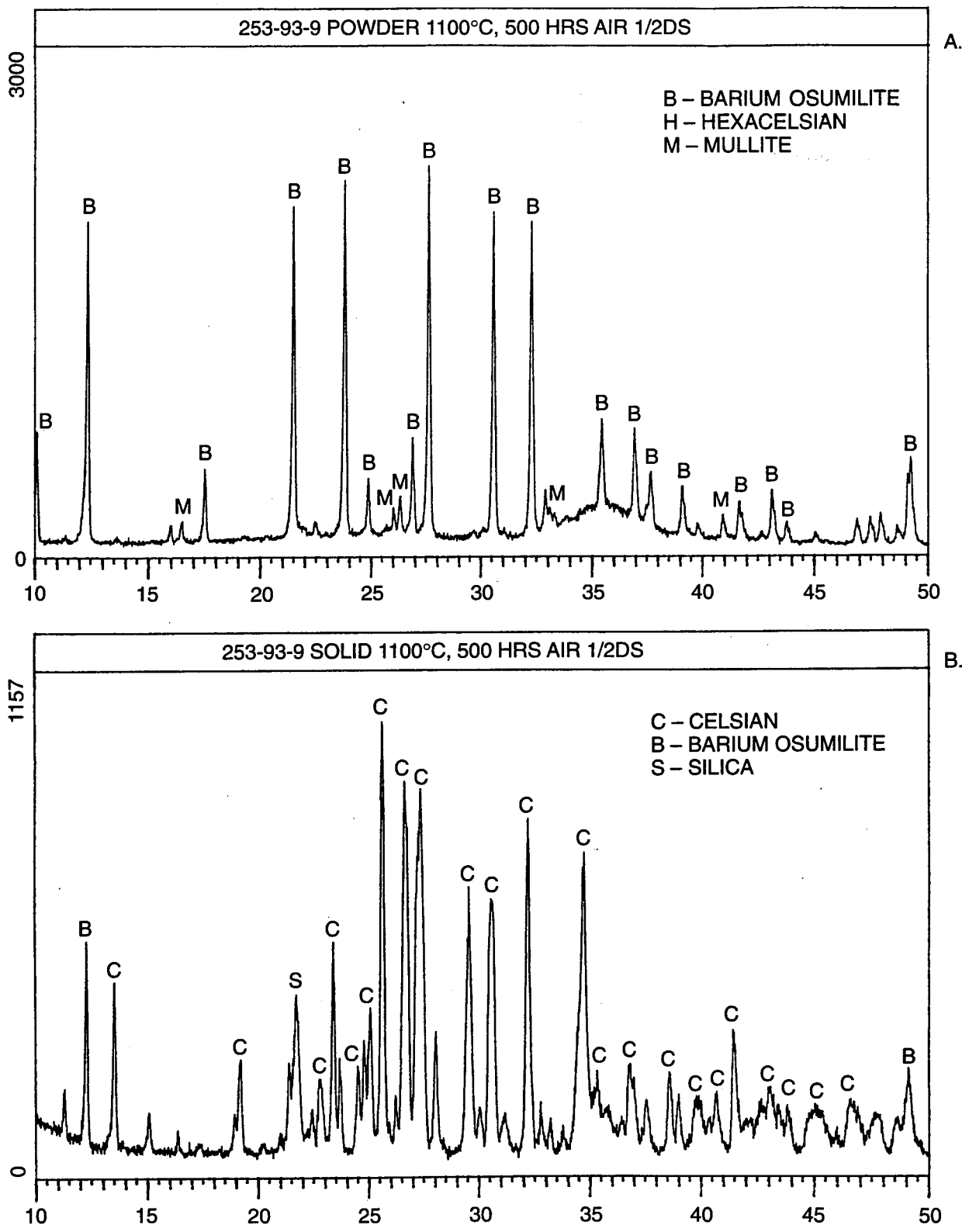

Figure 27 X-ray Diffraction Patterns for BMAS/BN/Nicalon Fiber Composite #253-93 After 1100°C, 500 Hrs, Air, (A) Powdered, (B) Surface

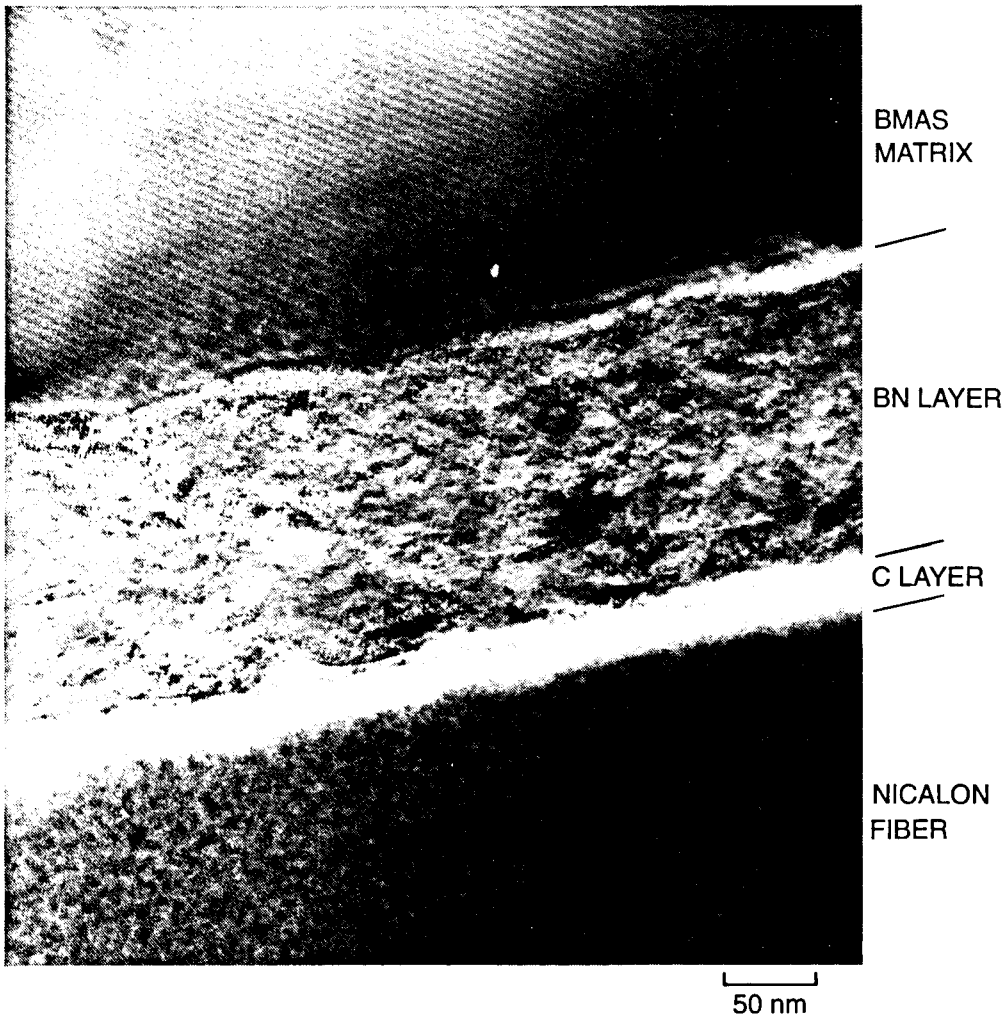

Figure 28 TEM Thin Foil Analysis of Interfacial Region of BMAS Matrix/BN Coated Nicalon Fiber Composite #253-93, After 1100°C, 500 Hrs, Air (90° Fiber)

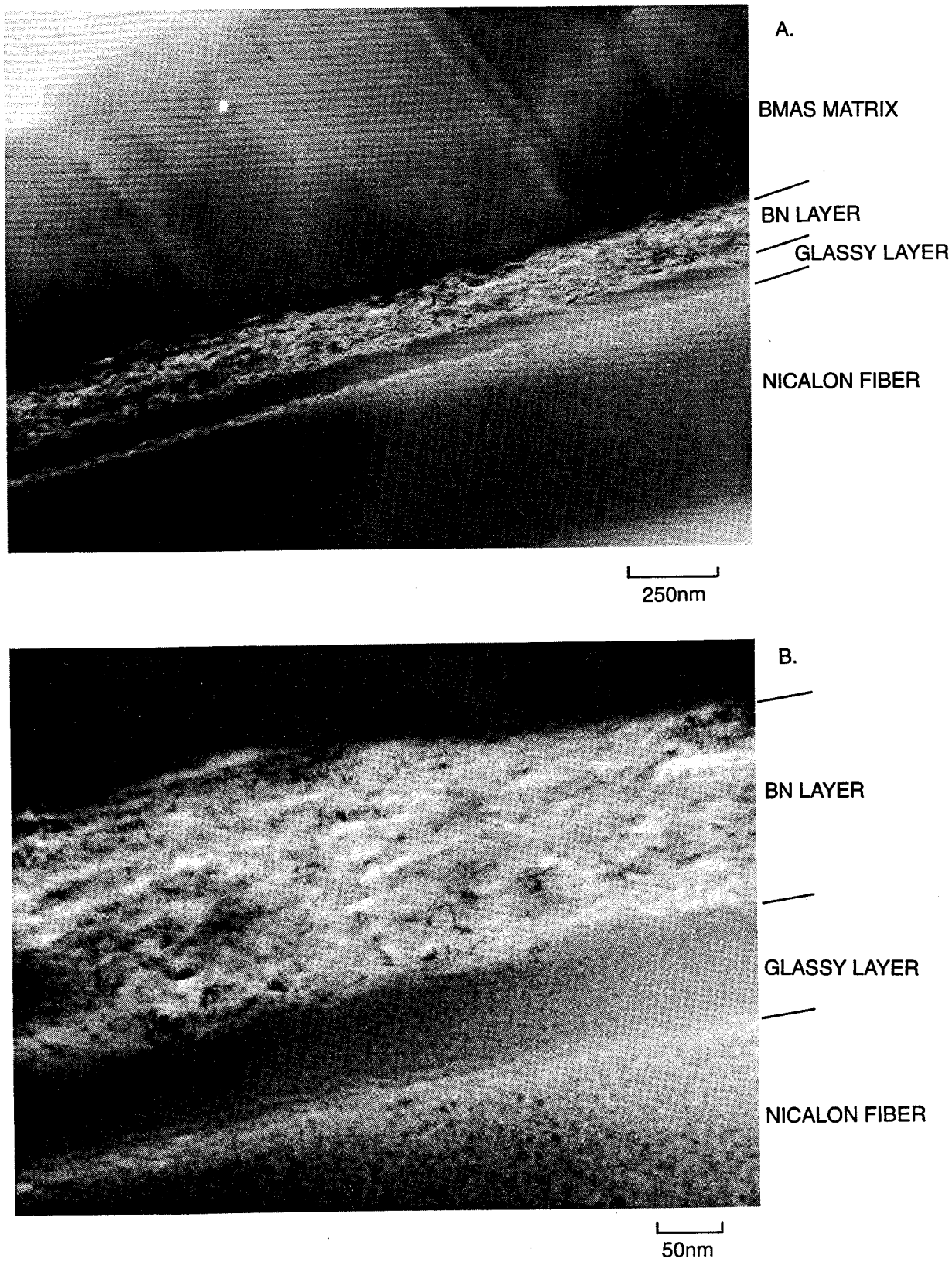

Figure 29 TEM Thin Foil Analysis of Interfacial Region of BMAS Matrix/BN Coated Nicalon Fiber Composite #253-93, After 550°C, 500 Hrs, O_2 (90° Fiber)

PG315.30

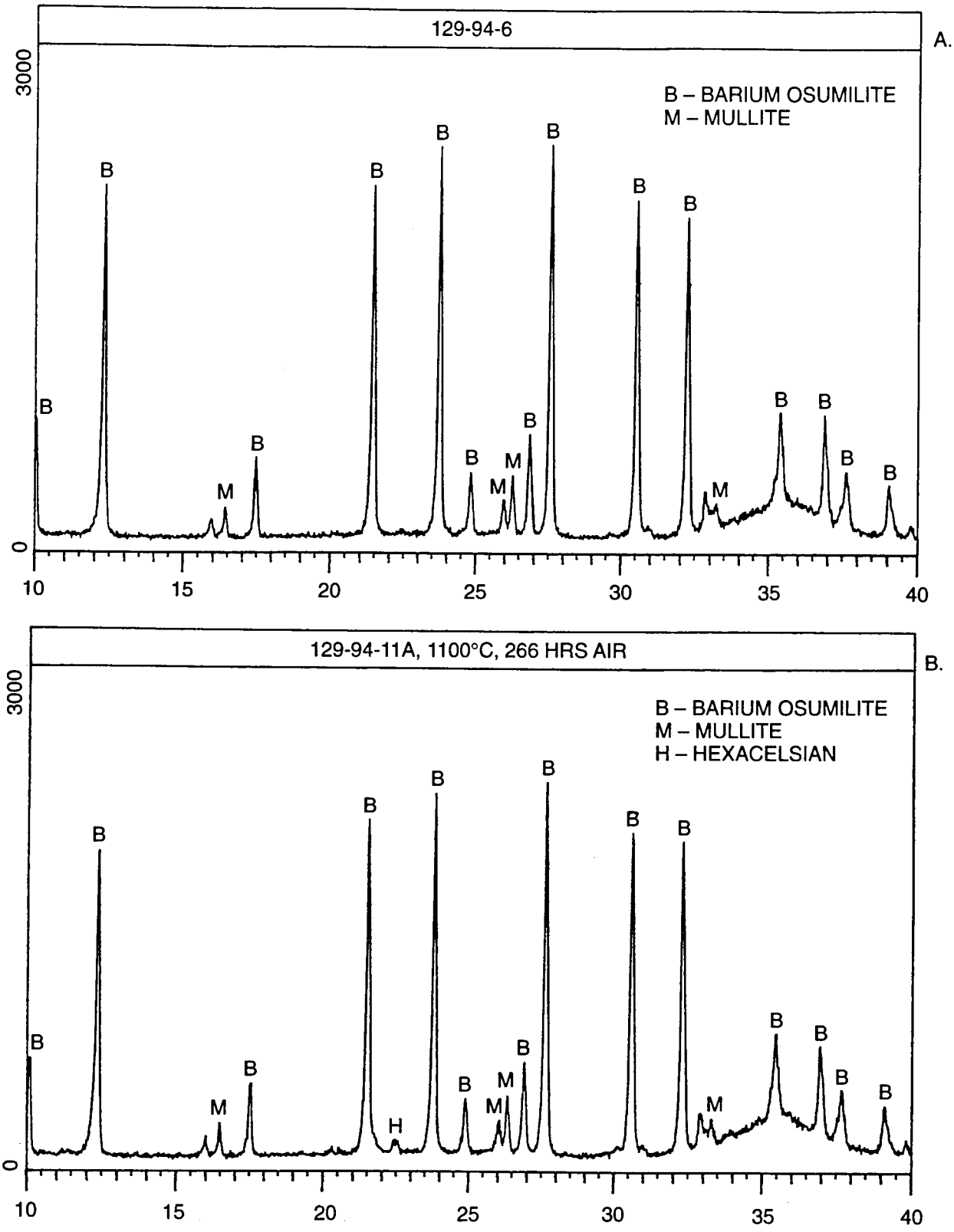

Figure 30 X-ray Diffraction Patterns for Modified BMAS Matrix/SiC/BN/Nicalon Fiber Composite #129-94 (A) As-Ceramed, (B) After 1100°C, 266 Hrs, Air

APPENDIX I

FLEXURAL CREEP BEHAVIOR OF SiC/BN DUAL COATED NICALON FIBER REINFORCED GLASS-CERAMIC MATRIX COMPOSITES

Flexural Creep Behavior of SiC/BN Dual-Coated-Nicalon-Fiber-Reinforced Glass-Ceramic Matrix Composites

Ellen Y. Sun

Division of Engineering, Brown University, Providence, RI 02912

Steven R. Nutt

Department of Materials Science, University of Southern California,

Los Angeles, CA 90089-0241

John J. Brennan

United Technologies Research Center, East Hartford, CT 06108

submitted to:

Journal of the American Ceramic Society

June 15, 1994

11-29-94

Flexural Creep of Coated SiC Fiber-Reinforced Glass-Ceramic Composites

Ellen Y. Sun*
Division of Engineering, Brown University, Providence, RI 02912

Steven R. Nutt*
Department of Materials Science, University of Southern California
Los Angeles, CA 90089-0241

John J. Brennan*
United Technologies Research Center, East Hartford, CT 06108

Presented in part at the 18th Annual Cocoa Beach Conference and Exposition on Composites and Advanced Ceramics, Cocoa Beach, Florida, January 1994, Mechanical Behavior I - Fatigue and Creep in Ceramic/Ceramic Composites Symposium (Paper No. C-9-94F)

Supported by the Air Force Office of Scientific Research (contract F49620-92-0001) and by the National Science Foundation (EYS and SRN) through a Materials Research Group (grant DMR-9002994)

*Member, American Ceramic Society

Abstract

The creep and creep-rupture behavior of a continuous fiber-reinforced ceramic matrix composite was investigated. The materials were produced by incorporating SiC fibers into a barium magnesium aluminosilicate (BMAS) glass-ceramic matrix. The fibers were coated with a dual layer of SiC/BN designed to impart high fracture toughness as well as oxidative stability at high temperatures. Flexural creep and creep-strain recovery experiments were conducted at 1000°-1200°C under applied stresses of 100 - 670MPa using three-point and four-point loading fixtures. The steady state creep rates were extremely low (~10E-9 s^{-1}) and were relatively insensitive to stress and temperature below 1130°C. The creep-rupture strength of the composite at 1100°C was about 75-80% of the fast fracture strength, although creep-rupture occurred rapidly above 1160°C.. Creep-strain recovery experiments showed recovery of up to 90% under prolonged unloading. TEM observations of crept specimens indicated that the interface microstructure was stable under the stress-temperature conditions employed.

1. Introduction

Fiber-reinforced glass-ceramic composites are being developed for high temperature applications because of the inherent thermal and chemical stability of ceramics, the suitability of glass-ceramics to composite fabrication, and the benefits of fiber reinforcement.[1, 2] Critical to the success of fiber-reinforced ceramic matrix composites (CMCs) is the presence of a "weak" fiber/matrix interface that is also stable at high temperatures.[3, 4] Recently, CVD-coated fiber-reinforced glass-ceramic matrix composites have shown excellent mechanical properties and good thermal stability.[5] These composites are candidate materials for high-temperature structural applications, particularly in gas turbine engines. However, before the materials can be reliably used in structural applications at high temperatures, it is necessary to know and understand the long-term mechanical behavior, particularly the resistance to creep and fatigue. Under conditions of high temperature and applied stress, deformation, diffusion and interfacial reactions often occur, and these processes can lead to microstructural damage. Accumulation of microstructural damage degrades critical mechanical properties and eventually results in composite failure. Knowledge of the creep behavior is thus important both for material evaluation and as a basis for design of composite structures.

In recent years, research on the mechanical properties of fiber-reinforced composites has focused on fracture mechanisms and on improving room-temperature toughness. Relatively few studies have been carried out to determine the creep and creep-recovery behavior of these composites, especially at temperatures above 1000°C, the temperature range targeted for future applications. The objective of the present study is to determine the creep and creep-strain recovery behavior of a fiber-reinforced glass-ceramic composite. The creep deformation mechanisms are investigated by correlating the creep properties of the composite with those of the matrix material and the reinforcement, and also with macro- and microstructural observations of the crept samples.

2. Experimental Procedure

2.1 Material

(1) Composites

The composite material selected for the present study consisted of a barium-magnesium aluminosilicate (BMAS) matrix reinforced with small-diameter SiC fibers@ coated with dual layers of BN and SiC deposited by CVD. The SiC fibers are reportedly synthesized by pyrolysis of a polycarbosilane-type precursor, resulting in nanocrystalline grains (~2 nm) and excess carbon and oxygen.[6] The BN coating was applied to the fibers by CVD at 1000°C using a proprietary precursor# chosen to give an approximate composition of 40at% B, 40at% N, and 20at% C. Carbon was deliberately added to prevent decomposition and strength degradation of fibers during the process. The oxygen content of both the SiC and BN layers was measured by Auger spectroscopy to be <3%. The tensile strength of the coated fibers was 1860 ± 255 MPa. The BMAS matrix was formulated to yield the barium osumilite composition on crystallization ($BaMg_2Al_3(Si_9Al_3O_{30})$), following the procedures described in Reference 7. Composite panels (100 × 100 mm) were fabricated by hot-pressing a lay-up of 0/90° plies at 1450°C for 5 minutes under 6.9 MPa pressure, resulting in fiber loadings of ~50vol%. After hot-pressing, the composite panels were cut into bars and heat-treated in argon at 1200°C for 24 hours in order to crystallize (or "ceram") the BMAS matrix to the barium osumilite phase. Composites consisting of lay-ups of eight or sixteen alternating 0/90° plies were produced. The flexural and tensile properties of the 8-ply composite are listed in Tables 1(a) and 1(b) respectively.

(2) BMAS Glass-Ceramic

The unreinforced BMAS glass-ceramic samples were fabricated by the same procedure as the composites, although slightly different processing conditions were required. Hot-pressing

---

@ Product designation Nicalon NLM 102, from Nippon Carbon Co., Ltd, Tokyo.
# 3M Company, St. Paul, MN.

was performed under 6.9 MPa pressure at 1050°C for 10 minutes under 14 MPa pressure, instead of at 1450°C for 5 minutes. This modification was required because at 1450°C in the absence of fiber-reinforcement, the viscosity of the glass is too low to allow pressing without loss of material. The samples were then ceramed in argon at 1200°C for 24 hours, just as the composites were. The flexural properties of the BMAS glass-ceramic are listed in Table 2. The phase-distribution and the grain-morphology were slightly different from the composite matrix because of the different processing conditions and nucleation mechanisms. (In the composites, the fibers provide abundant nucleation sites for crystallization of the glass.) Barium osumilite was the dominant phase in the unreinforced glass-ceramic, although there was more cordierite and celsian than in the composite. Nevertheless, the glass-ceramic microstructure was sufficiently similar to the composite matrix to be useful as a control for the investigation of creep.

2.2 Creep experiments

(1) Composites

Creep experiments were performed in air using three-point and four-point bending fixtures in a dead-weight loading system. For four-point flexural creep experiments, specimens with eight 0/90° plies (~75.0×5.1×1.3 mm) and sixteen 0/90° plies (~75.0×5.1×2.7 mm) were tested. A fixture with outer and inner spans of 63.5 mm and 19.0 mm was used for specimens 2.7 mm thick, while for specimens 1.3 mm thick, a fixture with outer and inner spans of 40.0 mm and 19.0 mm was used. Creep experiments were conducted at 1000°C to 1200°C under applied stresses of 100 MPa to 670 MPa. For three-point flexural creep experiments, specimens with sixteen 0/90° plies (~75.0×5.1×2.7 mm) were tested and a fixture with an outer span of 63.5 mm was used. Creep experiments were conducted at 1100°C and 1200°C with applied stresses of 100 MPa to 670 MPa. In both cases, the deflection was measured directly at the specimen so that creep effects in the loading rollers and the load train had no influence on the measurement. The displacement of the specimen was monitored with a linear variable-differential transducer. A

linear elastic analysis was employed to calculate the corresponding stress and strain values, based on the assumption that the stress gradient began and remained linear during the test.[8] All stresses reported were equal to the magnitude of the maximum outer-fiber stress. Because the analysis used is appropriate only for small deflections (~1-2% outer-fiber strain), the experimental creep strains generally were kept within this range, except for creep-rupture experiments. A plot of strain versus time was used to determine that a constant creep rate (or minimum strain rate) was reached and maintained. The stress (or the temperature) was then changed incrementally, and the procedure was repeated. Upon completion of a test, samples were cooled rapidly at an approximate rate of 50°C/min under constant load in an effort to retain the deformed microstructure.

The creep-strain recovery behavior of the composite was investigated by loading-unloading experiments. The specimens were first crept, then unloaded instantaneously and held at a stress of 10 MPa for 5 to 24 hours. A single experiment usually included two or three cycles.

(2) BMAS Glass-Ceramic

Three-point flexural creep experiments were performed on the glass-ceramic samples. The dimension of the specimens was ~100.0×5.1×3.4 mm. A fixture with outer span of 63.5 mm was used. Creep experiments were conducted at 1100°C to 1200°C under applied stresses of 40 to 130 MPa.

2.3 Macro- and microstructural observations

Direct observations of the crept specimens were made using optical microscopy. The microstructures of the crept specimens were studied using analytical and high-resolution transmission electron microscopy (HRTEM). Thin foils for TEM were prepared in a conventional manner by mechanical polishing, dimpling and ion milling. Specimens were examined using a JEOL 2010 microscope fitted with a Noran X-Ray spectrometer capable of light-element detection.

3. Results and Discussion

3.1 Flexural Creep Behavior

(1) Composites

A series of four-point flexural creep experiments were performed at constant temperature and incrementally increased stress to study the creep behavior of the composite over a wide range of stresses. The creep data from a typical experiment conducted at 1100°C is presented in Figure 1. The specimen was 1.3 mm thick in this case. For each value of stress, a brief (4-5 hours) period of transient creep was followed by a long period in which the creep rate was apparently constant. The creep rates during these prolonged periods were in the 10^{-9} s^{-1} range, and because the rates were so low, the stress dependence of the creep rate could not be accurately measured. For this sample, creep-rupture occurred at 560 MPa. Similar creep behavior was observed for thicker specimens (2.7 mm in thickness), except that thicker specimens tended to fail at lower stress levels (~400MPa). The fast fracture strength for thin and thick specimens was 760 and 500 MPa, respectively. Thus, both thick and thin samples failed in flexural creep at ~75-80% of the fast fracture strength.

The peculiar creep behavior presented in Figure 1 was unexpected. To test the validity of the measured strain rates and to explore possible effects of loading geometry, three-point flexural creep experiments were conducted under similar conditions. The results from three-point bending tests were consistent with those from four-point tests. The strain-time curves were similar in shape and the measured creep rates were also in the 10^{-9} s^{-1} range. The specimens, which were 2.7 mm thick, typically failed at ~400 MPa, just as in the four-point flexure experiments. In addition to flexural creep experiments, a tensile creep experiment was conducted in air at 1100°C under an applied stress of 103 MPa.[9] The specimen survived the 266 hour-test and the steady-state creep rate also was in the 10^{-9} s^{-1} range. Thus, the results from the four-point flexural creep experiments were deemed reliable.

The effect of temperature on creep rate was also investigated. Figure 2 shows the result of an experiment conducted under a constant stress of 250 MPa, periodically increasing the temperature in 30°C increments. The specimen was held for at least 24 hours at each temperature level. From 1000°C to 1130°C, the nominally constant creep rates were all on the order of $10^{-9}s^{-1}$, while creep-rupture occurred quickly above 1160°C at this stress level (250 MPa). An attempt to determine an activation energy for creep from an Arrhenius plot of log(ε)-log(1/T) was inconclusive because the creep rates were so low that differences between them were undetectable. However, there was clearly an effect of temperature that became apparent above ~1150°C. For example, at 1200°C, the steady-state creep rates of the composites were in the 10^{-8} s^{-1} range, an order of magnitude larger than those at 1100°C. Furthermore, the creep-rupture strength at 1200°C was only half of that at 1100°C and 45% of the corresponding fast fracture strength. These results indicate a critical temperature between 1130°C and 1160°C, above which the flexural creep properties of the composite degrade significantly.

(2) BMAS Glass-Ceramic

The BMAS glass-ceramic was extremely brittle and exhibited negligible strain-to-failure in flexural creep experiments. Upon loading, a constant strain rate was obtained after a period of transient deformation. The constant strain rates were in the range of 10^{-9} s^{-1} at all stress levels from 40 to 115 MPa. At ~130 MPa, the samples failed catastrophically. By fixing the applied stress and incrementally increasing the temperature from 1100°C to 1200°C, the softening temperature of the BMAS glass-ceramic was found to be ~1140°C.

The creep deformation mechanisms of the composite were studied by correlating the creep properties with those of the matrix material and the reinforcement. The tensile creep behavior of the SiC fibers at high temperatures was first investigated by Simon and Bunsell.[10] Using the same SiC fiber (NLM 102 Nicalon), they found that there existed a temperature-dependent threshold stress for creep in the 1100-1300°C temperature range. Below the threshold stress, the

creep rates were lower than 10^{-8} s^{-1}, while above the threshold, the creep rates were in the range of 10^{-8} s^{-1}. The threshold stresses for tensile creep at 1100°C and 1200°C were 600 MPa and 50 MPa, respectively. Comparing their data with the results presented here, it appears that the creep behavior of the composite is controlled by the creep response of the SiC fibers. For example, at 1100°C, the creep-rupture strength of the composite was below the threshold stress for fiber creep, and presumably the SiC fibers did not undergo appreciable creep. Most if not all of the deformation that occurred in the fibers was elastic, resulting in composites with creep rates comparable to the fibers (~10^{-9} s^{-1}). On the other hand, most of the stress levels investigated at 1200°C were above the threshold stress (50 MPa), and the composite creep rates were comparable to those of the fibers alone (~10^{-8} s^{-1}). The difference in the reported threshold stress for fiber creep at 1100°C and 1200°C indicates that the fibers are less resistant to creep at 1200°C. This phenomenon, plus the fact that the observed softening temperature of the BMAS glass-ceramic was ~1140°C, resulted in degradation of the composite creep properties at 1200°C.

Creep behavior of composites similar to those studied in the present work has been reported in the literature, and comparisons provide useful insights. For example, flexural and tensile creep experiments have been conducted on calcium aluminosilicate (CAS) composites reinforced with 0° and 0/90° SiC fibers, resulting in transient creep behavior (decelerating creep rates) for all stress levels employed.[11] Unlike the composites used in the present study, however, the fibers were uncoated, and the test temperature was slightly higher (1200°C).[11-13] During creep deformation, abnormal grain growth reportedly occurred in the SiC fibers, initiating at the interface and advancing radially inward. If a diffusional creep mechanism is assumed, an increase in the average fiber grain size should reduce the creep rate of the fibers, contributing to the transient decrease observed in the creep rate of the composite. Recent work has revealed that microstructural changes such as grain growth in embedded fibers are stimulated by diffusion of oxygen and/or other matrix species from the matrix.[14] However, in the present study, abnormal grain growth was prevented by the fiber coatings, which effectively prevented diffusion across

the interface. As a result, the fiber microstructures were stable for long-term exposures up to 1200°C (section 3.4). Thus, the differences in creep response between the CAS composites and the BMAS composites studied here can be attributed partly to the dynamic changes in fiber microstructure that occurred in the former material.[11] Multiple processes may be occurring during the initial period of primary creep. The weak BN coating applied to the fibers in this study may allow stresses to redistribute efficiently during initial loading, leading to a constant creep rate after a relatively short period (4-5 hours) of transient creep. In addition, provided the stress and temperature are sufficient, matrix flow can permit the fibers to straighten upon loading.

3.2 Creep-Strain Recovery Behavior of the Composites

The creep-strain recovery behavior of a composite provides an indication of the amount of recoverable deformation introduced during a loading period as well as indicating how a simple loading history of practical relevance influences the accumulated creep strain. A sample time-strain curve for two loading-unloading periods is shown in Figure 3. During loading, the total deformation consists of an instantaneous deformation (ε_{in}) and the creep deformation (ε_{cr}). During unloading, the deformation recovered instantaneously is $\varepsilon_{in,\ R}$, while the (time-dependent) creep-strain recovery is $\varepsilon_{cr,R}$. The creep-strain recovery ratio R_{cr} has been used to quantify the amount of creep-strain recovery that occurs during unloading. R_{cr} is defined as the creep-strain recovered during a particular unloading cycle divided by the creep strain for the cycle.[15]

$$R_{cr} = \varepsilon_{cr,R} / \varepsilon_{cr} \qquad (1)$$

The creep and strain recovery behavior of the BMAS composite was studied through loading-unloading experiments. Figure 4 shows the results of a typical creep-recovery experiment involving three cycles with increasing loads for each cycle. (The specimen was 2.7 mm thick and typically failed at about 400 MPa.) For the first cycle, the instantaneous

deformation (ε_{in}) upon loading was larger than the strain recovered upon unloading ($\varepsilon_{in,\,R} + \varepsilon_{cr,\,R}$), implying that permanent deformation occurred during loading. The permanent deformation was caused primarily by matrix cracking and crack propagation along the fiber/matrix interface, because both the stress and strain levels (222 MPa and ~0.40%) were well above the failure strength and the failure strain of the BMAS glass-ceramic (~110 MPa and 0.13%). The creep-strain recovery ratio was about 55% for the first two cycles (unloaded for 5.6 hours), and 70% for the third cycle, for which the unloading period was 20 hours. In recent creep recovery experiments on similar composites, Wu and Holmes reported a 49% creep-strain recovery ratio for 0/90° SiC fiber reinforced CAS composites during tensile creep at 1200°C in argon.[12] Figure 5 shows the creep and strain recovery for three cycles using identical loads but different unloading periods. The creep-strain recovery ratios were different for the three cycles. For the first cycle, which had the shortest unloading period, R_{cr} was 50%. For the second cycle, the unloading period was nearly three times as long, and R_{cr} was 58%. This recovery ratio was similar to the recovery observed in Figure 4 for the same applied stress (222 MPa). The third cycle involved a longer recovery period, and the measured recovery ratio was 91%.

The large creep-strain recovery observed in this composite system derives from several factors, including the creep properties of the constituents, the interfacial bonding, and the fiber distribution. For example, at 1100°C, the stress applied to the composite generally was below the threshold stress for fiber creep. Consequently, the SiC fibers deformed elastically while the matrix underwent creep. Upon unloading, elastic contraction of the fibers supplied a driving force for recovery. Because the temperature of the composite was maintained after unloading, the fibers and the matrix relaxed, resulting in anelastic strain recovery of the composite. The recovery process was also affected by the degree of interfacial debonding that in turn, controlled the load transfer between the fibers and the matrix. In this composite system, the BN layer provided a weakly bonded interface that also achieved effective load transfer, reducing the time needed to reach stress equilibrium between the fibers and the matrix. Holmes and Wu recently

reported that significantly more strain recovery could be obtained from 0/90° composites than from unidirectional composites.[16] They concluded that the 90° (transverse) fibers provided significant resistance to axial creep deformation through lateral constraint. Thus, in the present study, residual stresses in the transverse direction should also contribute to the driving force for axial contraction upon unloading.[16] However, large strain recovery is only obtained when the applied stress during loading is low or moderate. If the stress level is close to the failure strength, extensive microstructural damage is generally introduced during the loading period. Such damage results in permanent strain that cannot be completely recovered during unloading. This can be shown by comparing the R_{cr} value of the third cycle in these two cases. For an applied stress of 303 MPa, or ~75% of the ultimate strength, only 69% of the creep-strain was recovered after a 20-hour unloading period, while for 222 MPa applied stress (~55% of the ultimate strength), 91% recovery was obtained after a 25-hour unloading.

3.3 Failure Features of the Composites

Microscopic examination of the creep-ruptured specimens revealed the distribution of damage in creep-rupture samples. Failure consistently occurred under the load pins during both four-point and three-point creep-rupture experiments. Figure 6 shows that beneath the loading points, transverse cracking and delamination cracking initiated in the 90° plies and propagated through the matrix into the 0° plies, resulting in fiber/matrix debonding. The composite eventually failed by fiber rupture with extensive fiber pull-out in the 0° plies. The stress concentration under the loading pins became progressively severe as damage accumulated, although our results indicate that extensive fiber rupture occurred only at the highest stress levels.

Composite failure under three-point loading involved formation of a hinge under the loading pin. At 1200°C, the creep-rupture strength of the composite was ~240 MPa, although hinge formation was observed at lower stress levels (212 MPa). The profile of a typical creep-rupture sample is shown in Figure 7(a). Fiber buckling on the compression side of the sample was often observed in the top ply. A similar specimen crept at 1200°C under 184 MPa applied

stress was uniformly bent with no hinge formed under the load pin, as shown in Figure 7(b). In general, hinge formation did not occur until the applied stress approached the ultimate strength of the composite, leading to the conclusion that at stress levels lower than ~70% of the creep-rupture strength, the aforementioned linear elastic analysis could be applied to obtain valid flexural stress and strain values.

3.4 TEM Observations of Composites after Creep Tests

The microstructure of the crept specimens was examined by transmission electron microscopy. Oxidation was generally confined to the near-surface region and the reacted layer was less than 30 μm thick. No major changes were observed in the sample interiors (beneath the near-surface region). Figure 8 shows a typical interface region after creep at 1100°C. Both the BN coating and the SiC overlayer are intact and show no evidence of change from the pre-tested condition. Likewise, the fiber shows no evidence of grain growth or reaction with the matrix or coating. The only change apparent in such images is the formation of subtle dual sublayers at the fiber/BN interface, evident as light and dark strips. These nano-scale layers were carbon-rich (fiber side) and silica-rich (BN side) respectively and were produced by a carbon-condensed solid state oxidation reaction.[17] Occasionally, slight coarsening of the BN layer occurred because of matrix element diffusion or liquid infiltration, possibly through cracks in the SiC overlayer.[17] Analysis of SAD patterns and EDS spectra indicated that neither the microstructure nor the composition had changed significantly in the SiC fiber, the BN coating, the SiC coating or the matrix during creep at 1100°C. These observations indicate that the composite microstructure was stable under the stress-temperature conditions employed.

4. Conclusions

The flexural creep and creep-rupture behavior of dual-coated fiber-reinforced glass-ceramic composites was investigated. At temperatures up to 1130°C, the constant creep rates were in the range of $10^{-9}s^{-1}$, while at 1200°C, the constant creep rates were an order of magnitude larger. At 1100°C, the composite failed in flexural creep at ~75-80% of the fast fracture strength.

The 0/90° fiber-reinforced composites exhibited large creep-strain recovery, indicating that the creep deformation of the composites was viscoelastic. Furthermore, the results suggest that creep strains can be totally recovered after long-term heat-treatment at high temperatures and under zero loading condition, provided that the applied stress is sufficiently low to prevent extensive microstructural damage during initial loading and subsequent creep.

The dual SiC/BN coating applied to the SiC fibers provided an effective barrier to reaction and diffusion, resulting in composites that were microstructurally stable under long-term exposure to high temperatures and stresses. In addition, the BN coating has proven to provide the desired weak interfacial bond between the fibers and the matrix. Under low and moderate applied stress, this interfacial layer allows stress redistribution to occur efficiently. During initial loading, stress redistribution leads to steady-state creep after a brief transient, while during prolonged unloading, it results in large strain recovery. On the other hand, when the applied stress is close to the ultimate strength of the material, the BN coating allows debonding to occur, resulting in extensive fiber pull-out. These energy-absorbing processes contribute to the good toughness of the composite, as reported previously.[5] The results described here lead to the conclusion that the dual coating of fibers constitutes a valid approach to design interfaces in continuous fiber-reinforced composites, resulting in a combination of good toughness, strength and creep resistance.

An additional outcome of the present work concerns the experimental technique. Tensile creep experiments provide important information about composite behavior, although there are usually substantial technical difficulties associated with the experiments, as well as high costs. Flexural creep experiments, on the other hand, are intrinsically problematic because of the more complex stress state, but are attractive because of the simplicity of the testing procedure and

sample preparation. For the stress-temperature conditions employed in the present study, both loading methods yielded extremely low strain rates that were difficult to measure accurately. Improved extensometry would be valuable to future investigations of fiber-reinforced ceramics. While experiments could easily be conducted at higher temperatures to achieve larger strain rates, the kinetics for oxidation of the fiber and coatings are also much more rapid, and the fiber is also more susceptible to recrystallization. Consequently, the microstructure rapidly becomes unstable at extremely high temperatures. Creep experiments in controlled (non-oxidizing) atmosphere are currently being planned to evaluate the effect of oxidation on creep behavior.

Acknowledgments

The authors would like to thank Mr. Jim O'Kelly of 3M for coating the Nicalon fibers used in the study, Mr. Stan Kustra of UTRC and Mr. Gary Linsey of Pratt & Whitney for the composite flexural and tensile testing respectively, and Dr. Alexander Pechenik of the Air Force Office of Scientific Research for sponsorship of this program.

References

[1]K. M. Prewo and J. J. Brennan, "High Strength Silicon Carbide Fiber-Reinforced Glass Matrix Composites," *J. Mat. Sci.*, **15**, 463-468 (1980).

[2]K. M. Prewo and J. J. Brennan, "Silicon Carbide Fiber Reinforced Glass-Ceramic Matrix Composites Exhibiting High Strength and Toughness," ibid., **17**, 2371-2383 (1982).

[3]J. J. Brennan, "Interfacial Characterization of Glass and Glass-Ceramic Matrix/Nicalon SiC Fiber Composites"; pp 546-560 in *Material Science Research,* Vol. **20**, Plenum Press, New York, 1986.

[4]R. F. Cooper and K. Chyung, "Structure and Chemistry of Fibre-Matrix Interfaces in SiC Fibre-Reinforced Glass-Ceramic Composites: An Electron Microscopy Study," *J. Mat. Sci.,* **22**, 3148-60 (1987).

[5]J. J. Brennan, B. Allen, S. R. Nutt, and Y. Sun, "Interfacial Studies of Coated Fiber Reinforced Glass-Ceramic Matrix Composites"; *Annual Rept. R92-970150-1 on AFOSR Contract F49620-92-C-0001,* Nov. 30, 1992.

[6]S. Yajima, K. Okamura, T. Matsuzawa, J. Hasegawa, and T. Shishido, "Anomalous Characteristics of the Microcrystalline State of SiC Fibers," *Nature,* **279**, 706-707 (1979).

[7]K. M. Prewo, J. J. Brennan, and G. K. Layden, "Fiber Reinforced Glasses and Glass-Ceramics for High Performance Applications," *Am. Ceram. Soc. Bull.,* Vol. **65**, No. 2 (1986).

[8]E. M. Passmore, R. H. Duff, and T. Vasilo, "Creep of Dense, Polycrystalline Magnesium Oxide," *J. Am. Cer. Soc.,* **49** [11] 594-600 (1966).

[9]J. J. Brennan, S. R. Nutt, and E. Y. Sun, "Interfacial Studies of Coated Fiber Reinforced Glass-Ceramic Matrix Composites"; *Annual Rept. R93-970150-2 on AFOSR Contract F49620-92-C-0001,* Nov. 30, 1993.

[10]G. Simon and A. R. Bunsell, "Creep Behaviour and Structure Characterization at High Temperatures of Nicalon SiC Fibers" *J. Mat. Sci.,* **19**, 3658-70 (1984).

[11]C. H. Weber, J. P. A. Lofvander, and A. G. Evans, "The Creep Behavior of CAS/Nicalon Continuous-Fiber Composite," submitted to *Acta Metall. Mater.*

[12]X. Wu, and J. W. Holmes, "Tensile Creep and Creep-Strain Recovery Behavior of Silicon Carbide Fiber/Calcium Aluminosilicate Matrix Ceramic Composite," *J. Am. Cer. Soc.*, **76** [10] 2695-700 (1993).

[13]X. Wu and J. W. Holmes, "Static and Cyclic Creep Behavior of a SiC-fiber Glass-Ceramic Matrix Composite," to be submitted to *J. Am. Cer. Soc.*

[14]E.Y. Sun, "Microstructure and Mechanical Properties of Coated Fiber-Reinforced Glass-Ceramic Matrix Composites," *Ph.D Thesis*, Brown University, Providence, Rhode Island, 1994.

[15]J. W. Holmes, Y. H. Park and J. W. Jones, "Tensile Creep and Creep Recovery Behavior of a SiC-Fiber-Si_3N_4-Matrix Composite," *J. Am. Cer. Soc.*, **76** [5] 1281-93 (1993).

[16]J. W. Holmes and X. Wu, "Elevated Temperature Creep Behavior of Continuous Fiber-Reinforced Ceramics", in *Elevated Temperature Mechanical Behavior of Ceramic Matrix Composites*, edited by S. V. Nair and K. Jakus, Butterworth Hienneman, to be published in 1994.

[17]E. Y. Sun, S. R. Nutt, and J. J. Brennan, "Interfacial Structure and Chemistry of SiC/BN(C) Dual Coated Nicalon Fiber Reinforced BMAS Glass-Ceramic Composites"; to be published in *J. Am. Cer. Soc.*

Figure Captions

Figure 1 Strain vs. time curve of a 1.3 mm-thick specimen subjected to different stress levels at 1100°C (four-point).

Figure 2 Strain vs. time curve of a creep experiment performed with incrementally increased temperature and constant stress level (four-point).

Figure 3 Definition of some variables used to characterize the creep deformation and the strain recovery during loading-unloading experiments.[15]

Figure 4 Creep and strain recovery (four-point), with increasing loads for each cycle.

Figure 5 Creep and strain recovery (four-point), with same loads for each cycle.

Figure 6 Failure occurred at the loading points during creep-rupture experiment.

Figure 7 (a) Profile of a specimen creep ruptured at 212 MPa (1200°C, 3-pt). Notice hinge formed under the loading pin. (b) Profile of a specimen crept at 184 MPa without failure. No hinge formed.

Figure 8 Interfacial region in crept composites (1100°C, four-point).

Table 1(a). Flexural (3-pt) properties of 2D BMAS/SiC/BN/Nicalon fiber composites (8 plies)

Room Temp σ (MPa)				High Temp σ (MPa)		
as-pressed	ceramed	550°C, O_2, 100 hrs	1200°C, air, 500 hrs	1100°C	1200°C	1300°C
655	675	620	510	648	565	248

Table 1(b). Elevated temperature tensile properties of 2D BMAS/SiC/BN/Nicalon fiber composites (8 plies)

Temperature	UTS (MPa)	PL (MPa)	E (GPa)	ε_f (%)
1100°C	300	61	69	0.78
1200°C	294	28	62	0.88

Table 2. Flexural (3-pt) properties of the BMAS glass-ceramic.

Temperature	MOR (MPa)	E (GPa)	ε_f (%)
RT	137	100	0.14
1100°C	115	93	0.12

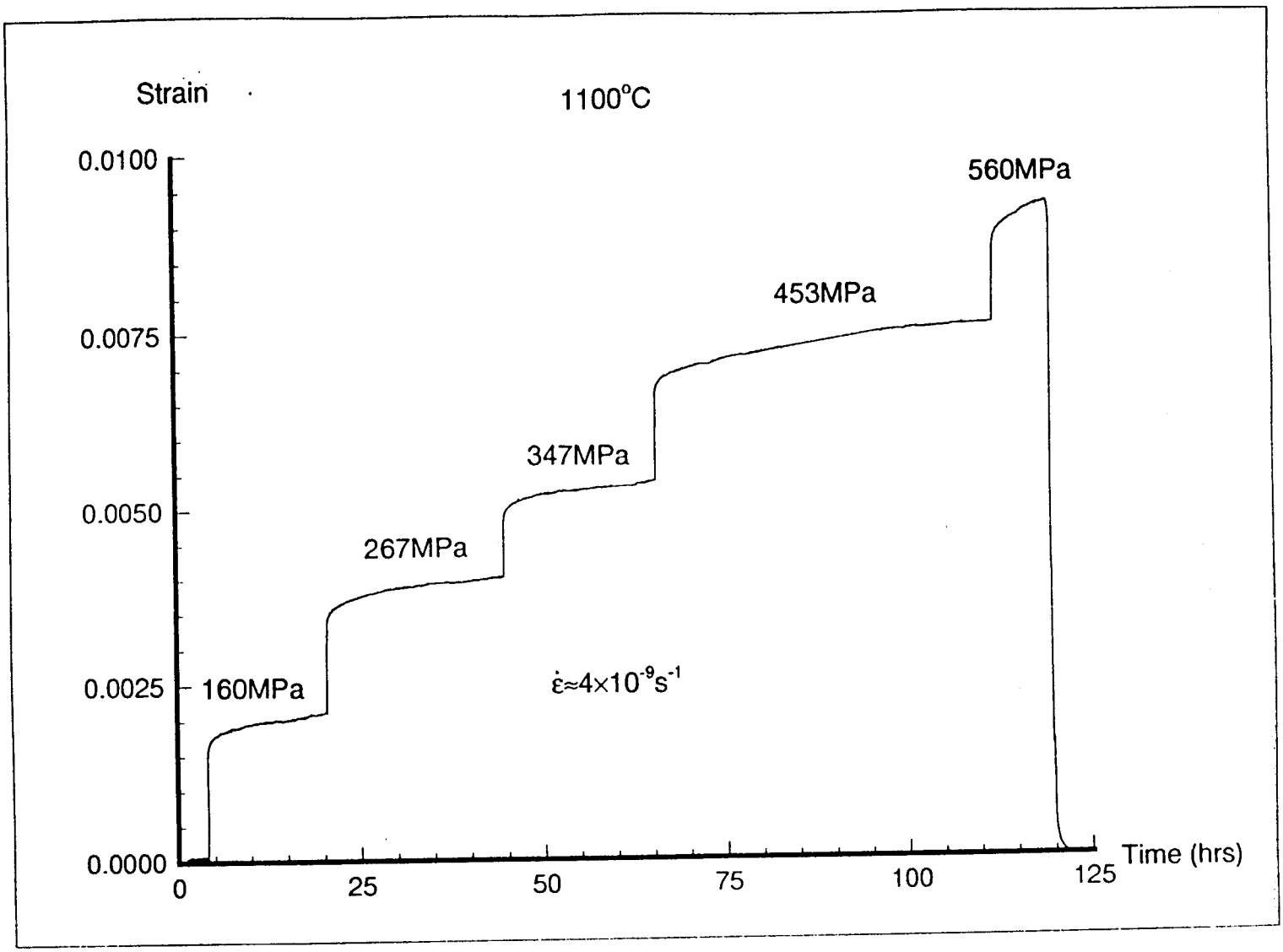

Fig. 1 Strain vs. time curve of a 1.3 mm-thick specimen subjected to different stress levels at 1100°C (four-point).

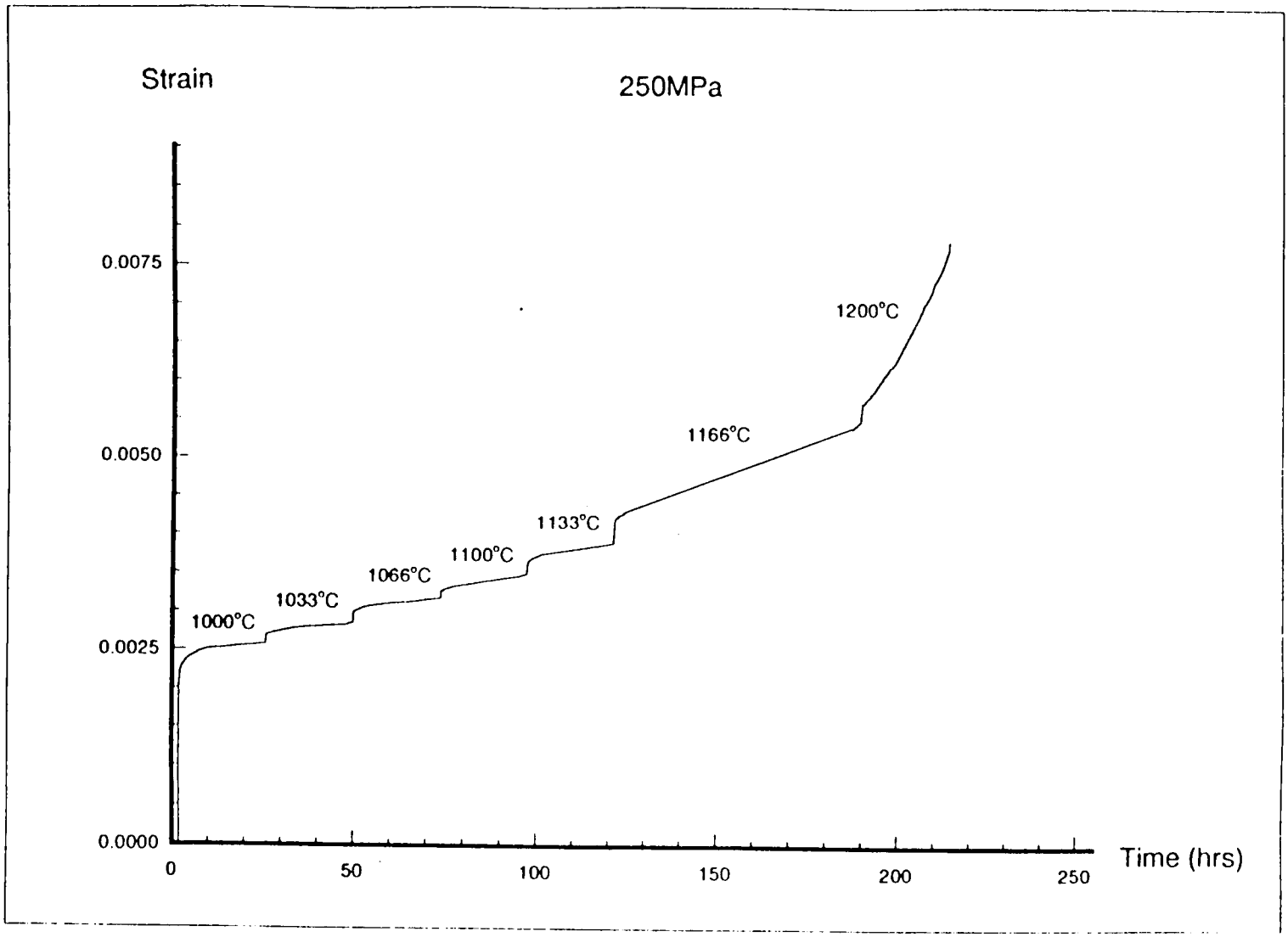

Fig. 2 Strain vs. time curve of a creep experiment with incrementally increased temperature and constant stress level (four point).

Creep Strain Recovery

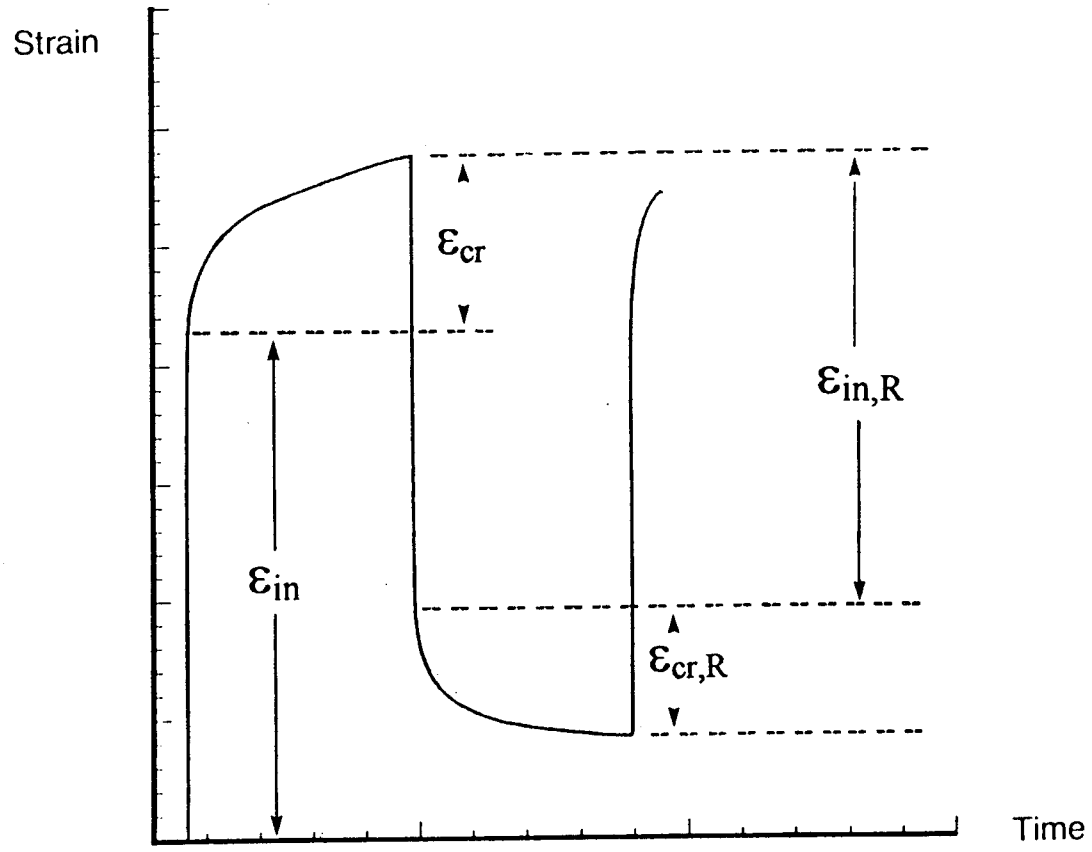

- the creep-strain recovery ratio: $R_{cr} = \varepsilon_{cr,R} / \varepsilon_{cr}$

Fig. 3 Definition of some variables used to characterize the creep deformation and the strain recovery during loading-unloading experiments.

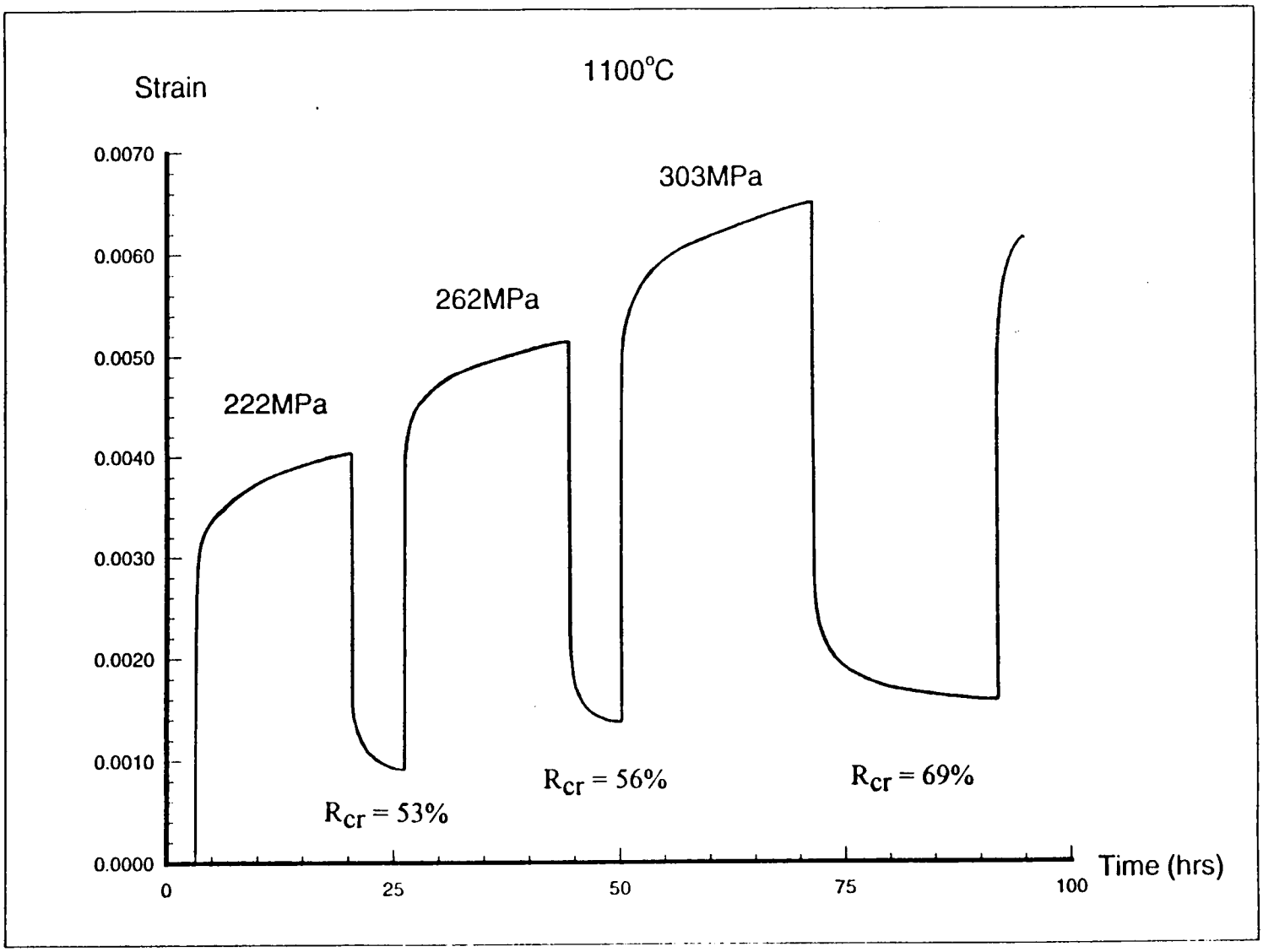

Fig. 4 Creep and strain recovery (four-point), with increasing loads for each cycle.

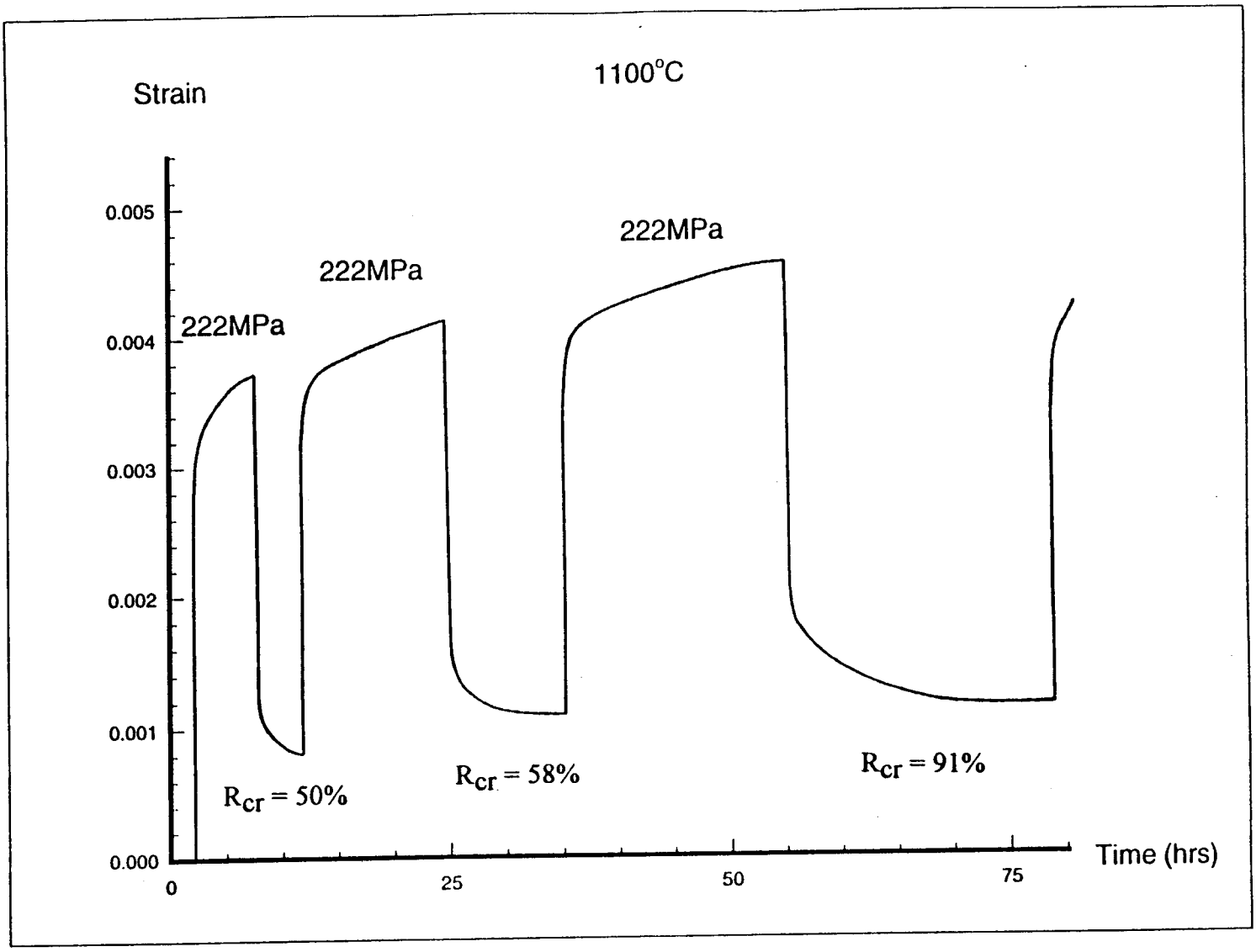

Fig. 5 Creep and strain recovery (four-point), with same loads for each cycle.

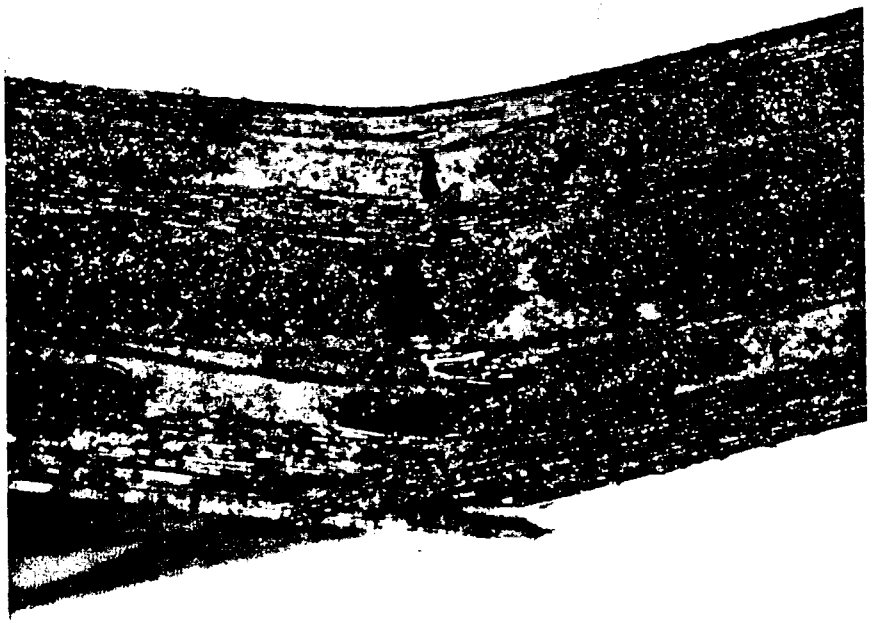

Fig. 6 Failure occurred at the loading points during creep-rupture experiment.

Fig. 7 (a) Profile of a specimen creep ruptured at 212 MPa (1200°C, 3-pt). Notice hinge formed under the loading pin. (continued)

Fig. 7(b) Profile of a specimen crept at 184 MPa without failure. No hinge formed..

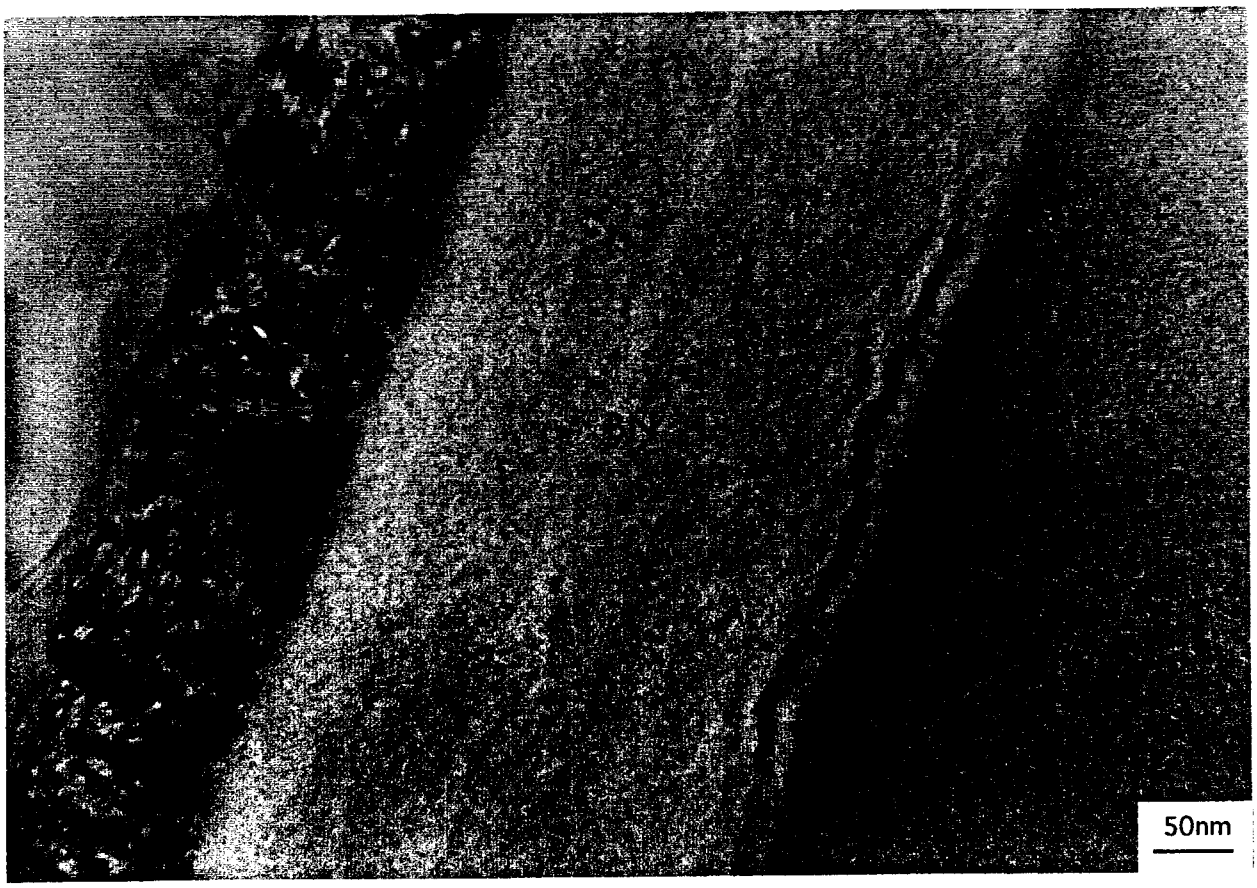

Fig. 8 Interfacial region in crept composites (1100°C, four-point).

APPENDIX II

HIGH TEMPERATURE TENSILE PROPERTIES OF COATED SiC FIBER REINFORCED GLASS-CERAMIC MATRIX COMPOSITES IN AEROBIC ENVIRONMENTS

High-Temperature Tensile Properties of Coated SiC Fiber Reinforced Glass-Ceramic Matrix Composites in Aerobic Environments

Ellen Y. Sun*
Division of Engineering, Brown University, Providence, Rhode Island 02912

Steven R. Nutt*
Department of Materials Science, University of Southern California, Los Angeles, California 90089-0241

John J. Brennan*
United Technologies Research Center, East Hartford, Connecticut 06108

Submitted to:

Journal of the American Ceramic Society

October 31, 1994

High-Temperature Tensile Properties of Coated SiC Fiber Reinforced Glass-Ceramic Matrix Composites in Aerobic Environments

Ellen Y. Sun*
Division of Engineering, Brown University, Providence, Rhode Island 02912

Steven R. Nutt*
Department of Materials Science, University of Southern California, Los Angeles, California 90089-0241

John J. Brennan*
United Technologies Research Center, East Hartford, Connecticut 06108

Presented in part at the 1994 TMS Annual Meeting, San Francisco, CA, February 1994, Control of Interfaces in Metal and Ceramic Composites Symposium.

Supported by the Air Force Office of Scientific Research (contract F49620-92-C-0001) and by the National Science Foundation (EYS and SRN) through a Materials Research Group (grant DMR-9002994).

*Member, American Ceramic Society.

Abstract

Tensile properties of an advanced glass-ceramic composite were investigated by conducting fracture, creep and fatigue experiments at both room temperature and high temperatures in air. The composites consisted of a barium magnesium aluminosilicate (BMAS) glass-ceramic matrix reinforced with SiC fibers with a SiC/BN coating. The material exhibited excellent tensile properties up to 1200°C. During monotonic tensile fracture tests, no degradation in ultimate strength was observed at high temperatures (1100 and 1200°C). Under long-term creep conditions at 1100°C, steady-state creep was established after a period of transient creep, with very low creep rates in the 10^{-9} s^{-1} range. Tensile fatigue experiments were conducted in which the maximum applied stress was slightly above the proportional limit stress of the matrix, and in these experiments, the composite survived 10^5 cycles at temperatures up to 1200°C. Microscopic failure mechanisms were investigated by TEM and microstructural observations were correlated with the mechanical behavior. The SiC/BN fiber coatings were stable at high temperatures and effectively inhibited diffusion and reaction at the interface. The BN layer also provided a weak interfacial bond which resulted in damage-tolerant fracture behavior. Limited oxidation of the SiC fibers occurred during prolonged exposure at high temperatures when oxygen diffused into the interior of the composite along microcracks. Under certain thermomechanical conditions, spinodal decomposition occurred in the intergranular glassy phase of the matrix.

1. Introduction

Fiber-reinforced ceramic matrix composites are being developed for potential use in gas-turbine engines, hypersonic airframes, and other applications involving high service temperatures and both static and dynamic loads. Ceramic materials are natural candidates for such applications because of the relatively low density and excellent thermal stability, although damage tolerance and brittle fracture would seem to be insurmountable limitations. However, ceramic composites have shown enhanced fracture toughness and higher damage tolerance compared to monolithic materials.[1, 2] Critical to the successful implementation of fiber-reinforced ceramic matrix composites in the aforementioned applications is the presence of a suitably weak fiber/matrix interface that is also stable at high temperatures.[1-5] High strength and toughness have been demonstrated in graphite fiber-reinforced composites and SiC fiber-reinforced composites with a carbon interfacial layer at room temperature.[1, 2, 6, 7] However, both of these materials are susceptible to oxidation during long-term elevated temperature exposure. Recently, research has been devoted to designing interfaces to improve the thermal stability of the composite, and several approaches have been investigated, including the use of fiber coatings and matrix doping.[8-10] However, approaches have achieved only modest success, and most of the basic research on failure mechanisms in CFCCs (continuous fiber ceramic composites) has been confined to studies of stress distribution during loading, and experimental work has been restricted to anaerobic ambients. Few studies have been conducted in aerobic ambients above 1000°C, despite the fact that this regime is the target for the future applications driving the development. Consequently, there has been little effort to correlate environmental effects and microscopic failure mechanisms of fiber-reinforced composites under the aforementioned thermal conditions.

Recently, an advanced composite material has been developed at United Technologies Research Center. Initial research indicated that this composite system exhibited high flexural strength and toughness, good flexural creep resistance, and good thermal and environmental stability up to 1200°C.[11-13] The objective of the present study was to assess the tensile

properties of this composite. Specifically, tensile fracture, tensile creep and tensile fatigue experiments were conducted in air at both room temperature and high temperatures. The composites were subjected to controlled stress and temperature conditions, and microscopic failure mechanisms were determined. In this systematic study, the role of thermal oxidation in fiber-reinforced composites is investigated, and the oxidation behavior under monotonic and cyclic stress conditions is compared.

2. Materials and Experimental Procedure

2.1 Composite fabrication

The matrix material selected for the present study was barium-magnesium aluminosilicate (BMAS), formulated to yield stoichiometric barium osumilite ($BaMg_2Al_3(Si_9Al_3O_{30})$) on crystallization. The reinforcement was a Si-C-O fiber (CG-Nicalon) with a dual SiC/BN coating. The coatings were deposited on the fiber by chemical vapor deposition, and the thicknesses of the SiC and the BN layers were approximately 100 and 300 nm respectively. The BN coating had an approximate composition of 40at% B, 40at% N, 17% C and 3at% O. Carbon was deliberately added to the BN precursor to minimize reactivity during deposition between the BN and the Nicalon fibers. The SiC overcoat was applied to the BN-coated fibers to prevent boron diffusion into the matrix during composite fabrication. The oxygen content of both the SiC and the BN layers was found to be <3% as determined by Auger spectroscopy. The measured tensile strength of the coated fiber (2220±565 MPa) indicated that essentially no degradation in ultimate strength was caused by the coating.

Composites were fabricated by hot-pressing a layup of 0/90° plies at 1450°C for 5 minutes under 6.9 MPa pressure. The resulting composites were generally greater than 98% of theoretical density at the completion of this process, and the resulting fiber loading was ~50vol%. After hot-

pressing, the panels were cut into tensile and flexural test samples and ceramed in argon at 1200°C for 24 hours, in order to crystallize the BMAS matrix to the barium osumillite phase. After ceraming, the amount of residual intergranular glassy phase in the BMAS matrix was about 3-5 vol%.

2.2 Mechanical testing

All of the mechanical testing was conducted in air. Uniaxial tensile experiments were performed at 20°C, 1100°C and 1200°C. The load was increased at a rate of 0.05 cm/min until fracture occurred. Tensile creep experiments were performed at 1100°C. In these experiments, specimens were gripped outside the hot zone.

Tension-tension fatigue testing was conducted at room temperature, 1100°C and 1200°C. The loading apparatus consisted of an articulated gripping system, $MoSi_2$ susceptor heating, and quartz rod extensometry, all of which were on a closed loop servohydraulic testing system. The gripping system consisted of cold pin-loaded friction grips. All tests were conducted at a stress ratio of 0.1. The samples were subjected to 10^5 cycles or until failure occurred, whichever came first. The frequency was between 2-3 Hz, which resulted in a 10^5 cycle runout time of 9-13 hours. An acoustic emission sensor (70-150 KHz resonant frequency) was mounted on the cold grip, and the signal was sent to a PAC Loron 320 system for data acquisition and analysis. In addition, the cycle count signal was sent from the waveform generation to the PAC system so that acoustic emission activity could be correlated with each cycle.

2.3 Composition and Microstructure observations

The fracture surfaces of tensile tested samples and of samples failed during creep and fatigue experiments were examined using scanning electron microscopy (SEM). Structural analysis of tensile creep samples was conducted using X-ray diffraction, and the results were compared with the as-ceramed composites. Microstructures of the composites were characterized using transmission electron microscopy (TEM). Thin foils were sectioned from ~5mm below the

fracture surface in fractured samples. Sections taken closer to the fracture surface were prohibitively fragile, implying an extensive damage zone. Specimens were prepared in a conventional manner by mechanical polishing, dimpling and ion milling. Thinned sections were examined using a JEOL 2010 microscope equipped with a thin-window X-ray spectrometer and a Gatan parallel detection electron energy loss spectrometer (PEELS). The local composition of selected regions of interest in TEM specimens was measured using energy dispersive spectroscopy (EDS) and PEELS. Probe sizes of 10 nm or 15 nm were used.

3. Results and Discussion

3.1 Tensile experiments

3.1.1 Tensile properties

The composite exhibited high ultimate tensile strengths at all test temperatures. Figure 1 shows stress-strain curves for tests conducted at 20°C, 1100°C and 1200°C respectively, and the tensile properties are listed in Table 1. In all cases, the composites exhibited elastic deformation upon initial loading, manifest as the linear part of the curve, from which the elastic modulus of the composite was determined. The stress at which the curve deviated from linearity marked the proportional limit (PL), normally attributed to initiation of microcracking in the matrix. Beyond the PL, the stress continued to increase, reaching an ultimate tensile strength (UTS) in the range of 230-300 MPa, whereupon the composites failed. Remarkably, no degradation in ultimate tensile strength was observed at high temperatures. The ultimate tensile strength and the strain-to-failure (ε_f) of the composites increased with increasing temperature, while the elastic modulus decreased. However, the proportional limit was unchanged from 20°C to 1100°C, and decreased by about 20% at 1200°C. The observed behavior is discussed in further detail in *Section 3.1.3*.

3.1.2 Fracture surface

The fracture surfaces of composite samples tested at 20°C (RT) and 1100°C were fibrous in nature, indicating extensive fiber pullout and crack deflection along interfaces during fracture (Figure 2(a)). These energy-absorbing processes enhanced the toughness of the composite. The length of the pulled-out fibers in the 0° plies was ~50-200 microns, and appeared slightly greater in the samples tested at high temperature. Further examination of the RT sample revealed that debonding occurred primarily in the coating layer, and fibers frequently showed regions in which the coating was partly debonded and partly adherent. The experiment at 1100°C lasted for about 20 minutes, during which time there was no dramatic change in the microstructure or degradation in strength or toughness. These observations indicate that a weak interfacial bond was achieved by the dual coating, as intended. The weak bond allowed transverse cracks in the matrix to be deflected along the fiber/matrix interface, resulting in strong and tough composites.

The fracture surface of the composite tested at 1200°C was quite different in appearance. A glassy, bubbly, surface layer was observed on the matrix regions of the fracture surface, as shown in Figures 2(b). The newly formed glass was porous, and the pores tended to be clustered around the 0° fibers. The formation of the glassy layer and bubbles are very likely a result of oxidation of the SiC fibers and the coating layers *after* composite failure, resulting in formation of siliceous glass and carbon monoxide gas. Before the fractured composite has time to cool, this glassy phase can penetrate into cracks and/or delaminations formed as a result of composite fracture.

3.1.3 Microstructure observations

Microstructural analysis of the tensile tested composites was conducted using TEM. Particular attention was paid to the fiber/matrix interfacial region and the intergranular glass phase in the BMAS matrix. Compared to the ceramed condition, no distinct changes were observed at the matrix-coating interface, the SiC-BN interface, or the BN-fiber interface in any of the tested samples. The SiC fibers, the BN coating and the SiC coating were stable during the experiments, except when exposed to air at the fracture surface and at microcracks. Debonding appeared to

occur primarily in the BN coating, an observation consistent with results described in the previous subsection.

Intergranular glassy phase was prevalent in the matrix and had important effects on the tensile properties of the composites. The BMAS matrix crystallized primarily to the barium osumilite phase, but contained ~3-5vol% residual glassy phase present as thin intergranular films, as shown in Figure 3. (The glass phase in this particular region is unusually thick.) The glass composition was measured by EDS and showed a conspicuous absence of magnesium, but was otherwise similar to the barium osumilite grains. At high temperatures (1100°C and 1200°C), these intergranular glass films became less viscous and facilitated boundary sliding. This phenomenon caused the matrix to soften and become more ductile, contributing to the observed decrease in modulus. The glassy phase also rendered the matrix more susceptible to damage processes, such as cracking and cavitation. In contrast, the strength of the Nicalon fibers was not expected to degrade appreciably at this temperature, particularly for the times involved.[14, 15] Because of the strength retention, the fibers carried most of the load, and the matrix carried relatively little. Thus the overall effect of matrix softening at high temperature was that the composite became less flaw sensitive, resulting in an increase in both ultimate tensile strength and strain-to-failure. However, increasing amounts of microstructural damage also contributed to a lower proportional limit.

A secondary phase was formed in samples tested at 1200°. Rectangular non-crystalline inclusions developed within barium osumilite grains.[16] The inclusions were approximately 35 nm in diameter, with broad facets along the (002) osumilite planes. The inclusions grew larger with increasing time at temperature, and cavities were occasionally observed to nucleate within them. Although the process by which the phase nucleates is presently unclear, these inclusions may be associated with the aforementioned depletion of magnesium, because like the intergranular phase, the inclusions tend to be magnesium deficient. These observations suggest that the BMAS matrix may not be stable under prolonged exposure to air at 1200°C, and this temperature may in fact constitute an approximate upper limit for BMAS-based composites in service applications.

3.2 Tensile creep

3.2.1 Creep properties

Tensile creep experiments were performed on composites at 1100°C and stress levels of 103 MPa and 138 MPa. The stress level of 103 MPa was slightly above the proportional limit stress at 1100°C (88 MPa). The tensile creep strain versus time curve is shown in Figure 4, along with a photograph of the as-tested sample. A transient creep mode in which the strain rate gradually decreased lasted ~50 hours (the data gap shown was caused by an electronic malfunction). The sample then experienced a very low constant creep regime that lasted until the experiment was terminated (without failure) at 266 hours. The measured creep rate in this regime was 8.32×10^{-4}% hr^{-1}, corresponding to a rate of 2.3×10^{-9} s^{-1}. A second sample was crept for 65 hours at 138 MPa, and failed when uploaded to 165 MPa. The creep behavior of this sample was similar to the first sample, and the creep rate after the transient regime was also ~10^{-9} s^{-1}.

The tensile creep behavior of the composite was similar to the behavior observed during flexural creep experiments conducted in air at 1100°C.[13] In both cases, a nominally constant creep rate in the range of 10^{-9} s^{-1} was measured after a period of transient creep. The extremely low creep rates are attributed to the fact that nearly all of the load is carried by the fibers, and the fibers are extremely resistant to creep under these stress-temperature conditions. In addition, the BN coating appears to provide the weak interfacial bond desired. Under low and moderate applied stresses, this interfacial layer may allow stress redistribution to occur efficiently so that a steady-state creep is established after a brief transient. Overall, the composite exhibits good creep resistance up to 1100°C at stress levels of ~50% of the ultimate strength.

3.2.2 Microstructural observations

Microstructural analysis of the tensile creep samples revealed a variety of changes in the interface microstructure. In the first sample, crept for 266 hours at 103 MPa, no gross changes were observed at the fiber/matrix interface in either the 0° or 90° plies, although a subtle

interlayer formed at the BN/fiber interface, as shown in Figure 5(a). Previous studies have shown that this interlayer results from a carbon-condensed oxidation of the SiC fiber.[12] The SiC coating, the BN coating and the SiC fibers were generally stable under the conditions employed. These observations were consistent with previous results from flexural creep experiments, which showed no major changes in the microstructure after flexural creep at 1100°C.[13] However, the interfacial microstructures in the second sample, which was crept for 65 hours at 138 MPa, then uploaded to 165 MPa, was quite different from the first sample. As shown in Figure 5(b), a porous reaction product was formed between the BN coating layer and the SiC fiber in the 90° plies. (The crack between the porous reaction product and the SiC fiber was formed during TEM specimen preparation.) Compositional analysis of the reaction product using EDS and PEELS revealed that the porous phase contained only silicon and oxygen, and microdiffraction patterns showed that it was non-crystalline. No compositional changes were detected in the adjoining BN coating or in the fiber interior. A gaseous product apparently evolved during the oxidation reaction, resulting in the observed porosity.

The formation of porous glass phase is believed to result from oxidation of fibers exposed to air during creep crack growth. During the latter creep test, the applied stress (138 MPa) was well above the proportional limit (88 MPa), inevitably causing matrix microcracking. Previous studies of similar composites have shown that cracking usually occurs in the BN layer or at the BN/fiber interface.[12] Thus, gaseous diffusion of oxygen along the crack path would lead to the passive oxidation reaction:

$$2\,SiC + 3\,O_{2\,(g)} \rightarrow 2\,SiO_2 + 2\,CO_{(g)} \qquad (1)$$

Such a reaction is consistent with the observed microstructure, in which the pores were caused by CO evolution, leaving behind porous silica. Oxidation of the SiC fiber was not observed in the composite crept at 103 MPa (without failure), evidently because of the low stress level and lower density of microcracks.

Although gross changes in the microstructure were not observed in interfacial regions, substantial changes occurred in the BMAS matrix after creep at 1100°C and 103 MPa. Figure 6 shows evidence of spinodal decomposition that initiated within the intergranular glassy phase that was present in the as-ceramed composites. The dark phase in the image forms a continuous network of tubules, ~100 nm in width, surrounded by a light-colored glassy phase. These phases were identified by electron diffraction and EDS as hexacelsian (dark phase), and a siliceous glass (light phase).[17] Furthermore, X-ray diffraction analysis indicated that the amount of hexacelsian phase increased considerably compared to the as-ceramed composite. (This phenomenon is discussed in detail in Ref. 17.) No decomposition of the matrix was observed in the second sample, in which the period of creep was of much shorter duration.

3.3 Tensile fatigue

3.3. 1 Fatigue properties

The tensile fatigue experiments conducted at 1100°C involved two maximum stress levels (103 MPa and 138 MPa), equivalent to the constant stress levels used in the creep experiments. The results of the fatigue experiments are summarized in Table 2. At the lower maximum stress, all of the samples survived 10^5 cycles without failure. However, at the higher maximum stress, failure occurred at 13,000 cycles. In addition, changes in the stiffness of the composites during fatigue experiments were monitored by measuring the elastic modulus at the first cycle, and after 100, 1000, 10,000 and 100,000 cycles. The results, plotted in Figure 7, show that the elastic modulus of all the samples dropped 6-11% from the first to the 100th cycle, and stayed relatively constant through the additional cycles. The observed changes in modulus were generally consistent with the acoustic emission data collected during the fatigue experiments, which showed significant activity at cycle one, corresponding to cracking and/or interface debonding in the material, followed by decreasing activity thereafter. Thus, the initial drop in modulus was associated with an accumulation of both microcracking and/or fiber-matrix debonding. These damage processes appeared to saturate after a relatively small number of cycles. Surprisingly, an

apparent increase in stiffness of 7 GPa was evident between 10^4 and 10^5 cycles in one of the fatigue samples (T = 1100°C and σ_{max} = 103 MPa). Recovery of the elastic modulus during cyclic loading has been reported in other fiber-reinforced glass or glass-ceramic matrix composites.[18] Although the causes of this phenomenon are not fully understood, Zawada *et al.* have speculated that several mechanisms might be responsible, including an increase in the frictional sliding coefficient, crack closure, and/or realignment of the fibers.[18]

The fatigue life of the composite can be estimated using a power-law relation, often applied to similar composite systems.[19] The constitutive equation is of the form

$$\sigma_{app} = \sigma_{uts} (2N_f)^b \quad (2)$$

where σ_{app} is the applied maximum stress, $2N_f$ is the number of reversals to failure (1 cycle = 2 reversals), σ_{uts} is the monotonic tensile strength, and b is the fatigue strength exponent. At 1100 °C, σ_{uts} was measured in the tensile experiment to be 272 MPa, and N_f was 13,000 when σ_{app} was 138 MPa. Using these data, b is calculated to be -0.0667. Substituting b and σ_{uts} into equation (2) yields a fatigue life of ~9×10^5 cycles (for σ_{max}=103 MPa). This value can be used to approximate the total fatigue life of the composite system for a given for σ_{max}.

3.3.2 Microstructural observations

Microstructural analysis of the tensile fatigue samples revealed several features.

(1) In samples fatigued at σ_{max}=103 MPa, cracks in the matrix occurred in both the 0° and 90° plies. The cracks initiated in the matrix, propagated toward the fibers, deflected at the fiber/matrix interface and continued propagating along the interface, as shown in Figure 8. In most cases, the cracks propagated either within the BN layer (Figure 8(a)) or at the BN/fiber interface (Figure 8(b)). Therefore, the BN layer functioned as a debond layer, allowing crack deflection and energy absorption during fracture.

(2) The fatigue samples tested at 1100°C and 103 MPa exhibited fiber oxidation in the 90° plies. Figure 9(a) shows the reaction in an early stage, with affected regions visible as light spots which appear to be on the fiber side of the interface. This is more clearly visible in Figure 9(b), in which the original fiber surface is highlighted by a dashed line. The affected region is clearly on the fiber side of the interface, while the BN coating is unaffected. Compositional analysis by EDS and PEELS revealed that such areas contained only silicon and oxygen (no carbon or boron). The absence of carbon is attributed to the oxidation reaction, which results in evolution of gaseous CO,[17, 19] while the absence of boron indicates that the BN layer was not involved in the reaction. When the oxidation reached an advanced stage, a non-crystalline porous layer formed at the BN/fiber interface, exhibiting a characteristic mottled appearance shown in Figure 10. The thickness of the reacted zone was about 150 μm.

(3) In fatigue samples tested at 1200°C, additional changes were observed in the interior of the SiC fibers. The homogenous appearance of the nanocrystalline fibers was changed, and the microstructure was partitioned into equiaxed domains, which were nanocrystalline and ~1 μm in diameter. Figures 11(a) and 11(b) are PEELS spectra collected from the fibers in the fatigued sample and in the ceramed sample respectively, along with diffraction patterns. Both EDS and PEELS measurements indicated that the oxygen concentration increased. The diffraction pattern from the domains in the fatigued fibers revealed an additional set of reflections. The inner diffuse ring, which was not present in pretested fibers, corresponds to lattice planes in a group of SiO_2 polymorphs that have a 0.342 nm spacing. Apparently, the SiC fibers were partly oxidized and the oxygen concentration was substantially increased. In contrast, oxidation of the SiC fiber was not observed in composites heat-treated in air at the same temperature (1200°C for 500 hours).[12]

The observations described above indicate that oxidation of the SiC fibers was more extensive under cyclic loading conditions than under static loads, even for similar stress levels, times and temperatures. The critical phenomenon involved here is crack healing, or crack closure. Crack closure in CFCCs can reportedly occur by the oxidation of silicon carbide to produce

siliceous glass, as observed in SiC/C/SiC composites.[20] Consider first the case of static applied loads. Recall that under *constant* tensile load at 1100°C (creep), no oxidation of the SiC fibers was observed (in the bulk) when the applied stress was moderate (103 MPa). Although matrix cracking probably occurred under these conditions, the crack openings were presumably small enough to be closed by reaction products. Consequently, oxidation was generally confined to near-surface regions of the composite when the stress level was moderate. Furthermore, thermal exposure alone caused negligible microstructural changes, as in the case of heat-treatment in air at the same temperature (1200°C) for 500 hours.[12] However, when the (static) applied stress was increased to 138 MPa, matrix cracks (or crack opening displacements) were more extensive, and the crack openings were presumably too large to be sealed by the oxidation product. In this case, oxygen diffused along cracks into the bulk, resulting in oxidation of SiC fibers (*Section 3.2.2)*.

In contrast, under cyclic tensile loads, crack-wake contact prevented accumulation of the oxidation product, thus precluding the possibility of crack-healing through the generation of reaction products. Consequently, even with a maximum applied stress of only 103 MPa, oxidation of SiC fibers was observed in bulk of the composite. Thus, when microcracking occurred, crack-healing was prevented, leading to fiber oxidation. This was especially true in the case of fatigue loading at 1200°C, which caused extensive oxidation to the SiC fibers.

4. Conclusions

The tensile properties and corresponding microstructural changes reported have shown that the fiber-reinforced glass-ceramic composite was microstructurally stable at high temperatures. No significant degradation in tensile strength or change in fracture mode was observed up to 1200 °C, and the composite exhibited good tensile creep resistance up to 1100°C. Under cyclic loading to a maximum stress of 103 MPa, the material survived 10^5 cycles at temperatures up to 1200°C.

The short-term and long term properties observed in this study derived largely from the degree to which the interface microstructure was controlled by the SiC/BN dual coating. In particular, the BN coating provided the desired weak interface necessary for toughness, while the SiC overlayer provided a barrier to diffusion and reaction at high temperatures. Both layers were more stable in oxidizing atmospheres than either BN coatings alone, or previously studied carbon-rich interfaces.[3, 4]

Although the focus of this investigation has undoubtedly been on the interface, the role of the matrix microstructure and associated properties is also critical. Residual glassy phase in the matrix had important implications on the high-temperature response of the composite. Above 1000°C, viscous flow of intergranular glassy phase facilitated boundary sliding and contributed to matrix softening, allowing the matrix to creep and the fibers to carry most of the applied load. On the other hand, glassy phase in some instances contributed to damage-tolerance, allowing microcracks to heal. The matrix properties also controlled the proportional limit stress, the stress at which microcracking initiated. Microcracking affected not only the elastic modulus, but also the oxidation resistance, as observed in the creep and fatigue experiments. Microstructural modifications to increase the matrix proportional limit stress should directly benefit the composite properties. Thus, a potentially important area for future research is the design of matrix compositions and microstructures with improved resistance to microcracking. Undoubtedly, there will be tradeoffs in designing composites based on glass-ceramics, in that optimizing stiffness and toughness of the composite by controlling the amount of residual glassy phase may also reduce damage-tolerance.

The work presented here has also shown that the microstructures that develop under cyclic stress fields can be quite different than those that evolve under monotonic loading despite similar stresses and temperatures. In fact, environmental effects had a more significant effect on the material during cyclic loading compared to static or quasi-static loading conditions. Oxidation was enhanced during fatigue experiments, apparently because of crack-wake contact which impeded gaseous diffusion of oxygen. Consequently, material life-time predictions based on

experimental data from static loading conditions or in anaerobic environments are likely to be inaccurate. A more complete understanding of the micromechanisms involved in fatigue damage and the effects of oxidation is needed before introducing the material into high-temperature structural applications.

Acknowledgments

The work was support by the Air Force Office of Scientific Research (contract F49620-92-C-0001) and by the National Science Foundation (EYS and SRN) through a Materials Research Group (grant DMR-9002994). The authors thank Mr. Jim O'Kelly of 3M for coating the Nicalon fibers used in the study, Mr. Stan Kustra of UTRC and Mr. Gary Linsey of Pratt & Whitney for mechanical testing of the composites, Miss Anne Staples of Brown University for TEM specimen preparation, and Dr. Alexander Pechenik of AFOSR for sponsorship of this program.

References

[1]K. M. Prewo and J. J. Brennan, "High Strength Silicon Carbide Fiber-Reinforced Glass Matrix Composites," *J. Mat. Sci.*, **15**, 463-468 (1980).

[2]K. M. Prewo and J. J. Brennan, "Silicon Carbide Fiber Reinforced Glass-Ceramic Matrix Composites Exhibiting High Strength and Toughness," ibid., **17**, 2371-2383 (1982).

[3]J. J. Brennan, "Interfacial Characterization of Glass and Glass-Ceramic Matrix/Nicalon SiC Fiber Composites"; pp. 549-560 in *Materials Science Research,* Vol **20**, Plenum Press, New York, 1986.

[4]R. F. Cooper and K. Chyung, "Structure and Chemistry of Fiber-Matrix Interfaces in SiC Fibre-Reinforced Glass-Ceramic Composites: An Electron Microscopy Study," *J. Mat. Sci.*, **22**, 3148-3160 (1987).

[5]R. L. Kerans, R. S. Hay, N. J. Pagano, and T. A. Parthasarathy, "The Role of the Fiber-Matrix Interface in Ceramic Composites," *Am. Ceram. Soc. Bull.*, Vol. **68**, 429-442 (1989).

[6]D. C. Phillips, R. A. Sambell, and D. H. Bowen, "The Mechanics Properties of Carbon Fiber Reinforced Pyrex Glass," *J. Mat. Sci.*, 7, 1454-1464 (1972).

[7]S. R. Levitt, "High-Strength Graphite Fiber/Lithium Aluminosilicate Composites," *J. Mat. Sci.*, **8**, 793-806 (1973).

[8]R. W. Rice, "BN Coating of Ceramic Fibers for Ceramic Fiber Composites," *US Patent 4,642,271,* Feb. 10 (1987).

[9]J. J. Brennan, "Interfacial Studies of SiC Fiber Reinforced Glass-Ceramic Matrix Composites," *Final Rept. R87-917546-4 on ONR Contract N00014-82-C-0096,* Oct. 15, 1987.

[10]R. Naslain *et al,* "Boron Nitride Interphase in Ceramic-Matrix Composites," ibid., **74** [10] 2482-88 (1991).

[11]J. J. Brennan, B. Allen, S. R. Nutt, and Y. Sun, "Interfacial Studies of Coated Fiber Reinforced Glass-Ceramic Matrix Composites," *Annual Rept. R92-970150-1 on AFOSR Contract F49620-92-C-0002,* Nov. 30, 1992.

[12]E. Y. Sun, S. R. Nutt, and J. J. Brennan, "Interfacial Structure and Chemistry of SiC/BN(C) Dual Coated Nicalon Fiber Reinforced BMAS Glass-Ceramic Composites," *J. Am. Cer. Soc.*, 77 [5], 1329-39 (1994).

[13]E. Y. Sun, S. R. Nutt, and J. J. Brennan, "Flexural Creep Behavior of SiC/BN Dual-Coated-Nicalon-Fiber-Reinforced Glass-Ceramic Matrix Composites," submitted to *J. Am. Cer. Soc.*

[14]B. A. Bender, J. S. Wallace, and D. J. Schrodt, "Effect of Thermochemical Treatments on the Strength and Microstructure of SiC Fibers," *J. Mat. Sci,* **26** (1991), 970-976.

[15]G. Simon, and A. R. Bunsell, "Creep Behaviour and Structural Characterization at High Temperatures of Nicalon SiC Fibers," ibid., 19 (1984), 3658-3670.

[16]E. Y. Sun, S. R. Nutt, and J. J. Brennan, "Microscopic Failure Mechanisms in SiC Fiber-Reinforced Glass-Ceramic Composites"; pp. 175-185 in *Control of Interfaces in Metal and Ceramics Composites,* edited by R. Y. Lin and S. G. Fishman, TMS, 1994.

[17]E. Y. Sun, S. R. Nutt, and J. J. Brennan, "Thermal Stability of Glass-Ceramic Matrix Composites Reinforced with Dual Coated Silicon Carbide Fibers," to be submitted to *J. Am. Cer. Soc.*

[18]L. P. Zawada and L. M. Butkus, "Tensile and Fatigue Behavior of Silicon Carbide Fiber-Reinforced Aluminosilicate Glass," *J. Am. Cer. Soc.*, **74** [11] 2851-58 (1991).

[19]Y. Ramakrishnan and N. Jayaraman, "Fatigue Behaviour of Borosilicate Glass-Ceramic Matrix, Nicalon (Silicon Carbide) Fiber Composites," *J. Mat. Sci,* **28** (1993), 5580-91.

[20]L. Filipuzzi, G. Camus, and Roger Naslain, "Oxidation Mechanisms and Kinetics of 1D-SiC/C/SiC Composite Materials: I, An Experimental Approach," *J. Am. Cer. Soc.*, 77 [2] 4591-66 (1991).

Figure Captions

Fig. 1 Stress vs. strain response of BMAS/SiC/BN/Nicalon fiber composites tensile tested at 20 °C, 1100°C and 1200°C.

Fig. 2 Fracture surface of the composites: (a) tested at 1100°C, and (b) tested at 1200°C.

Fig. 3 Residual intergranular glassy phase in the BMAS matrix.

Fig. 4 Tensile creep curve and tested sample (1100°C, 103 MPa, air).

Fig. 5 (a) Interfacial region in the composite after tensile creep experiment (1100°C, 103 MPa, air, 266 hours); and (b) oxidation occurred at the BN/SiC fiber interface in the composite after tensile creep experiment (1100°C, 138 MPa, air, 65 hours).

Fig. 6 Spinodal decomposition occurred in the intergranular regions, in the composite after tensile creep at 1100°C for 266 hours.

Fig. 7 The elastic modulus of the composites determined at different cycle points during the fatigue experiments.

Fig. 8 Sample after fatigue testing at room temperature (103 MPa, 10^5 cycles): (a) crack propagating in the BN layer, in the 0° plies, and (b) matrix crack intersecting the BN coating layer, in the 90° plies.

Fig. 9 (a) Oxidation of the SiC fiber in an early stage, in the composite fatigued at 1200°C under 103 MPa; and (b) a high-resolution image of the arrowed area in (a).

Fig. 10 Oxidation of the SiC fiber in an advanced stage.

Fig. 11 PEELS spectra and diffraction patterns from (a) fibers in the pretested composite and (b) fibers in the fatigued sample (tested in air at 1200°C).

Table 1. Tensile properties of BMAS/SiC/BN/SiC fiber composites

Temperature	PL (MPa)	E (GPa)	UTS (MPa)	ε_f (%)
20°C	87.9	98.3	236.5	0.84
1100°C	88.0	54.3	271.6	0.94
1200°C	70.1	44.0	302.7	1.18

Table 2. Tensile fatigue results of BMAS matrix/SiC/BN/SiC fiber composites (tested in air)

Temperature	20°C	1100°C	1100°C	1200°C
Max. Stress (MPa)	103	103	138	103
Comments	10^5 cycles no failure	10^5 cycles no failure	13,000 cycles failed	10^5 cycles no failure

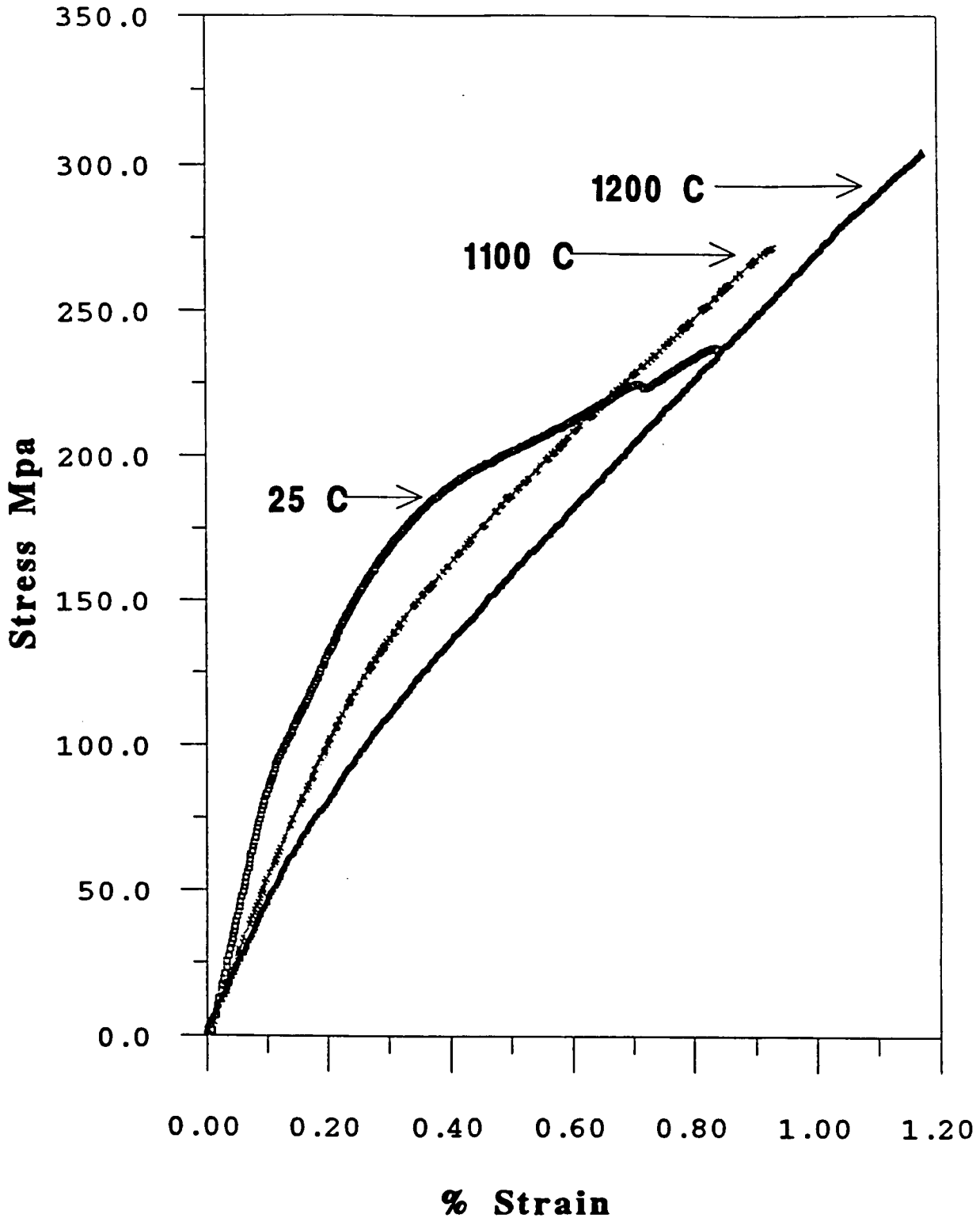

Figure 1 Stress vs. strain response of BMAS/SiC/BN/Nicalon fiber composites tensile tested at 20°C, 1100°C and 1200°C.

(a)

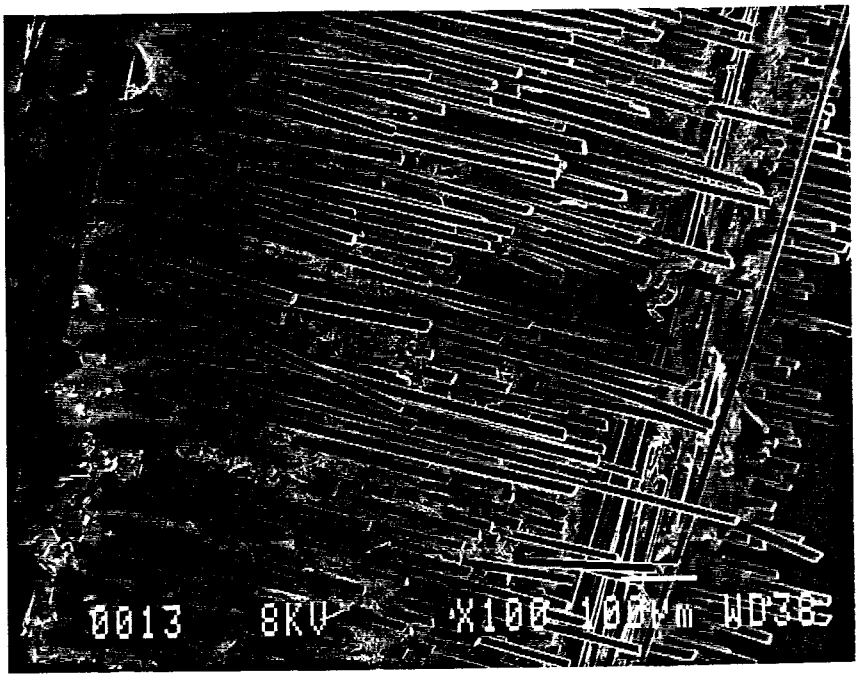

(b)

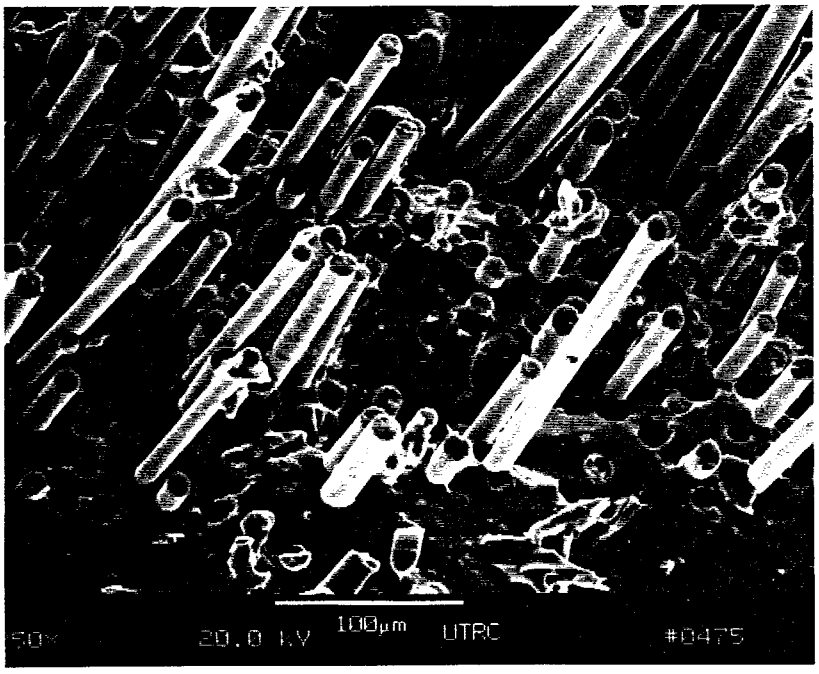

Figure 2 Fracture surface of the composites: (a) tested at 1100°C, and (b) tested at 1200°C.

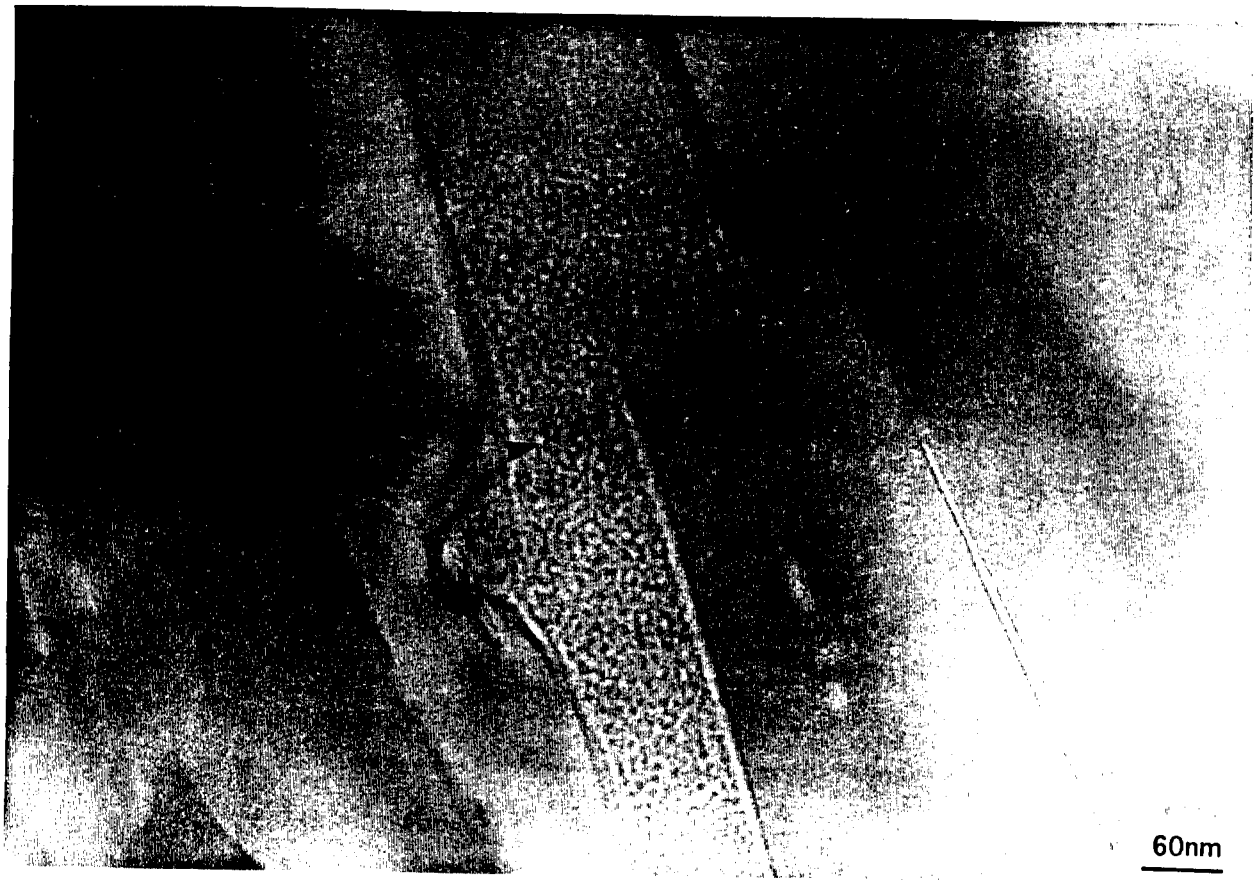

Figure 3 Residual intergranular glassy phase in the BMAS matrix.

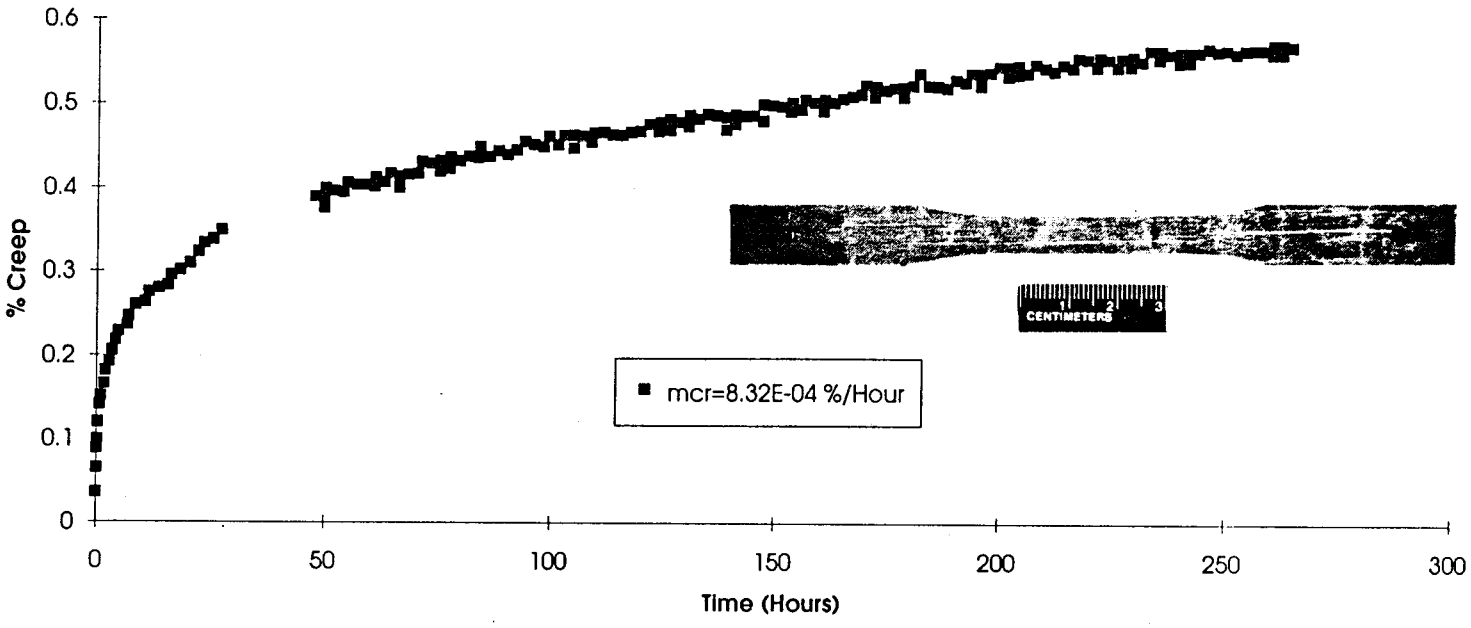

Figure 4 Tensile creep curve and tested sample (1100°C, 103 MPa, air).

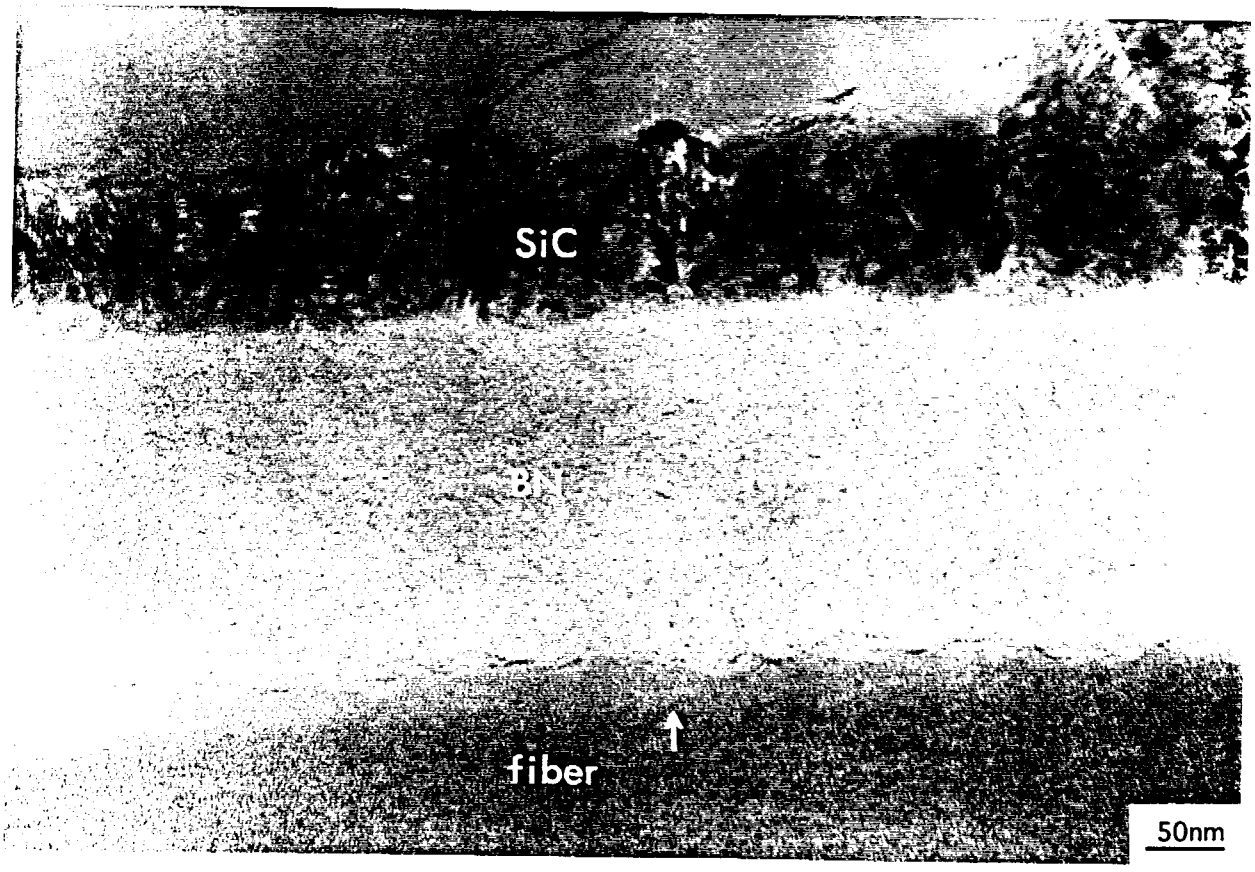

Figure 5(a) Interfacial region in the composite after tensile creep experiment (1100°C, 103 MPa, air, 266 hours).
(continued)

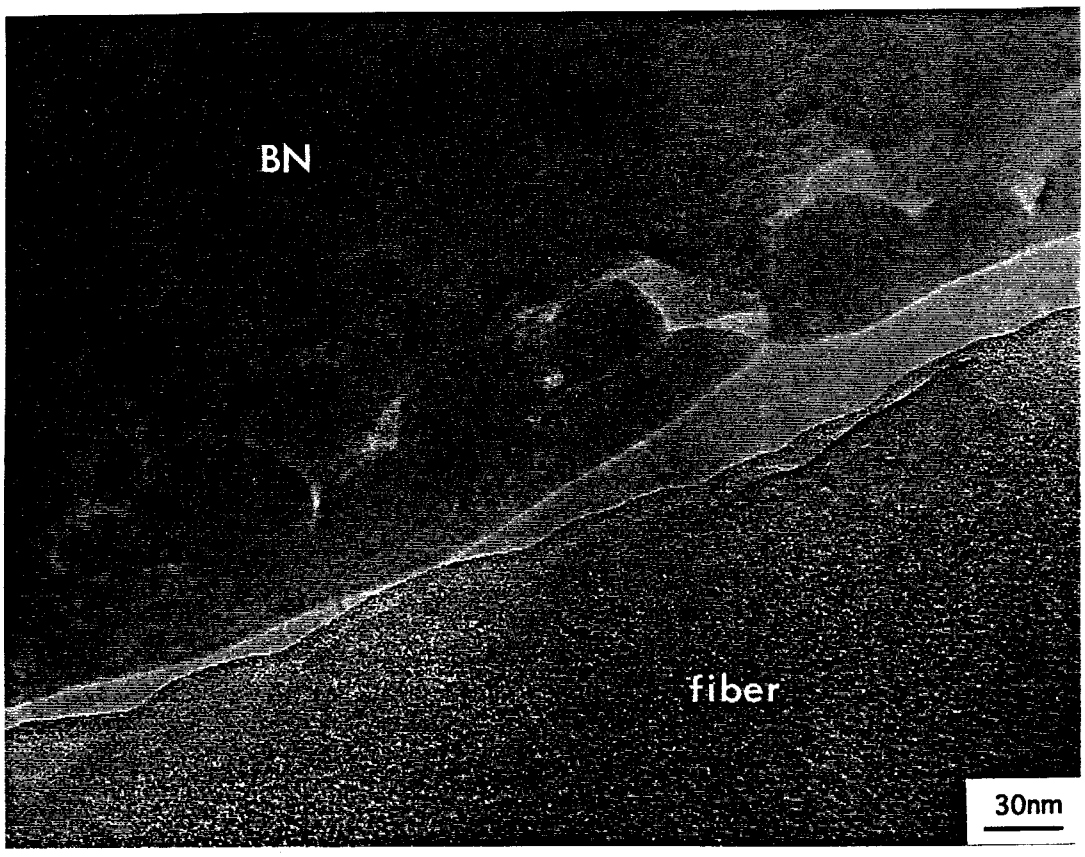

Figure 5(b) Oxidation occurred at the BN/SiC fiber interface in the composite after tensile creep experiment (1100°C, 138 MPa, air, 65 hours).

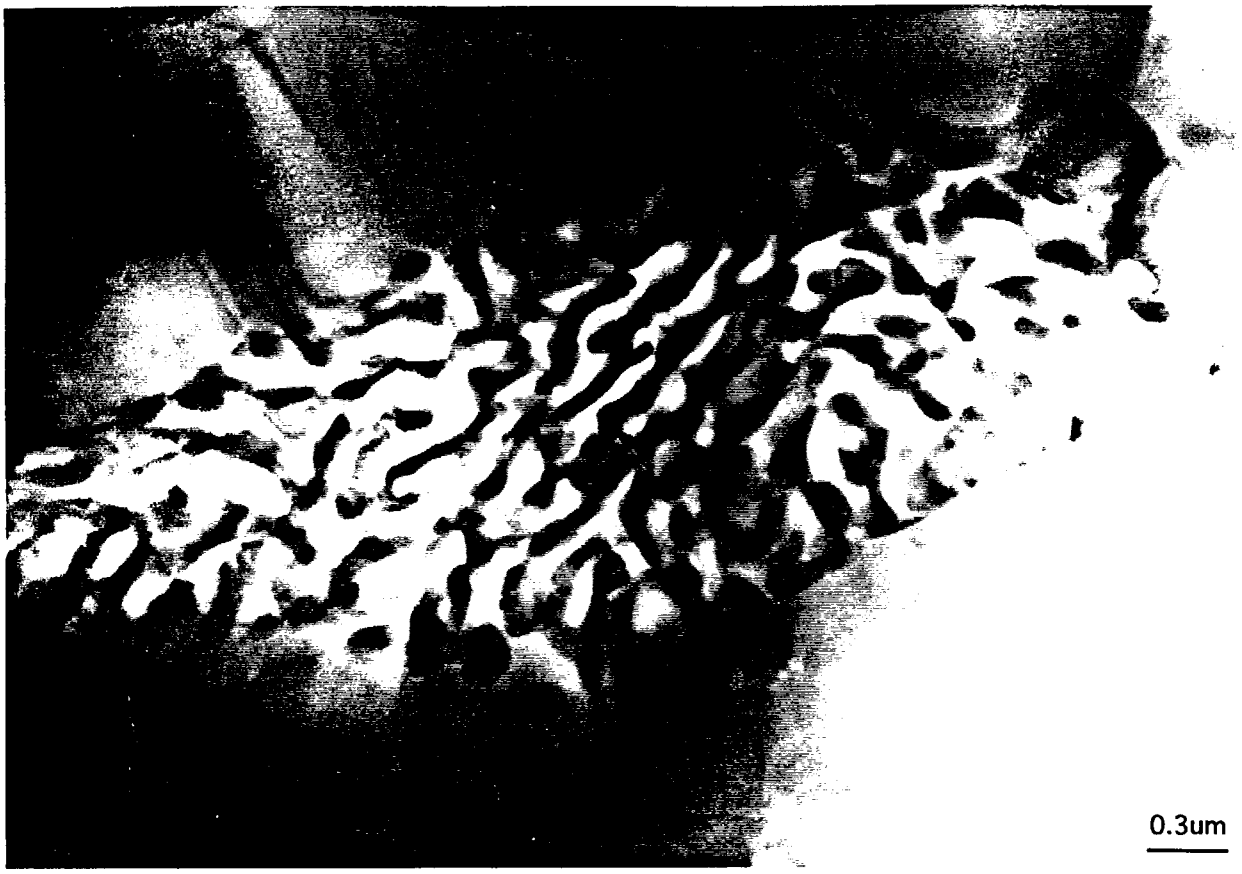

Figure 6 Spinodal decomposition occurred in the intergranular regions, in the composite after tensile creep at 1100°C for 266 hours.

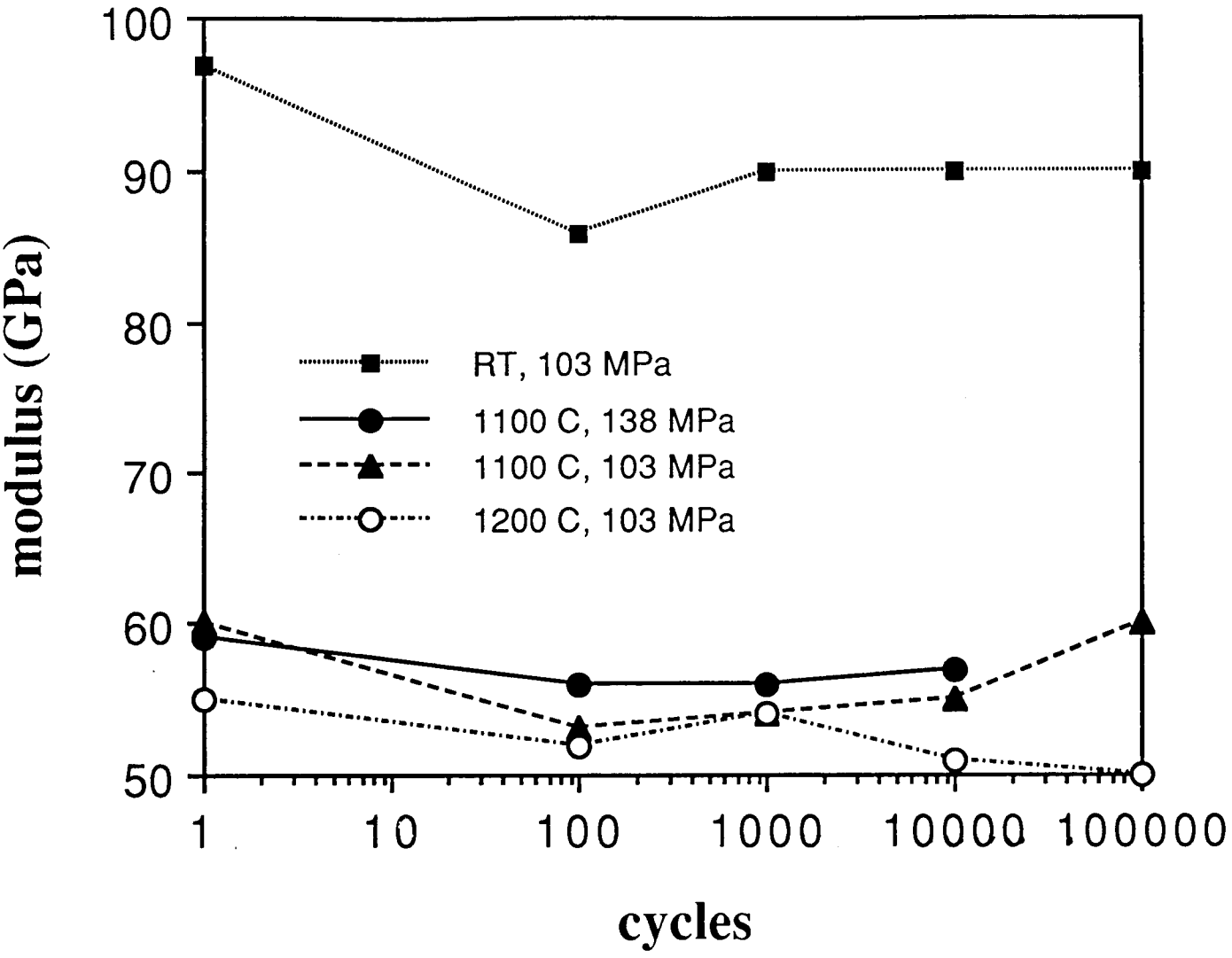

Figure 7 The elastic modulus of the composites determined at different cycle points during the fatigue experiments.

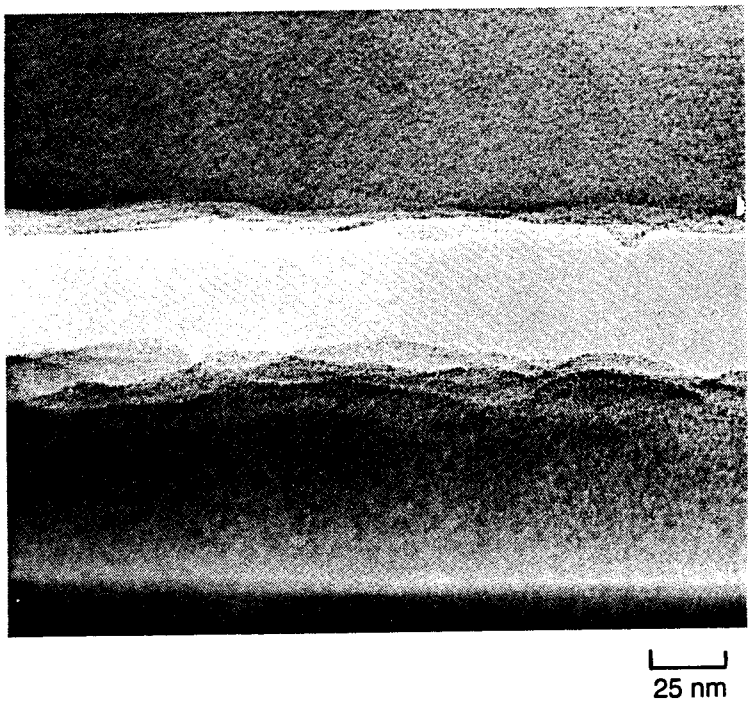

Figure 8 Sample after fatigue testing at room temperature (103 MPa, 10^5 cycles): (a) crack propagating in the BN layer, in the 0° plies. (continued)

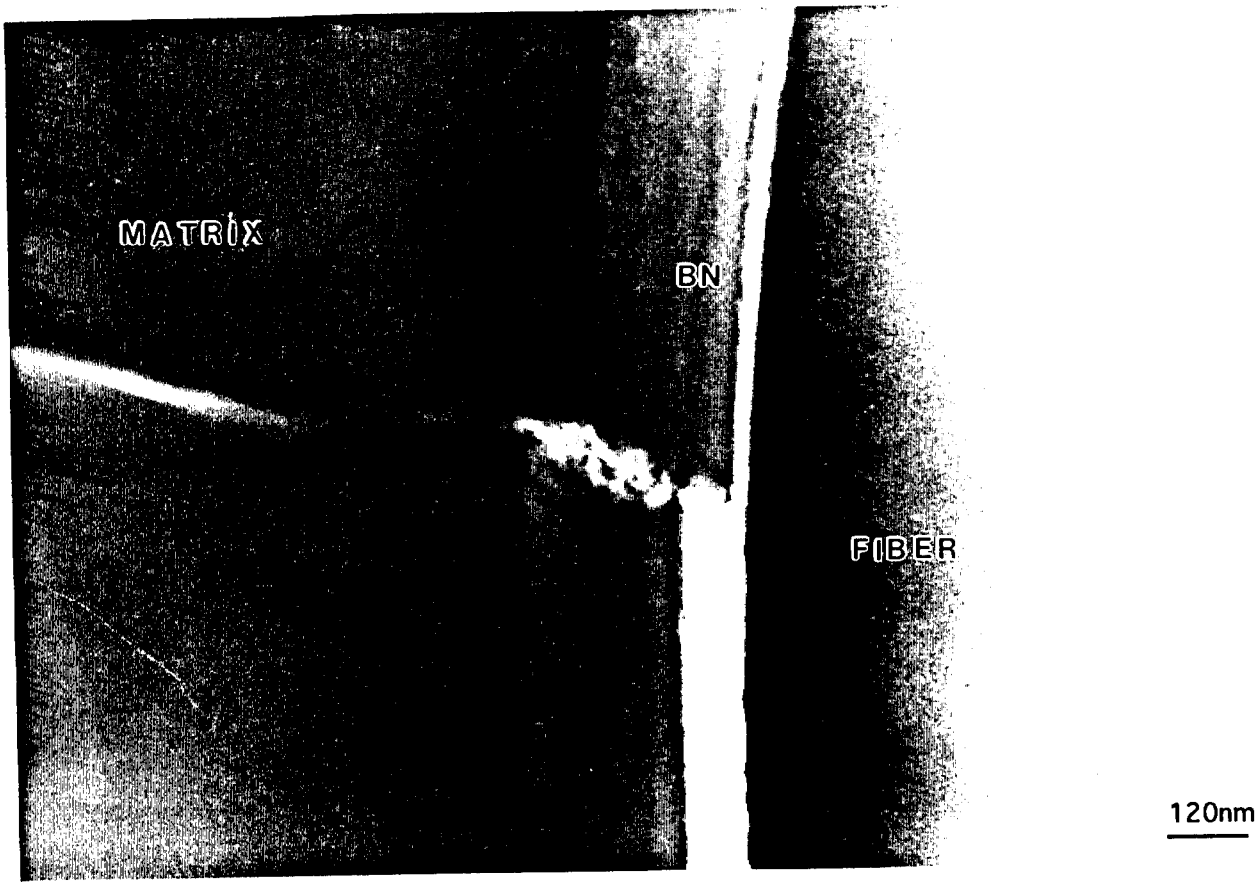

Figure 8 (b) matrix crack intersecting the BN coating layer, in the 90° plies.

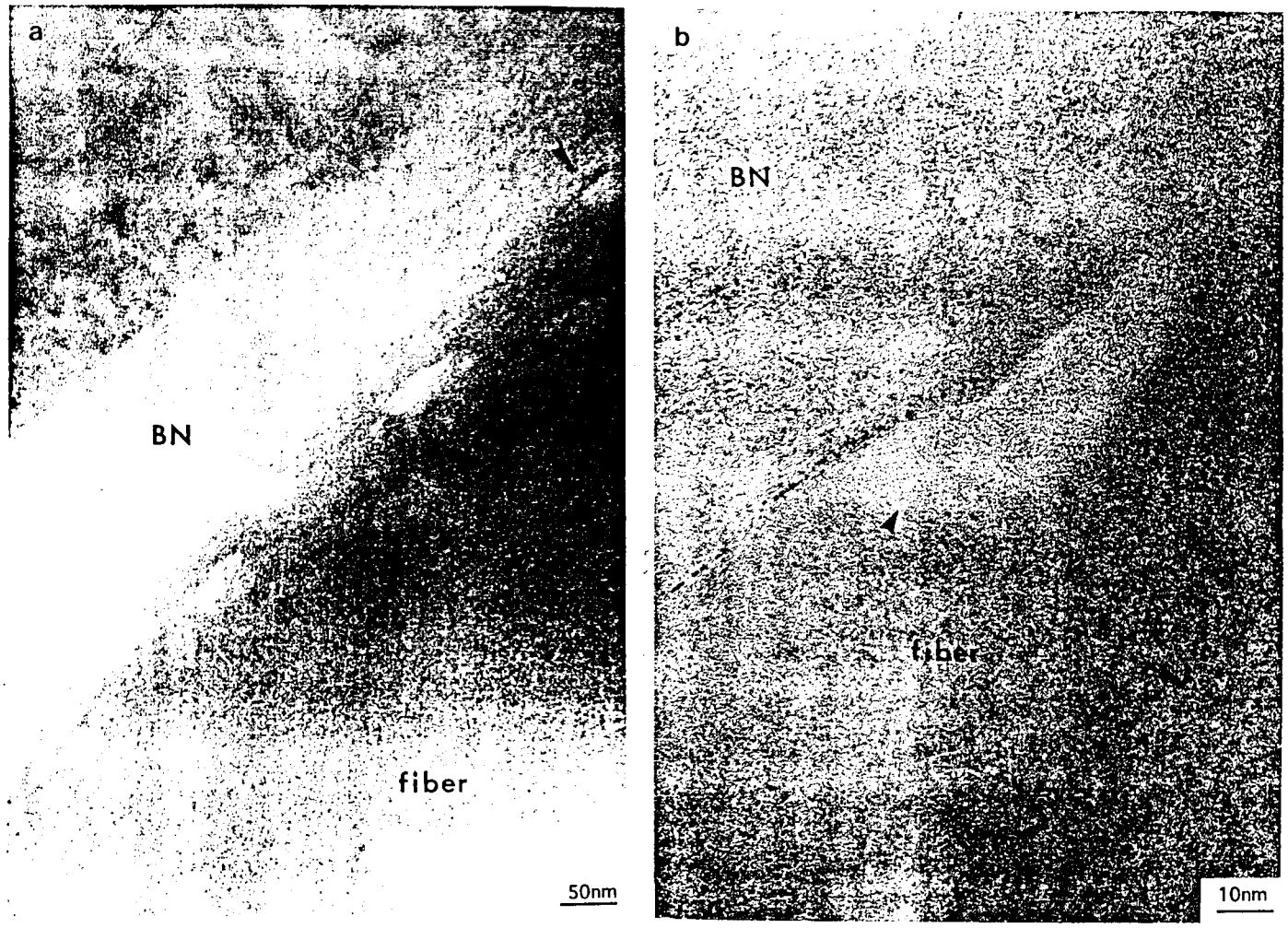

Figure 9 (a) Oxidation of the SiC fiber in an early stage, in the composite fatigued at 1200°C under 103 MPa;
and (b) a high-resolution image of the arrowed area in (a).

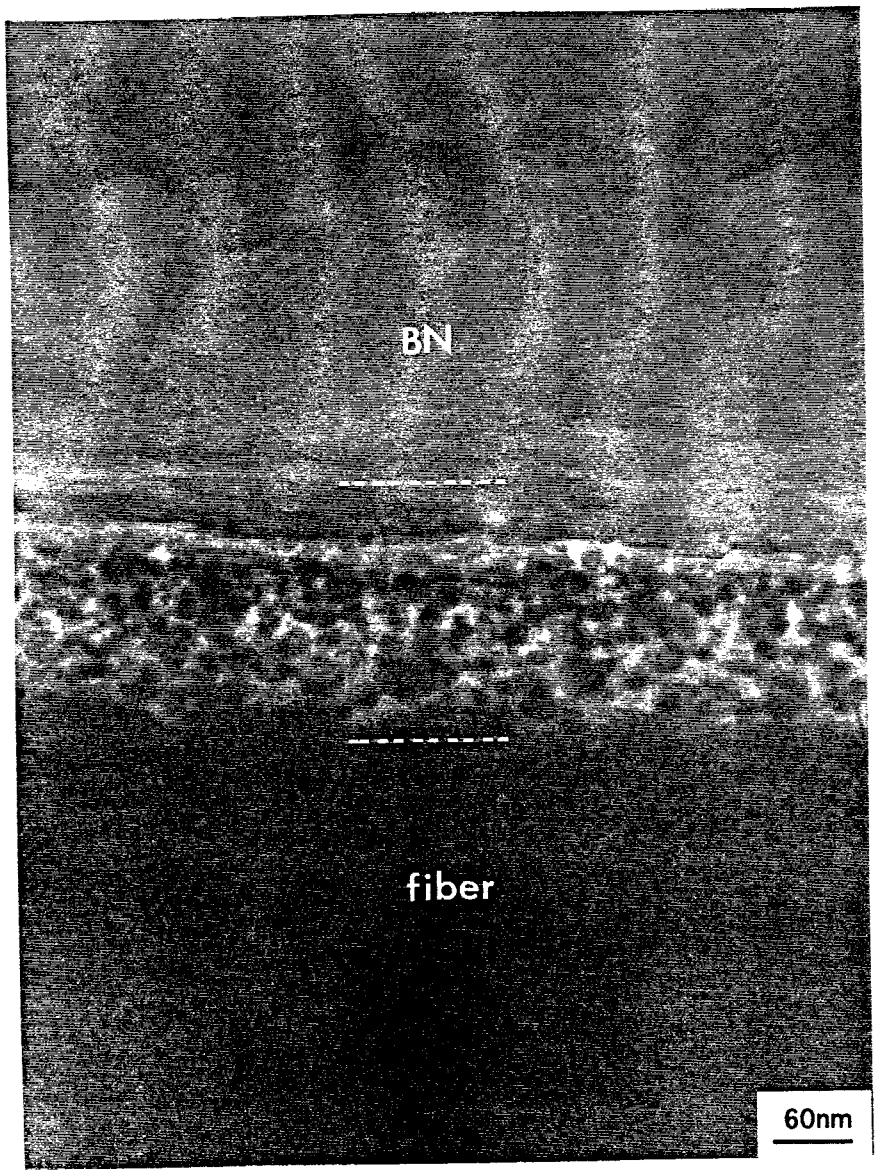

Figure 10 Oxidation of the SiC fiber in an advanced stage.

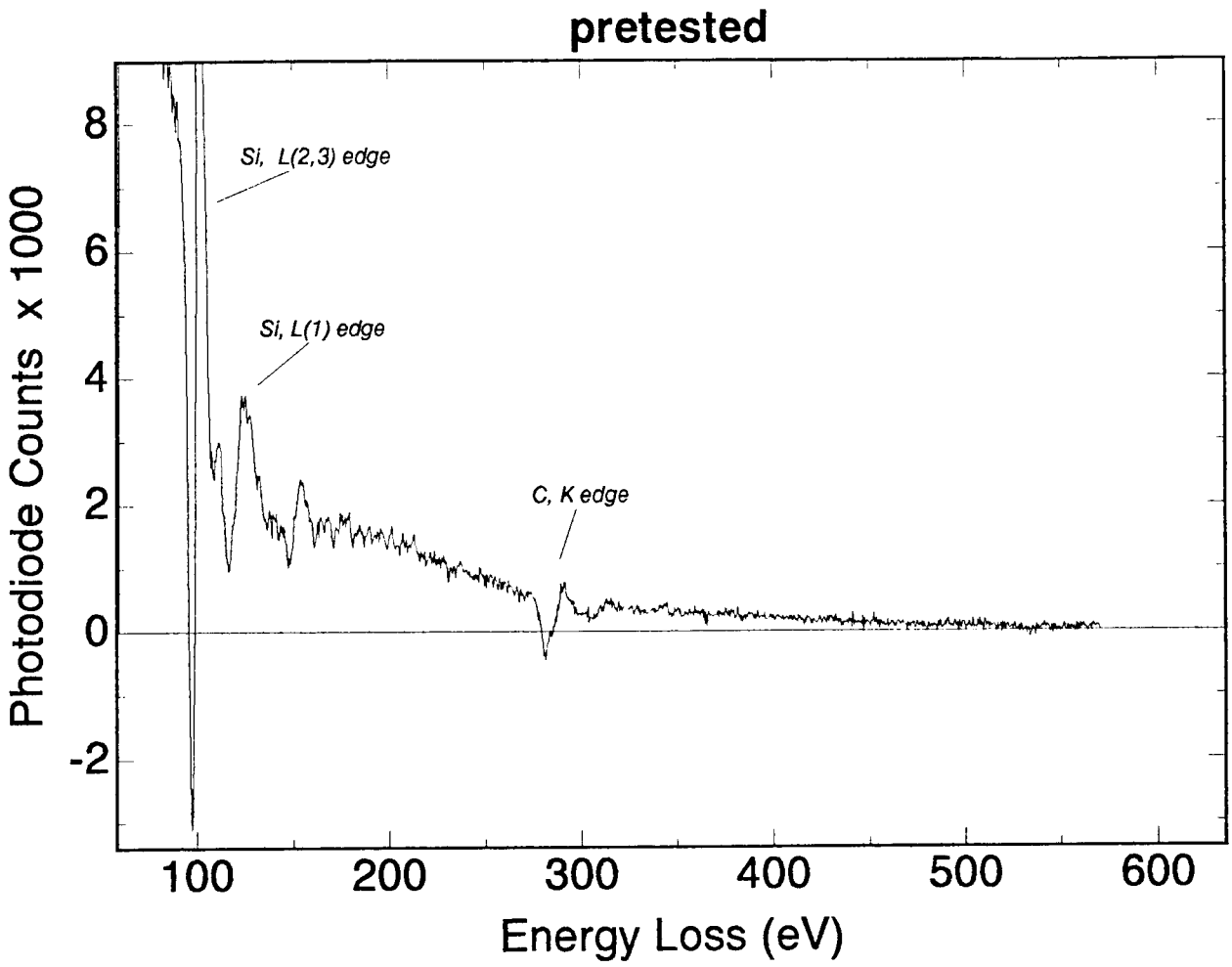

Figure 11 (a) PEELS spectrum and diffraction pattern from fibers in the pretested composite.

(continued)

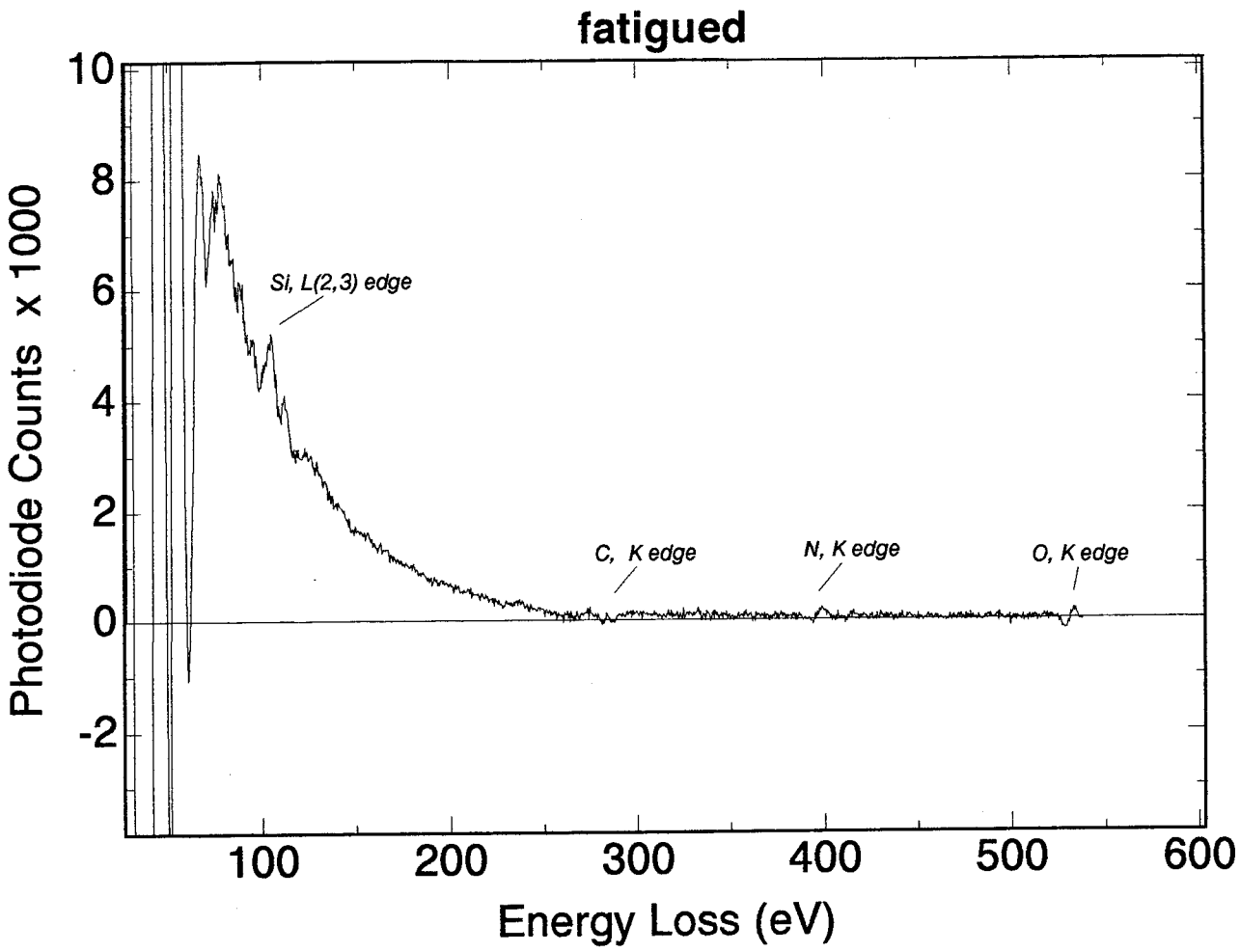

Figure 11 (b) PEELS spectrum and diffraction pattern from fibers in the fatigued sample (tested in air at 1200°C).